1-29-2015

Analytical and Experimental Methods for Studying Novel Cavity Geometries in Quantum Dot Mode Locked Lasers

David Murrell

David A. Murrell

Candidate

Optical Science and Engineering (ECE)

Department

This dissertation is approved, and it is acceptable in quality and form for publication: *Approved by the Dissertation Committee:*

Christos Christodoulou

Dr. Christos Christodoulou, Chair

Luke Lester

Prof. Luke Lester, Co-Chair

Ravi Jain

Dr. Ravi Jain, Member

Jean-Claude Diels

Dr. Jean-Claude Diels, Member

Sayan Mukherjee

Dr. Sayan Mukherjee, Member

Analytical and Experimental Methods for Studying Novel Cavity Geometries in Quantum Dot Mode Locked Lasers

by

David A. Murrell

B.S. Engineering Physics, Colorado School of Mines 2007
M.S. Applied Physics, Colorado School of Mines 2009
M.S. Optical Science and Engineering, University of New Mexico
2013

DISSERTATION

Submitted in Partial Fulfillment of the
Requirements for the Degree of

Doctor of Philosophy
Optical Science and Engineering

The University of New Mexico

Albuquerque, New Mexico

December 2014

Dedication

To my parents, Don and Amy Murrell, whose constant faith made my journey possible and reminded me that all things are in reach to those who strive.

Acknowledgments

I would like to acknowledge the steadfast support and wisdom of Professor Luke F. Lester; my longtime advisor and mentor who introduced an inquisitive young intern to the wonders that result when disciplines merge. I would like to extend my gratitude to my remaining committee members who have had significant effects on my understanding. Dr. Christos Christodoulou and his student Georgios Atmazakis provided me a new perspective to consider when working with mode locked lasers using their experience in the RF world. Dr. Jean-Claude Diels' skill in free space optics and mode locking were a bountiful well spring that I drew upon often. Dr. Ravi Jain's insight into laser sources and all things fiber provided the grounding I needed to venture beyond what I knew. And Dr. Sayan Mukherjee who showed me the dividends of rigor and relayed some of his wisdom purchased through experience. I also thank my colleagues and friends who I met at the Center for High Technology Materials and who have enlightened me either by direct aid or by stimulating conversation. Dr. Ravi Raghunathan provided exceptional insight into mathematical constructs of mode-locking. Dr. Jesse Mee's experimental prowess and skills at data visualization allowed me to see and reach farther than I could have without him. Dr. Mark Crowley's theoretical background was invaluable when teasing out the ideal device configurations informed by gain and loss observations. Also thanks to Dr. Yan Li who apprenticed me through experimental measurement, Nishant Patel who helped me to learn more about thermal conduction than I ever expected, and Dr. Nathan Withers whose breadth of knowledge made my ventures less of a leap. This work could not have been completed without collaborations with the National Science Foundation, Defense Threat Reduction Agency, Air Force Research Laboratory, University of Rochester, Rochester Institute of Technology, the Cancer Research Center at the University of New Mexico, and all of the other brilliant people who I had the pleasure of meeting on my own road to knowledge.

Analytical and Experimental Methods for Studying Novel Cavity Geometries in Quantum Dot Mode Locked Lasers

by

David A. Murrell

B.S. Engineering Physics, Colorado School of Mines 2007

M.S. Applied Physics, Colorado School of Mines 2009

M.S. Optical Science and Engineering, University of New Mexico 2013

Ph.D. Optical Science and Engineering, University of New Mexico, 2014

Abstract

In this dissertation, the insights provided using analytical methods to predict and refine Quantum Dot Mode Locked Lasers (QDMLLs) for use in multiple applications are explored. Experimental investigation guided by theory greatly reduces the number of iterations to find solutions to technical problems. The fitness of the theory and methods used for prediction of QDMLL operation are demonstrated. Experimental cases for QDMLLs in high temperature and radioactive environments are presented. Further avenues of pursuit for achieving high repetition rates in optical sources are also proposed.

Contents

List of Figures

List of Tables

Glossary

AFM	Atomic Force Microscopy
CW	Continuous Wave
DWELL	Dots-in-a-Well
FWHM	Full Width Half Maximum
MBE	Molecular Beam Epitaxy
OTDM	Optical Time Division Multiplexing
PL	Photoluminescence
QDMLL	Quantum Dot Mode Locked Laser
RF	Radio Frequency
WDM	Wavelength Division Multiplexing

Chapter 1

Introduction

1.1 Foreward

Novelty is a constant in the development of next generation laser sources. The field has progressed from the first GaAs [1] laser diode to branching families of devices each with brilliant innovations and unique implications. It is remarkable that the field of Optoelectronics has developed so rapidly in 50 years that the bulwarks of the field have had the opportunity to see their work advanced several generations by their colleagues. This dissertation illustrates and postulates based on my own experience with the Quantum Dot Mode-Locked Laser (QDMLL). It is a device that I have worked with extensively throughout my entire tenure as a graduate student in Optical Science and Engineering; my first research projects with the technology occurred even before then. I have been impressed with the versatility of the QDMLL to produce short pulses and to be dynamically adapted to many situations.

The theories that describe the operation of these devices are continuously evolving as the dynamics of these lasers are better understood. It is my hope that the next few chapters in this document will prove both enlightening and thought provoking on the topic of the fitness of these devices to operate in a wide range of applications.

1.2 The Growth of Data Demand

The consumption of bandwidth for all purposes has been increasing exponentially for many years and is expected to continue to do so for the foreseeable future [2]. The breakdown of this Internet traffic by type is shown in figure 1.1.

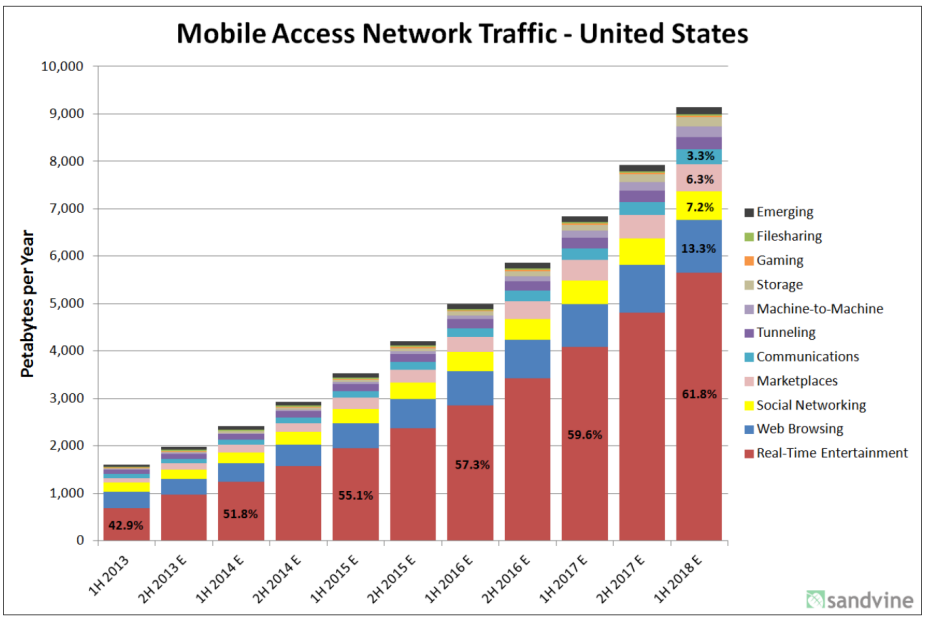

Figure 1.1: A breakdown of mobile bandwidth use in the United States and projections to 2018 [2]

The utilization of real time entertainment in figure 1.1 is driven primarily by video streaming services. Impressive growth in the demand for more services on the

Internet is already stressing our infrastructure and further considerations must be made going forward. Long haul communications have principally adopted fiber optic links because of their remarkable data bandwidth. Now, the stresses of bandwidth are being felt locally as the limitations of the Copper interconnects [3] in current processor technology are manifesting. A potential solution to the local bandwidth needs utilizes Silicon photonics [4] to replace the existing Copper interconnects in routing servers as well as in end user devices. Integration of photonic networks with high bandwidth [5, 6] using novel structures for routing [7, 8, 9] continues to be a popular area of research. Interest in laser sources for these networks is similarly shared by many [10, 11]. This research focuses on the fitness of the QDMLL for integration into similar networks by projecting mode locking behavior into environmental extremes and with novel cavity configurations.

1.3 The Quantum Dot Mode Locked Laser

The ideal source for providing the necessary optical signal for Silicon photonic networking techniques is a mode locked laser. These lasers use internal modulation of the elements inside the optical cavity to generate a continuous train of short pulses [4]. These pulses vary in width and repetition rate based on the laser design. There are two basic schools of mode locking which are employed independently or in hybrid configurations. The first school is active mode locking. This requires that an external high frequency source be used to create the pulse train which must be synchronized and carefully monitored. The technique requires extensive Radio Frequency (RF) generating equipment and is highly sensitive to temperature and other instabilities. Many of the components for such an active mode locking setup utilize a large amount of weight and power. However, this technique allows for the shortest possible pulses at a cost of increased complexity.

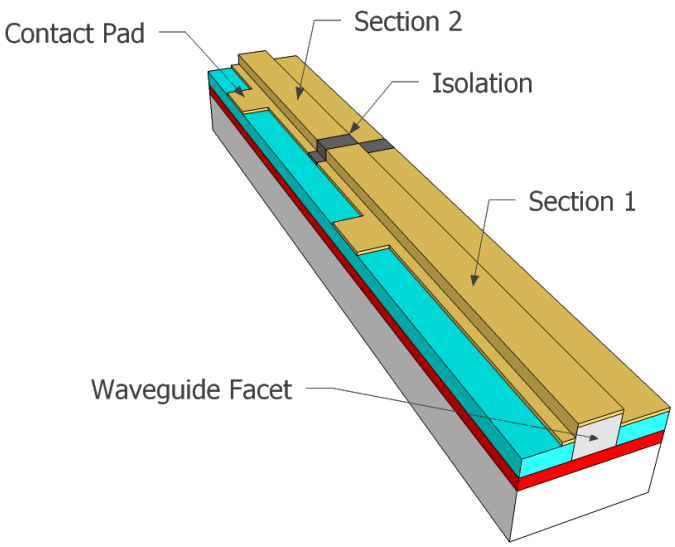

Figure 1.2: 2 Section QDMLL device schematic

Passive mode locking is the other school to achieve short pulses and is the technique of choice for the optoelectronics group at the University of New Mexico. Modulation within a passively mode locked laser is accomplished using a nonlinear saturable absorber [12]. A monolithic III-V semiconductor configuration of GaAs can produce a mode locked laser, like the one in figure 1.2, without the need for RF equipment required to maintain active mode locking. A complex system requiring extensive power and heat dissipation can be replaced with a single semiconductor merely millimeters in length. Operation of this laser requires only DC voltages in the most basic of implementations. One section of the semiconductor serves as the laser gain and the other as a mode locking element: the saturable absorber. A schematic diagram of a horizontally emitting semiconductor laser is shown in figure 1.2. Each section is electrically isolated to allow for independent gain and saturable absorption regions. The ridge waveguide is coated with a metal contact which allows direct integration into electrical systems for ease of use. Emission of light is along the waveguide facet; this light can be coupled into optical fiber or into silicon modulators for data

multiplexing. Properties of the QDMLL [13] that allow for low threshold current density [14], broad gain bandwidth from an inhomogeneously broadened system [15], low spontaneous emission noise in the output pulses [16], and abrupt gain saturation with carrier density [17] are all useful properties in communication systems.

1.4 Ultrafast Optical Networking

The concept of an ultrafast network on chip using assorted multiplexing methods has been well implemented in fiber optic telecommunications systems. The rush to develop fiber with the appropriate material properties took up much of the 1990s and remains well implemented to this day. The reason for substituting optical communications for Copper waveguides still holds today; higher bandwidth is possible using a smaller cable when optical techniques are employed. This is due to several unique properties of light and its conduits that make it an ideal communications medium [18, 19]. First, the frequency of light far exceeds that of microwaves which allows for a much higher data bandwidth. Additionally, light of different wavelengths can travel along the same waveguide while maintaining the information each color channel contains. This allows for many additional channels to be used in parallel along the same connecting channel. This technique is known as Wavelength Division Multiplexing (WDM) [6]. Mode locked laser sources deliver a continuous train of stable pulses of light that range in duration from fs to ns in temporal width depending on the method used. These pulse trains can be multiplexed in time creating a new pulse train that can carry data at integer multiples of the laser's initial mode locking repetition rate. Multiplexing in time, independent of wavelength, is known as Optical Time Division Multiplexing (OTDM) [20, 21].

OTDM allows for an additional method to increase the bandwidth of WDM techniques. A sample system based on passive delay lines constructed at the Rochester

Institute of Technology [9] is shown in figure 1.3. This system is used to split one pulse into many by offsetting optical pulses using variable delay lines. The optical signals coupled into the system pictured in figure 1.3 travel along the four waveguide paths with each circular section representing an optical delay path of equal length. Thus, the optical pulse that enters the OTDM multiplexer will be copied and time shifted so that the output appears to be an integer multiple of the initial repetition rate. That integer will be equal to the number of independent optical paths available in the multiplexer. In the case of figure 1.3, the frequency multiplication is a factor of four.

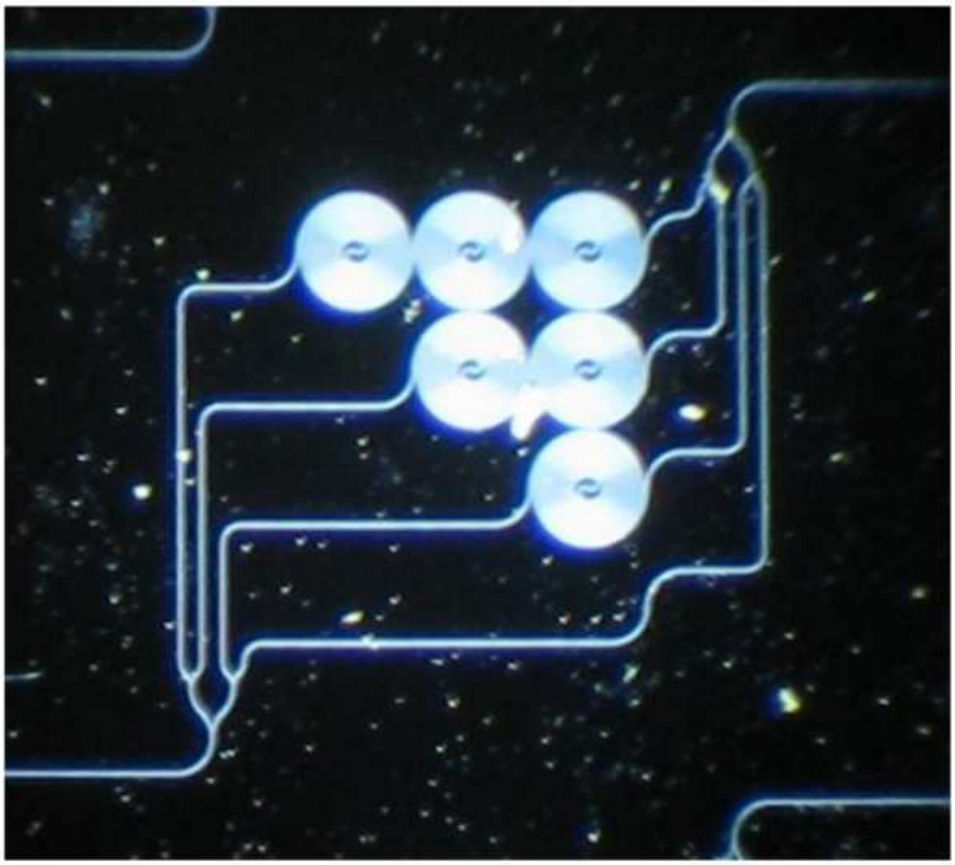

Figure 1.3: OTDM pulse multiplexer for increasing the output repetition rate signal

Integration of an optical modulator, like the ring resonators described later in this section [22, 23], into the OTDM setup in figure 1.3 allows for the transmission of binary information at a repetition rate of the input laser. This is done by increasing the loss on one of the waveguide paths electrically using the ring resonator. This would darken one of the pulses in the output multiplexed train allowing for the communication of binary data. For example, if the input repetition rate of the laser was 10 GHz, then the pictured OTDM setup would create an equivalent pulse train with a repetition rate of 40 GHz. Limitations of this increase in repetition rate are found in the total loss per unit length of the waveguide and the input pulse width. The number of channels can be increased so long as the attenuation from the waveguide does not mute the input pulses and the temporal spacing of the pulses in the output is greater than the initial pulse width. The advantage of this system is that the modulators operate at the frequency of the laser and not at the eventual data rate. Data is multiplexed to create an effective transmission that is higher than the laser pulse rate but modulation of each input channel only requires oscillators operating at the same frequency of the laser's pulse train. In the case of the example in figure 1.3, this means that an active system following the same geometry would require resonators only 1/4 of the speed of the output data transmission. This means that lower power modulators that operate at slower frequencies can be substituted at a savings in weight and power requirements. WDM operations applied to this allow for additional channels on top of the OTDM system; these channels are separated by color. Thus, even more data can be transmitted along the same waveguide when WDM techniques are applied in concert with OTDM.

For completeness, this conversation must include a comment on WDM setups. Modulation techniques can be applied to semiconductor waveguide systems using tunable ring resonators grown on silicon [22]. These devices have the ability to electrically shift their resonant wavelength at high speed. High speed and high resonator quality means that these rings can operate as switches for data communication by

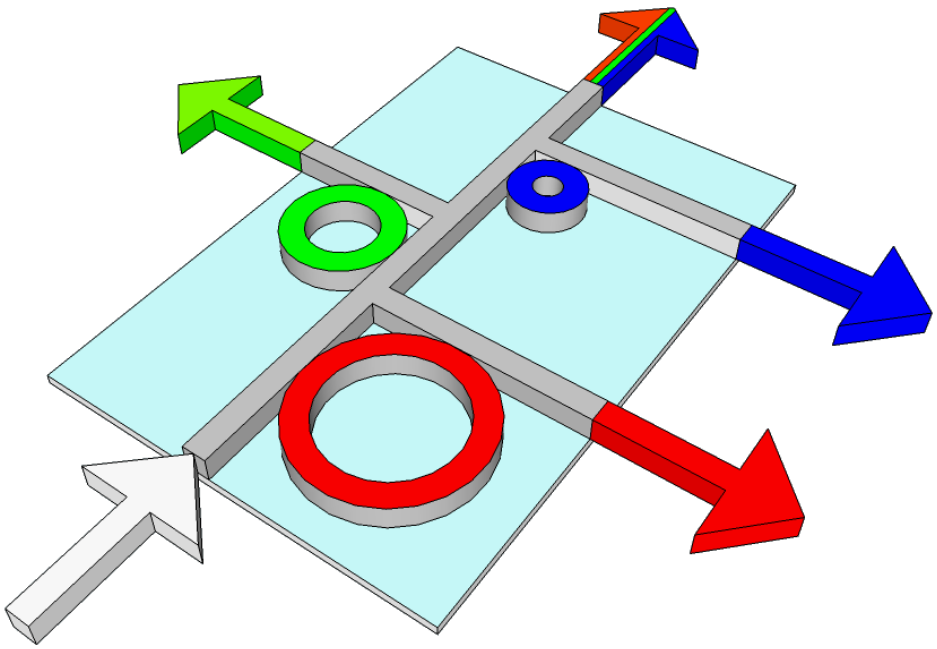

Figure 1.4: WDM functional illustration showing the isolation of data channels by wavelength

picking off wavelengths of interest. A schematic diagram of a hypothetical WDM system using ring resonators is shown in figure 1.4 [4]. The 90 degree bends in the waveguide structure do not couple well without the use of the ring resonator. Broad light sources represented by the white arrow can be partitioned into their component colors using active ring resonators. When these rings are active, light will couple into the perpendicular waveguide and reduce the intensity of that light along the main optical channel. This allows for Boolean communication of data using on and off settings. The resonance peak of each ring pictured in figure 1.4 is relative to the size of that ring in addition to the electrical bias on it [23]. Such a system provides the basic method for communicating binary data along multiple independent channels separated by wavelength. These technologies are state of the art and variations of the electrically tunable ring resonator are being tested all over the country. Individual modulators have been demonstrated as thermally tunable and quick responding.

State of the art resonators can achieve modulation frequencies beyond 12.5 GHz [22]. Combination of this technique with OTDM could expand the transmitted data bandwidth even further.

1.5 Modeling Mode Locking with Device Parameters

Modeling device performance based on collected data from the processed wafer itself [24] provides the best insight into the operation of lasers from that growth. This dissertation utilizes and advances models of mode locking based on a gain modulation phasor approach [25, 26] to forecast QDMLL operation. Input parameters into these models are taken from device modal gain and loss curves captured using the segmented contact method [27]. Analysis of new theoretical investigations and of resulting corroborating experiments allow for the complete characterization of the QDMLL using these gain curves as the principal informing quality. The details of these gain and absorption curves in concert with the properties of the Quantum Dot provide exceptional insight into the QDMLL.

References for Chapter 1

[1] R. Hall, G. Fenner, J. Kingsley, T. Soltys, and R. Carlson, "Coherent Light Emission From GaAs Junctions," *Physical Review Letters*, vol. 9, pp. 366–368, Nov. 1962.

[2] Sandvine, "Sandvine Global Internet Phenomena Report 1H-2013," tech. rep., Sandvine Corporation, Waterloo, ON, Canada, 2013.

[3] A. Shacham, K. Bergman, and L. P. Carloni, "Photonic Networks-on-Chip for Future Generations of Chip Multiprocessors," *IEEE Transactions on Computers*, vol. 57, pp. 1246–1260, Sept. 2008.

[4] B. Jalali, M. Paniccia, and G. Reed, "Silicon photonics," *IEEE Microwave Magazine*, vol. 7, pp. 58–68, June 2006.

[5] P. Rosenberg, S. Mathai, W. V. Sorin, M. Mclaren, J. Straznicky, G. Panotopoulos, D. Warren, T. Morris, M. R. T. Tan, and S. Member, "Low Cost, Injection Molded 120 Gbps Optical Backplane," *Journal of Lightwave Technology*, vol. 30, pp. 590–596, Feb. 2012.

[6] S. Manipatruni, L. Chen, and M. Lipson, "50 Gbit/s wavelength division multiplexing using silicon microring modulators," in *2009 6th IEEE International Conference on Group IV Photonics*, pp. 244–246, IEEE, Sept. 2009.

[7] K. Preston, B. Schmidt, and M. Lipson, "Polysilicon photonic resonators for large-scale {3D} integration of optical networks," *Opt. Express*, vol. 15, pp. 17283–17290, Dec. 2007.

[8] N. Sherwood-Droz, H. Wang, L. Chen, B. G. Lee, A. Biberman, K. Bergman, and M. Lipson, "Optical 4x4 hitless slicon router for optical networks-on-chip ({NoC})," *Opt. Express*, vol. 16, pp. 15915–15922, Sept. 2008.

[9] A. a. Aboketaf, A. W. Elshaari, and S. F. Preble, "Optical time division multiplexer on silicon chip," *Opt. Express*, vol. 18, pp. 13529–13535, June 2010.

[10] A. Pushparaghavan, V. Rajamani, and N. Malmurugan, "A Novel Scheme of Estimating Link Power Budget using {DBA} for a 10 Gbit/s {TDM}-{PON} Architecture," *Journal of Optical Communications*, vol. 31, pp. 234+, Dec. 2010.

[11] E. A. Avrutin, J. H. Marsh, and E. L. Portnoi, "Monolithic and multi-gigahertz mode-locked semiconductor lasers: constructions, experiments, models and applications," *Optoelectronics, IEE Proceedings* -, vol. 147, pp. 251–278, Aug. 2000.

[12] A. G. Vladimirov and D. Turaev, "Model for passive mode locking in semiconductor lasers," *Physical Review A*, vol. 72, pp. 033808+, Sept. 2005.

[13] M. G. Thompson, A. R. Rae, M. Xia, R. V. Penty, and I. H. White, "InGaAs Quantum-Dot Mode-Locked Laser Diodes," *Selected Topics in Quantum Electronics, IEEE Journal of*, vol. 15, pp. 661–672, May 2009.

[14] G. T. Liu, K. J. Malloy, A. Stintz, H. Li, and L. F. Lester, "Extremely low room-temperature threshold current density diode lasers using {InAs} dots in $\{In_{0.15}Ga_{0.85}As\}$ quantum well," *Electronics Letters*, vol. 35, pp. 1163–1165, July 1999.

[15] H. Su and L. F. Lester, "Dynamic properties of quantum dot distributed feedback lasers: high speed, linewidth and chirp," *Journal of Physics D: Applied Physics*, vol. 38, pp. 2112+, July 2005.

[16] C.-Y. Y. Lin, F. Grillot, N. a. Naderi, Y. Li, and L. F. Lester, "Rf Linewidth Reduction in a Quantum Dot Passively Mode-Locked Laser Subject To External Optical Feedback," *Applied Physics Letters*, vol. 96, no. 5, pp. 051118+, 2010.

[17] S. W. Osborne, P. Blood, P. M. Smowton, J. Lutti, Y. C. Xin, A. Stintz, D. L. Huffaker, and L. F. Lester, "Energy distributions of carriers in quantum dot laser structures," in *Proc. SPIE 5349, Physics and Simulation of Optoelectronic Devices XII* (M. Osinski, H. Amano, and F. Henneberger, eds.), vol. 5349, pp. 63–68, June 2004.

[18] D. Miller, "Rationale and challenges for optical interconnects to electronic chips," *Proceedings of the IEEE*, vol. 88, pp. 728–749, June 2000.

[19] M. J. Kobrinsky, B. A. Block, J.-F. Zheng, B. C. Barnett, E. Mohammed, M. Reshotko, F. Robertson, S. List, I. Young, and K. Cadien, "On-Chip Optical Interconnects," *Intel Technology Journal*, vol. 8, no. 2, pp. 129–141, 2004.

[20] B.-e. B.-E. Olsson, M. Karlsson, and P. Andrekson, "OTDM demultiplexer based on XPM-induced wavelength shifting in highly nonlinear fiber," *IEEE Photonics Technology Letters*, vol. 15, pp. 1770–1772, Dec. 2003.

[21] J. Yu and P. Jeppesen, "Simultaneous all-optical demultiplexing and regeneration of channel from 40 Gbit/s OTDM signals based on SPM and XPM in dispersion-shifted fibre," *Electronics Letters*, vol. 36, no. 21, p. 1798, 2000.

[22] P. Dong, R. Shafiiha, S. Liao, H. Liang, N.-N. Feng, D. Feng, G. Li, X. Zheng, A. V. Krishnamoorthy, and M. Asghari, "Wavelength-tunable silicon microring modulator," *Opt. Express*, vol. 18, pp. 10941–10946, May 2010.

[23] R. Soref, L. Fellow, and I. Paper, "The Past, Present, and Future of Silicon Photonics," *Selected Topics in Quantum Electronics, IEEE Journal of*, vol. 12, pp. 1678–1687, Nov. 2006.

[24] C. Y. Lin, Y. C. Xin, Y. Li, F. L. Chiragh, and L. F. Lester, "Cavity design and characteristics of monolithic long-wavelength InAs/InP quantum dash passively mode-locked lasers," *Optics express*, vol. 17, pp. 19739–19748, Oct. 2009.

[25] K. Lau and J. Paslaski, "Condition for short pulse generation in ultrahigh frequency mode-locking of semiconductor lasers," *Photonics Technology Letters, IEEE*, vol. 3, pp. 974–976, Aug. 1991.

[26] C. Y. Lin, Y. C. Xin, J. H. Kim, C. G. Christodoulou, and L. F. Lester, "Compact Optical Generation of Microwave Signals Using a Monolithic Quantum Dot Passively {Mode-Locked} Laser," *IEEE Photonics Journal*, vol. 1, pp. 236–244, Oct. 2009.

[27] Y. C. Xin, Y. Li, A. Martinez, T. J. Rotter, H. Su, L. Zhang, A. L. Gray, S. Luong, K. Sun, Z. Zou, J. Zilko, P. M. Varangis, L. F. Lester, and S. Member, "Optical gain and absorption of quantum dots measured using an alternative segmented contact method," *Quantum Electronics, IEEE Journal of*, vol. 42, pp. 725–732, July 2006.

Chapter 2

Quantum Dot Mode Locked Laser and Background

2.1 Novelty of Quantum Media

Advancements in the field of semiconductors have come quickly and with bountiful results. Interesting properties of these devices have been examined beginning with simple differential doping of a single semiconductor, to heterostructures that blend many semiconductors, and finally to more exotic structures that push boundaries further. Quantum confinement in semiconductor material allows for a unique definition of an energy band structure that is based mostly on the physical size of the nanostructure rather than just the crystallographic arrangement of the material. This quantum effect is a practical application of the "particle in a box" systems solved by novice students of modern physics. The physical condition comprising the "box" is a barrier potential on either side of a small physical space on the scale of the de Broglie wavelength of the particle to be trapped. It is the barrier potential caused by a buffer of dissimilar semiconductor material that provides the bounding

region and the dimensions to determine the energy levels themselves. To illustrate this mathematically, an example of the particle in a box in its most elementary case is presented: an infinite potential well.

Begin by envisioning a cube of material with uniform side lengths L. The symmetry of this problem allows us to focus on only one dimension as each of the three dimensions are linearly independent of each other. Next, proceed with the full time dependent Schroedinger Equation 2.1. This is the general form of the governing wave equation used for all quantum effects. This can be transformed into a time independent case when considering a wavefunction of a form like $\Psi(t) = Ee^{\frac{-it}{\hbar}}$. This time dependent oscillation cancels nicely resulting in equation 2.2.

$$-\frac{\hbar^2}{2m}\nabla^2\Psi + V\Psi = i\hbar\frac{\delta\Psi}{\delta t} \tag{2.1}$$

$$-\frac{\hbar^2}{2m}\nabla^2\Psi + V\Psi = E\Psi \tag{2.2}$$

Now, we can enforce boundary conditions in our system which produces solutions that are trigonometric functions. Graphically, the solutions take the form shown in figure 2.1 following the generalized expression in equation 2.3.

$$\Psi_N(x) = \sqrt{\frac{1}{2L}} sin\left(\frac{N\pi x}{L}\right) \tag{2.3}$$

Where L is the physical dimension of the quantum confinement and N is a positive integer representing the discrete energy levels allowed in the quantum state. The energy of the quantum state is solved using boundary conditions of the argument in the trigonometric function. These energy levels take the form shown in equation 2.4

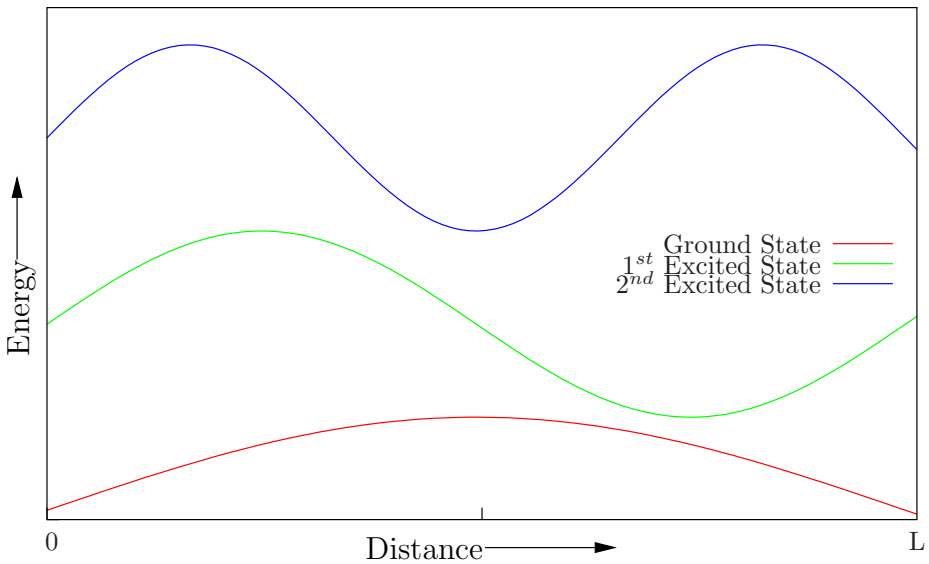

Figure 2.1: First three energy states $\Psi(x)$ offset by energy for a quantum particle in a box

$$E = N^2\pi^2\hbar^2/2mL^2 \tag{2.4}$$

where m is the mass of the particle trapped, N is again a positive definite integer, and L represents the physical dimension of the quantum confinement as before. This discretization of permissible energy levels within the quantum structure provides a method to adjust allowed states through the mechanical formation of the "box".

The general solutions to these expressions depend on the individual geometries of the quantum media; as some shapes allow for closed form solutions [1] while others rely on numerical approaches [2]. Quantum Dot approximations as cylinders (allow for closed form solutions) and pyramidal structures (which require numerical methods to solve) are the most common. These quantum effects allow for flexibility in energy states that would not be attainable simply by combining new heterostructures and provide a useful tool for band-gap engineering.

2.2 Variance in the Density of States

Shaping of the energy levels available in a material using quantum confinement is one benefit of the technique but the same mechanism that creates these levels also produces additional effects. Quantum confined media behave quite differently from bulk semiconductor materials. These differences are stark in the analysis of the available Density Of States (DOS) in quantum confined media and traditional materials. The quantum effect that generates the energy band-gaps from physical confinement also provides shaping of the DOS. The DOS is a measure of how many possible sites in a material are available to be filled based on the energy of the carrier in a semiconductor. These relations vary depending on the level of quantum confinement in a material as shown by the qualitative depiction in figure 2.2.

Bulk material has a parabolic DOS where the number of available sites for carriers to reside increases continuously as a function of applied energy. Quantum Wells have restrictive measurements in one physical dimension. Such constraints make the Quantum Well a 2D structure in terms of carrier transport. The 2D case allows for continuous filling of energy states in the well's two unconfined dimensions so long as the initial minimum energy value is met first in the confined direction.

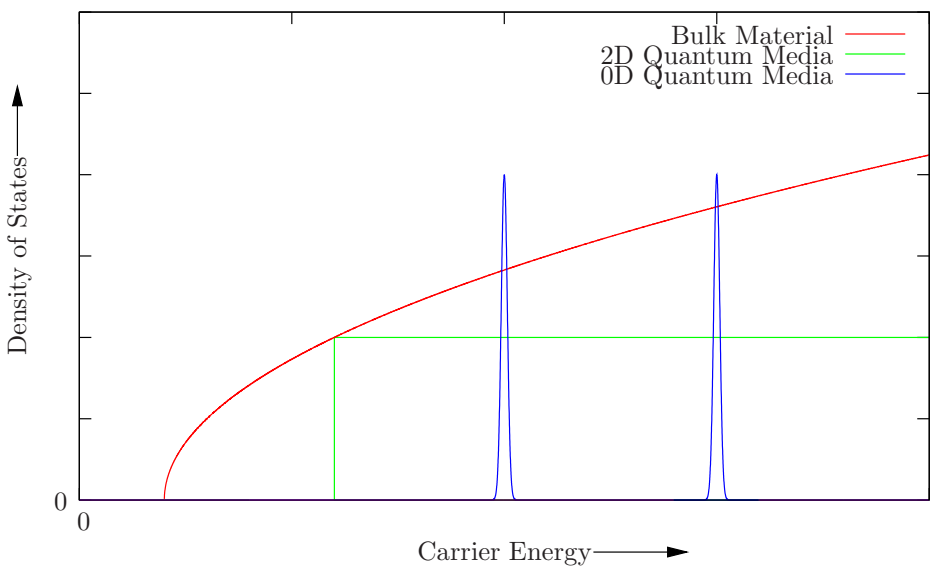

Figure 2.2: Examples of the Density of State curves for bulk semiconductors, 2D quantum confined material (Wells), and 0D quantum material (Dots)

Another interesting case is that of the 0D structure: the quantum dot. This structure, as shown earlier in the particle in a box example, has only discrete states for particular values of carrier energy. Intermediate energy levels are forbidden in the dot. The DOS plot for a large number of exactly identical Quantum Dots takes the form of discrete delta functions spaced by the allowed energy states and governed in height by the number of dots in the material. These Quantum Dots in practice are more like narrow Gaussians due to inhomogeneous broadening of the dot dimension in the material. The novelty here for the 0D structures is that the number of available energy states is adjustable by the number of dots in the material; their disposition within energy space can be tuned by varying the size of the structures themselves. For lasers, this is an extraordinarily powerful technique because it allows for more of the carrier energy put into a material to be directed at the lasing transition rather than to the bulk of the semiconductor states. This means that Quantum Dot Mode Locked Lasers (QDMLLs) exhibit remarkably low threshold current density [3, 4] by exploiting this physical effect.

2.3 Growth of Quantum Confined Media

Quantum confined materials are created in the growth process using techniques that become more sophisticated as the dimensions of confinement increase. To understand the techniques, one must first explain the cornerstone of microstructure engineering: lattice strain. Introducing additional elements to a binary semiconductor like GaAs can create ternary compounds like InGaAs or compounds with even higher numbers of constituent elements. Varying the fractional composition of semiconductor compounds allows for band gap engineering at the device level and can be used to manipulate strain as a function of the difference between the lattice constant of disparate crystals. The possible variances in lattice constants are shown in the chart reproduced in figure 2.3.

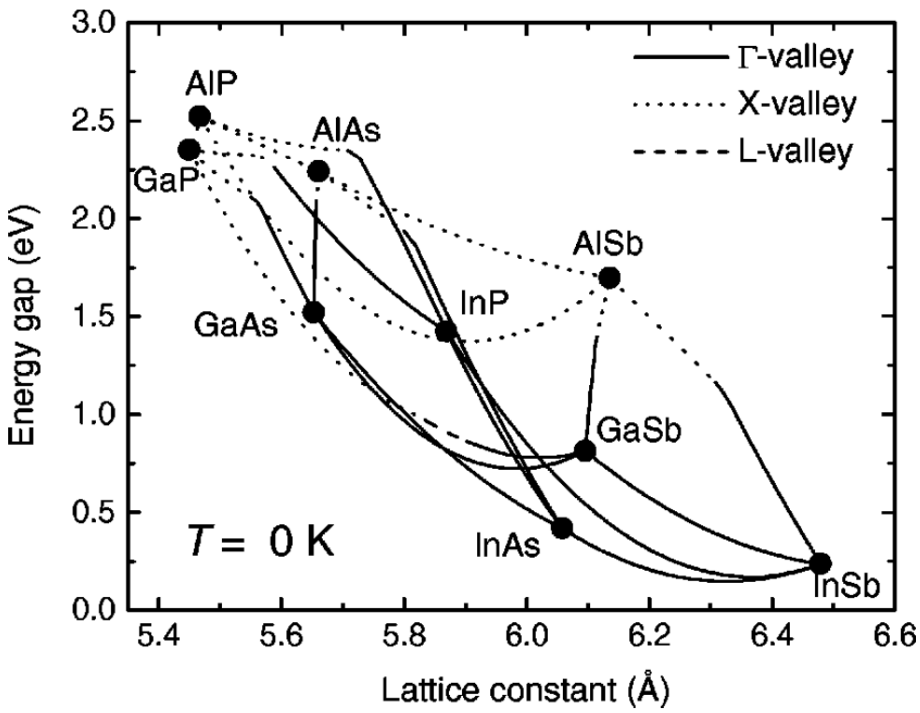

Figure 2.3: Energy gap values for various semiconductor alloys [5]

Structures like the quantum well or ultrathin layers [6] are grown by varying the product ratios in the reactors as the growth process proceeds. Quantum Dots [7] in particular have a fascinating growth method that utilizes material strain to induce islands of semiconductor material to form. This Stranski-Krastanov [8] growth mode is how quantum dots can self form in semiconductor devices when appropriate reactor parameters are set. These quantum dots are the closest we can get to true 3D quantum confinement. This growth mode utilizes lattice mismatch between semiconductor compounds to produce strain during the growth process. The size of these dots is controlled by the thickness of the grown dot layer beyond some minimum critical thickness [9]. These dots are grown with incredible density exceeding 10^{10} dots per square centimeter. These dots are difficult to visualize by microscopy in a completed device because one is limited to seeing the cross section. However, Atomic Force Microscopy (AFM) images taken without a capping layer can be used to truly gain an appreciation of the dots grown, as seen in figure 2.4. This image shows the dots themselves before they are embedded in further layering.

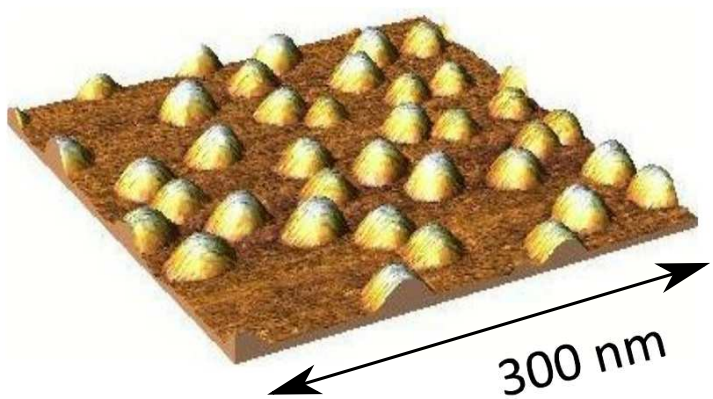

Figure 2.4: AFM image of a Quantum Dot layer showing the growth process

These dot layers can be stacked upon one another in a device structure to reap the benefits of increased material gain in the case of a laser and increased detector

sensitivity in the case of a sensing device. The addition of layers can detract from device function either by providing excessive recombination sites for detectors or through attenuation in active devices as a result of nonuniform pumping. The materials used in this study are principally InGaAs quantum dots grown on and covered by thin InGaAs layers and typically stacked 6-8 times. This growth pattern serves a double function as the dots are embedded in a quantum well creating a Dots-in-a-Well (DWELL) structure. The pattern enhances the carrier injection into the dots themselves to increase the efficiency of the devices [10]. Among these benefits, ultra low threshold current density is perhaps the foremost [3, 4].

2.4 Bandgap Tunability

Quantum dots inserted into a semiconductor behave as any heterojunction would in traditional treatment. The difference is that their bandgaps can be adjusted through varying the dot size to introduce additional energy transitions inside of the bandgap of the parent semiconductor. The doping values of the dot and surrounding material can shift the position of these intermediate gap states deliberately to create different effects for carriers moving through the junction [11]. There are two basic types of quantum dot as illustrated in figure 2.5 in traditional energy/space diagrams.

Type I Quantum Dots, such as the InAs dots in the InGaAs quantum well, have their forbidden region within the bandgap of the parent semiconductor it is embedded in. This means that both electrons and holes are trapped by the dot in the same space as those carriers travel through the semiconductor. Type II Quantum Dots have the energy band offsets that overlap with the parent semiconductor bandgap at either the conduction or valence bands. Thus, the Type II case either confines the electron carrier or the hole carrier as they travel through the semiconductor depending on how the band overlaps.

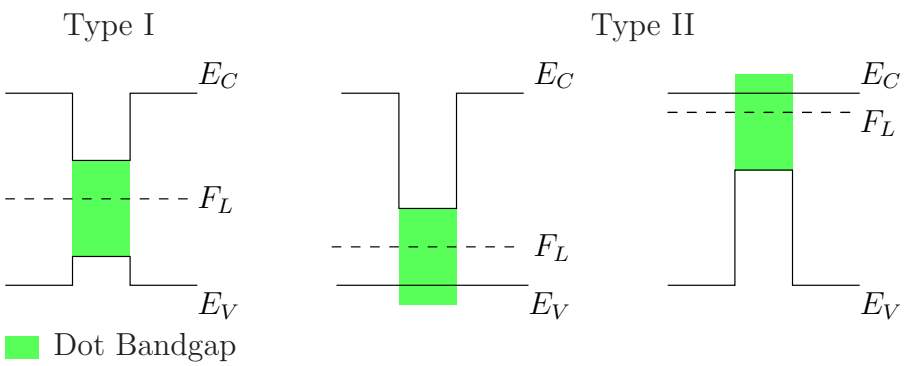

Figure 2.5: Quantum Dot band structures for Type I and Type II dots

The implications of this bandgap tunability lead to lasers that can have their output wavelength adjusted during the growth process beyond that of the limitations of binary compounds like GaAs. Device flexibility in output emission combined with the improved efficiently afforded by discretization in the Density of States provide powerful possibilities for lasers made with these quantum confined media.

2.5 DWELL Laser

The growth of the QDMLL structure [12] using Molecular Beam Epitaxy (MBE) produces layers similar to the first step in figure 2.6. Starting from the n-doped substrate, an n-type GaAs buffer layer is grown that is lattice matched to the substrate to provide a high-quality, low defect density material before growing the actual device structure. The next AlGaAs layer provides the thick optical cladding material for the waveguide portion of the laser. This layer is thick so that the maximum extent of the generated optical intensity does not interfere with the substrate or the buffer layer. Cladding layers that are too thin would leach some of the potentially generated light. Differences in relative concentrations of Al and Ga in the AlGaAs cladding layer affect the optical confinement factor of the finished devices which al-

lows for fine tuning of the mode shape within the cavity. The next layering set is the optical gain material itself. It consists of InAs quantum dots, InGaAs quantum wells surrounding them, and layers of GaAs that comprise most of the waveguide core. This layer sequence is repeated as needed to acquire the number of gain structures desired for lasing operation. Too few layers will mean that the gain provided will be insufficient. Excessive numbers of gain layers will be detrimental to the device as the extra layers will begin to absorb light at the emission wavelength which will cause an increase in the threshold current density. In practice, 6-8 DWELL layers provide an ideal number of stacks for device operation.

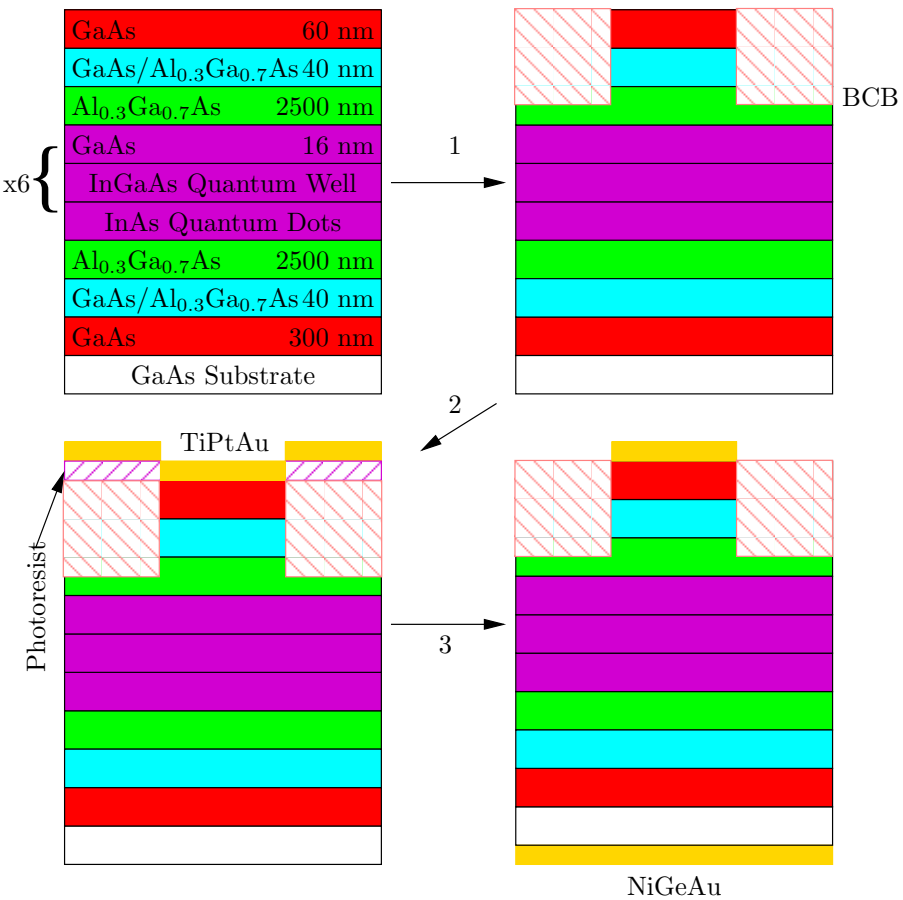

Figure 2.6: QDMLL processing procedure and layer structure depicted looking down the laser waveguide

The processing flow in figure 2.6 begins with the grown material and an initial patterning of photoresist that masks a waveguide trace. The device is then etched in step 1 to electrically and optically isolate each individual laser waveguide from its nearest neighbor. This is typically done with a plasma etch while monitoring the anisotropy to ensure that the laser waveguide does not suffer from undercutting. The etched groves are then filled with spin on Bisbenzocyclobutene (BCB) that provides electrical isolation between the p-type contacts and the underlying conductive AlGaAs cladding layers. The next patterning process applies a metalization layer of TiPtAu to provide an ohmic contact to the p-type material. Finally, the back contact is metalized with an appropriate alloy of NiGeAu and the remaining material is lifted off with an immersion bath resulting in a completed wafer of devices. Electrical isolation along the ridge waveguides to produce independent anodes is accomplished with ion implantation. The optical waveguide is continuous through the entire laser. The final pattered wafer, when viewed from above, takes the form shown in figure 2.7.

2.6 Analytical Modeling of Mode Locking

Understanding of any engineered device is greatly expanded with the application of analytical modeling where such formulations are possible. This section deals with the derivation of the sinusoidal mode locking model used in this dissertation to predict the performance of mode locked lasers [13]. Expansion of this model was vital to the projections and claims made in this work and in the work of other researchers working in this field. Expanding an existing model must always be done with respect to the assumptions made during the initial formulation shown here. Thus, I begin with the illustration of Lau's model [13] for the prediction of passive mode locking. The expression takes the form of a net gain modulation phasor of the form represented

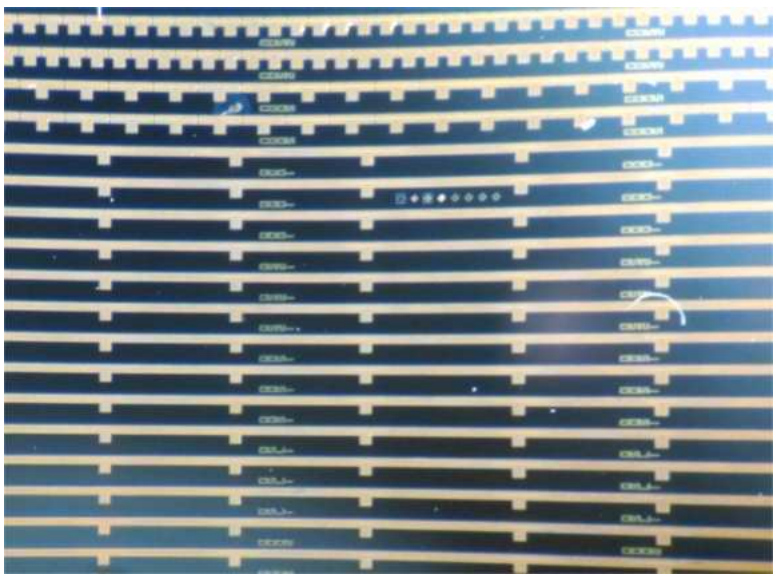

Figure 2.7: Example processed wafer pattern showing laser waveguide paths and multisection devices

in equation 2.5.

$$V_j\left(\left(-2\delta-\frac{1}{\tau}\right)(1+b_j^2)+g_o\right)=-|\hat{g}|(V_{j-1}e^{-i\theta}+V_{j+1}e^{i\theta}) \tag{2.5}$$

Where V_j is the field amplitude in the cavity of the j^{th} mode. Equation 2.5 relates each mode to the relative phases of the previous and the next in the laser gain profile. The photon lifetime of the device is represented by τ, the amplitude of the net modulation phasor is given by $|\hat{g}|$, and the phasor's phase is given by θ. Next, δ represents the difference between the the modulation frequency and the inter modal spacing. The parameter representing absolute gain in the device is given by g_o with a shaping parameter b_j for each mode that correctly defines the gain function when cast in the form $g_o/(1+b_j^2)$. The next step is to find a solution for V_j that satisfies equation 2.5 when j is allowed to vary. A Gaussian solution of the form shown in equation 2.6 results.

$$V(j) = e^{-(j/w)^2} \tag{2.6}$$

$$w^4 = \frac{4b}{\tau}|\hat{g}_{net}|cos(\theta) \tag{2.7}$$

$$g_{net} = \left[\frac{-G_g g_o}{i\omega + T_g^{-1}} - \frac{-G_a a_o}{i\omega + T_a^{-1}}\right] s e^{i\omega t} = \hat{g}_{net} e^{i\omega t} \tag{2.8}$$

Where the Gaussian parameter w is given by equation 2.7, T_a and T_g represent the respective effective carrier lifetime for the gain and absorption regions, and the gain modulation phasor $\hat{g}_{net}$ is given by equation 2.8. This is the pulse width. It is important to note that the actual shape of pulses measured from passively mode locked devices take the form of sech^2 rather than that of a pure Gaussian [14, 15]. However, this model is most valuable in projecting the existence and quality of mode locking by examining how the pulse width, w, varies with device parameters. The RHS of equation 2.7 contains the product of the magnitude of the net gain modulation phasor $|\hat{g}|$ with the cos of the phase difference θ. This is the mathematical transformation necessary to produce the real part of the phasor which is represented as a vector in the complex plane [16, 17]. We then can approximate the real part of $\hat{g}$ with equation 2.9 derived from the laser rate equations [16].

$$Re(g) \approx \frac{G_a^2 S_o^2 a_o - G_g^2 S_o^2 g_o}{\Omega^2} \tag{2.9}$$

$$\frac{\Gamma P}{\alpha_m v_g h\nu W dL} = S_o \tag{2.10}$$

Where G_g and G_a represent the differential gain or absorption that follow the behavior as shown in figure 2.8, a_o is the unsaturated absorption, g_o is the unsaturated gain, Ω is the device modulation frequency (repetition rate), and S_o is the cavity

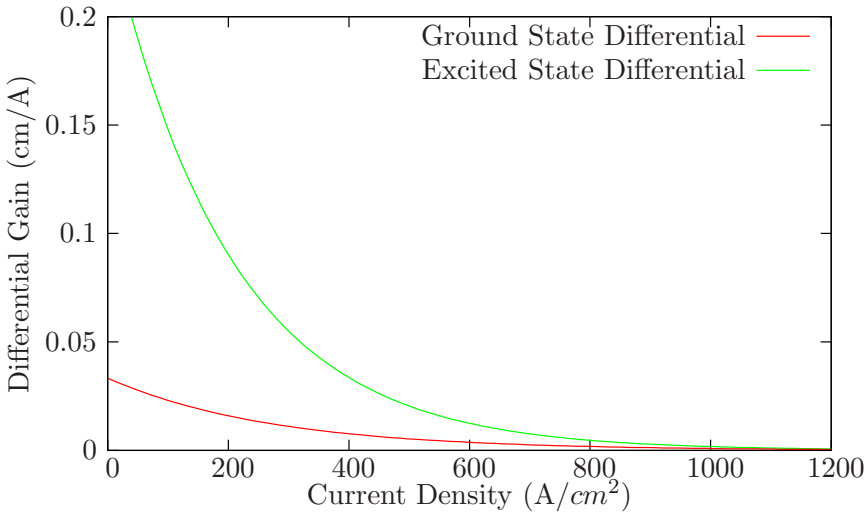

Figure 2.8: Differential gain values as a function of applied current bias on a QDMLL

photon density given in equation 2.10. In the photon density expression, L is the device length, v_g is the group velocity of the propagating mode, α_m is the mirror loss, α_i is the internal loss, d is the thickness of the active region, W is the ridge width of the device waveguide, Γ is the optical confinement factor, P is the peak pulse power, and ν is the emission frequency.

One can extract several physical limitations on the sinusoidal pulse model in that all valid solutions for active pulsing must be positive definite for arguments of equation 2.9. This is to say that the argument for the exponential in equation 2.6 is an oscillating solution and has a defined pulse width, w, given in equation 2.7. These expressions do not produce oscillating solutions when the differential gain term exceeds the differential absorption term in equation 2.9. This provides a bounding function on the appearance of mode locking in a device which lead to the development of an analytical model predicting mode locking under different absorber/gain conditions [18]. Further refinement of this model allows for the prediction of mode locking operation in regimes previously not considered.

References for Chapter 2

[1] Y. Li, J.-L. Liu, O. Voskoboynikov, C. Lee, and S. Sze, "Electron energy level calculations for cylindrical narrow gap semiconductor quantum dot," *Computer Physics Communications*, vol. 140, pp. 399–404, Nov. 2001.

[2] M. Grundmann, O. Stier, and D. Bimberg, "InAs/GaAs pyramidal quantum dots: Strain distribution, optical phonons, and electronic structure," *Physical Review B*, vol. 52, pp. 11969–11981, Oct. 1995.

[3] G. T. Liu, K. J. Malloy, A. Stintz, H. Li, and L. F. Lester, "Extremely low room-temperature threshold current density diode lasers using {InAs} dots in $\{In_{0.15}Ga_{0.85}As\}$ quantum well," *Electronics Letters*, vol. 35, pp. 1163–1165, July 1999.

[4] G. T. Liu, A. Stintz, H. Li, L. F. Lester, and K. J. Malloy, "Ultralow-threshold-current-density quantum dot lasers using the dots-in-a-well (DWELL) structure," in *Proc. SPIE 3944, Physics and Simulation of Optoelectronic Devices VIII* (R. H. Binder, P. Blood, and M. Osinski, eds.), vol. 3944, pp. 814–822, July 2000.

[5] I. Vurgaftman, J. R. Meyer, and Mohan, "Band parameters for {III}–V compound semiconductors and their alloys," *Journal of Applied Physics*, vol. 89, no. 11, pp. 5815–5875, 2001.

[6] J. Wagner, P. Ganser, D. Serries, T. Geppert, M. Maier, L. Kirste, and K. Köhler, "Epitaxy and characterisation of dilute III As 1 2 y N y on GaAs and InP," *IEE Proceedings - Optoelectronics*, vol. 151, no. 5, pp. 247–253, 2004.

[7] N. N. Ledentsov, V. A. Shchukin, M. Grundmann, N. Kirstaedter, J. Böhrer, O. Schmidt, D. Bimberg, V. M. Ustinov, Yu, A. E. Zhukov, P. S. Kop'ev, S. V. Zaitsev, Zh, A. I. Borovkov, A. O. Kosogov, S. S. Ruvimov, P. Werner, U. Gösele, J. Heydenreich, A. Y. Egorov, N. Y. Gordeev, and Z. I. Alferov,

"Direct Formation of Vertically Coupled Quantum Dots in Stranski–Krastanov Growth," *Physical Review B*, vol. 54, pp. 8743–8750, Sept. 1996.

[8] V. L. Tassev and D. F. Bliss, "Stranski, Krastanov, and Kaischew, and their influence on the founding of crystal growth theory," *Journal of Crystal Growth*, vol. 310, pp. 4209–4216, Aug. 2008.

[9] D. Leonard, K. Pond, and P. M. Petroff, "Critical layer thickness for self-assembled InAs islands on GaAs," *Physical Review B*, vol. 50, pp. 11687–11692, Oct. 1994.

[10] G. T. Liu, A. Stintz, H. Li, T. C. Newell, A. L. Gray, P. M. Varangis, K. J. Malloy, and L. F. Lester, "The influence of quantum-well composition on the performance of quantum dot lasers using InAs/InGaAs dots-in-a-well (DWELL) structures," *Quantum Electronics, IEEE Journal of*, vol. 36, pp. 1272–1279, Nov. 2000.

[11] X. M. Wen, L. V. Dao, P. Hannaford, S. Mokkapati, H. H. Tan, and C. Jagadish, "The state filling effect in p-doped InGaAs/GaAs quantum dots," *Journal of Physics: Condensed Matter*, vol. 19, p. 386213, Sept. 2007.

[12] Y.-C. C. Y. Xin, A. Stintz, H. Cao, L. Zhang, A. L. Gray, S. R. Bank, M. Osinski, J. Harris, and L. F. Lester, "Monolithic passively mode-locked lasers using quantum-dot or quantum-well materials grown on GaAs substrates (Proceedings Paper)," in *Integrated Optoelectronic Devices 2007* (M. Osinski, F. Henneberger, and Y. Arakawa, eds.), vol. 6468, International Society for Optics and Photonics, Mar. 2007.

[13] K. Lau and J. Paslaski, "Condition for short pulse generation in ultrahigh frequency mode-locking of semiconductor lasers," *Photonics Technology Letters, IEEE*, vol. 3, pp. 974–976, Aug. 1991.

[14] X. Huang, A. Stintz, H. Li, L. F. Lester, J. Cheng, and K. J. Malloy, "Passive mode-locking in 1.3 mu m two-section InAs quantum dot lasers," *Applied Physics Letters*, vol. 78, no. 19, pp. 2825–2827, 2001.

[15] M. G. Thompson, A. R. Rae, M. Xia, R. V. Penty, and I. H. White, "InGaAs Quantum-Dot Mode-Locked Laser Diodes," *Selected Topics in Quantum Electronics, IEEE Journal of*, vol. 15, pp. 661–672, May 2009.

[16] K. Y. Lau, "Narrow-band modulation of semiconductor lasers at millimeter wave frequencies (>100 GHz) by mode locking," *Quantum Electronics, IEEE Journal of*, vol. 26, pp. 250–261, Feb. 1990.

[17] J. Palaski and K. Y. Lau, "Parameter ranges for ultrahigh frequency mode locking of semiconductor lasers," *Applied Physics Letters*, vol. 59, p. 7, July 1991.

[18] C. Y. Lin, Y. C. Xin, Y. Li, F. L. Chiragh, and L. F. Lester, "Cavity design and characteristics of monolithic long-wavelength InAs/InP quantum dash passively mode-locked lasers," *Optics express*, vol. 17, pp. 19739–19748, Oct. 2009.

Chapter 3

Analytical Modeling of Mode Locking in QDMLLs

3.1 Theoretical Iteration

Investigations at the University of New Mexico have made considerable progress in development of mode locked laser theory over several iterations from the initial derivation illustrated by Lau and Paslaski [1]. This classic paper modeled the onset of passive mode locking in a semiconductor laser as a sinusoidal modulation of the optical intensity output of the laser. They described this boundary using a net gain modulation phasor approach and simultaneously derived expressions that ensured minimization of self-pulsation contamination.

Our recent work extended the aforementioned formalism to account for the discrete distribution of the gain and saturable absorber sections in a laser cavity and the internal loss [2]. The following equation 3.1 was derived in that study

$$\frac{L_a}{L_g} > \left(\frac{\frac{dg_o}{dJ}}{\frac{dg_o}{dJ}|_{g_o=0}} \right)^2 \frac{g_o}{a_o} \tag{3.1}$$

where L_a and L_g are the length of the absorber and gain sections respectively, g_o and a_o are the modal gain in the gain section and unsaturated absorption in the absorber region respectively, dg_o/dJ is the differential gain, and the differential quantity in the denominator of equation 3.1 represents a conservative approximation for the differential absorption [2]. The fundamental difference in the treatment of the pulse predicting phasor between this treatment and Lau's is that the bounding parameter is set to the internal loss α_i rather than simply zero. This extension enabled the prediction of functional device layouts using the measured gain and loss characteristics as input. The model has been employed for the cavity design of two-section passively mode locked lasers based on several different material systems [2, 3, 4]. The method is based on the assumption that the net gain modulation $(g_o - a_o)$ is sinusoidal and in phase with the photon density modulation. This formulation does not consider the fundamental limit of lasing in these devices. Consequently, an additional basic constraint within the model comes in the form of the threshold condition for lasing in equation 3.2.

$$\frac{L_a}{L_g} = \frac{g_o - \alpha_m - \alpha_i}{a_0 + \alpha_m + \alpha_i} \tag{3.2}$$

In equation 3.2 above, α_i is the internal loss, α_m is the mirror loss, while L_a and L_g are the lengths of the absorber and gain sections of two-section device respectively.

From equations 3.1 and 3.2, it is readily apparent that in order to strengthen the mode locking condition over temperature one can, for instance, reduce the variation of the modal gain with temperature by engineering the gain material and reducing the internal losses. On the other hand, one can optimize the ratio L_a/L_g; the latter is the approach examined in this work. Equations 3.1 and 3.2 can be considered as describing the hard boundary defining the onset of mode locking, the limiting case, or minimum requirement. Although the model does not have the capability to predict the pulse duration since a sinusoid is assumed, it is nevertheless a useful tool to predict the onset of mode locking over a broad temperature range. Proceeding from this point, the theoretical mode locking range of the wafer 967 is studied in detail in this chapter.

3.2 Initial Theoretical Projections

As mentioned in the previous section, equations 3.1 and 3.2 together provide robust boundary conditions for the prediction of mode locking operation. Applying this technique to gain data of the 967 wafer provided an initial mode locking prediction range in figures 3.1-3.6. These plots are presented with equation 3.1 providing the lower bound, equation 3.2 providing the upper bound, and plotted as a function of applied current density relative to the absorber section to gain section length ratio in the laser. Regions of mode locking projected in this model are enclosed on the right hand side of the projected device curves bounded from lasing threshold and gain/absorption balance. These theoretical contours were computed based on segmented contact method data taken between 20-70 C. Initial projections were promising, thus the next step with more detailed gain/loss analysis was taken with more confidence.

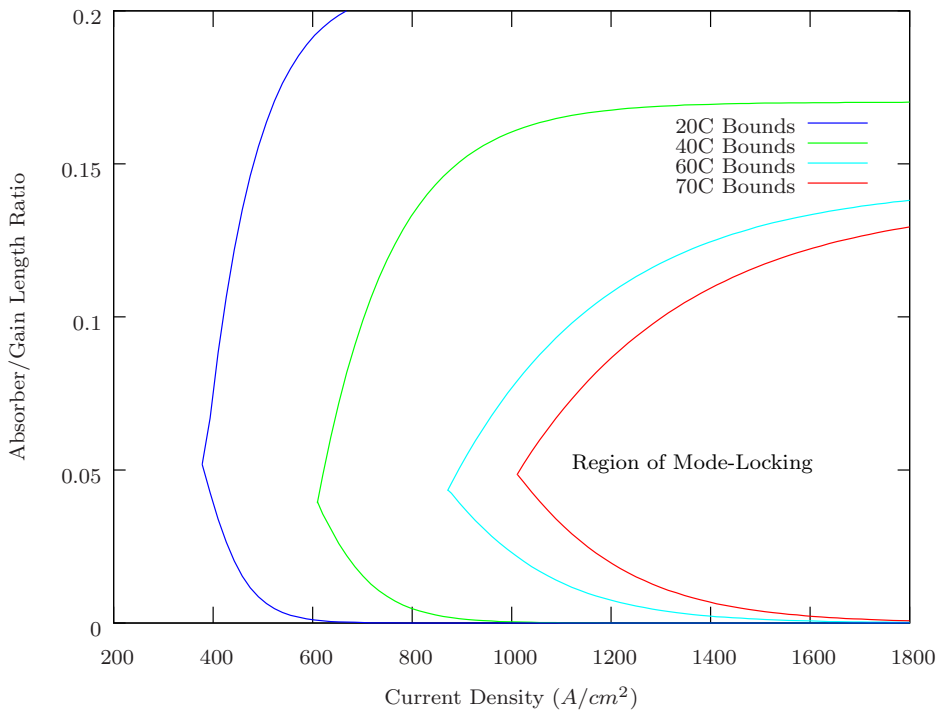

Figure 3.1: Projected mode locking map for device 967E with 0 V reverse bias on the saturable absorber

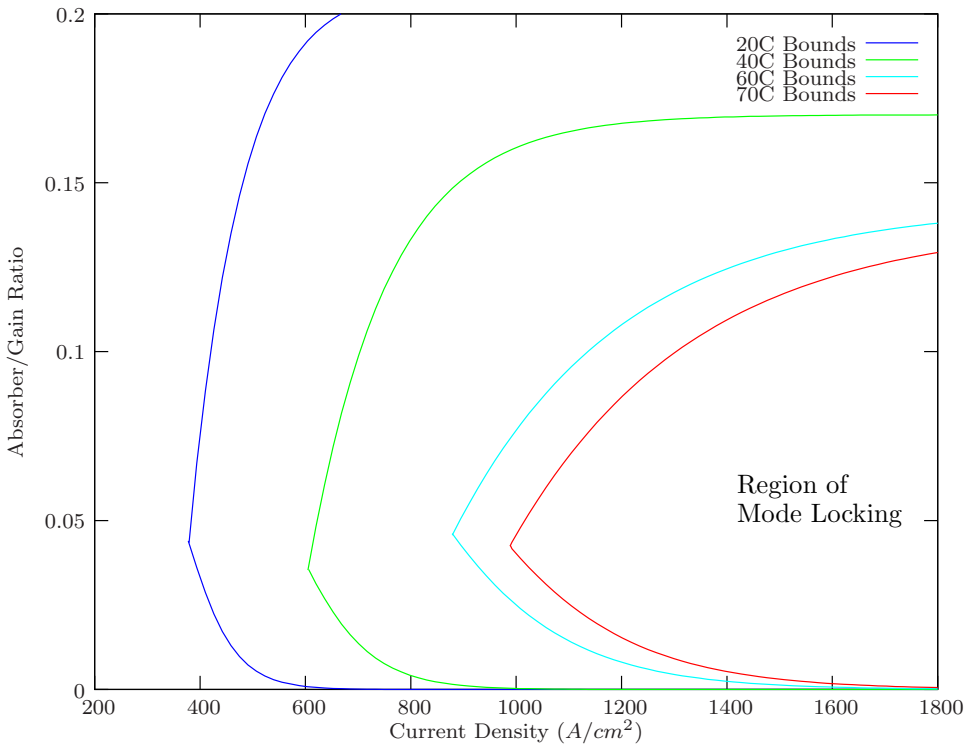

Figure 3.2: Projected mode locking map for device 967E with -1 V reverse bias on the saturable absorber

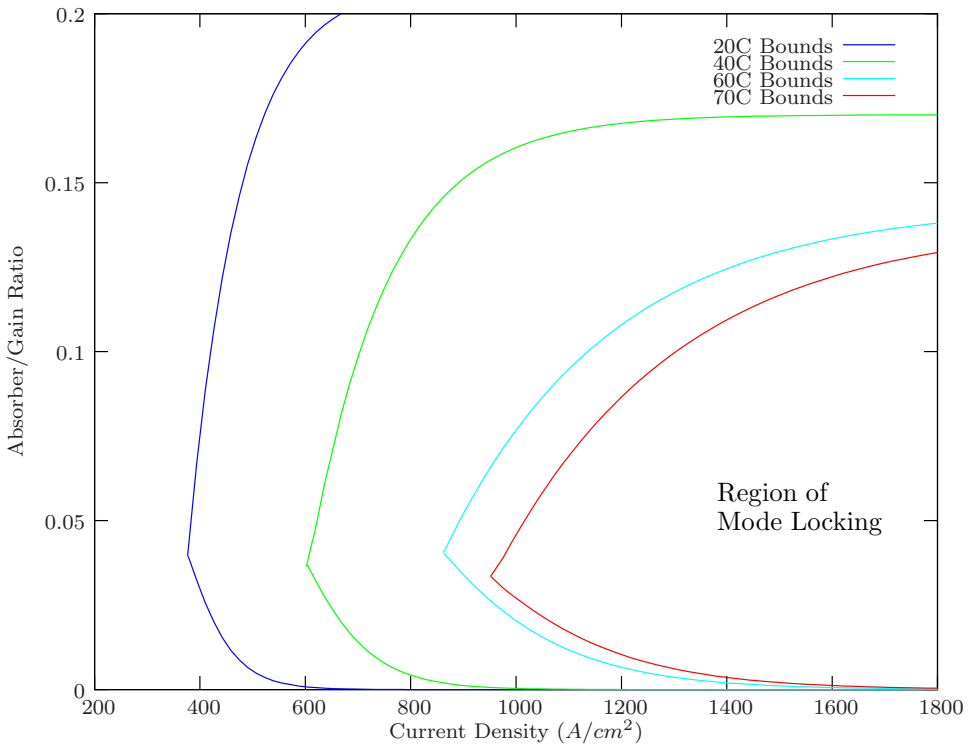

Figure 3.3: Projected mode locking map for device 967E with -2 V reverse bias on the saturable absorber

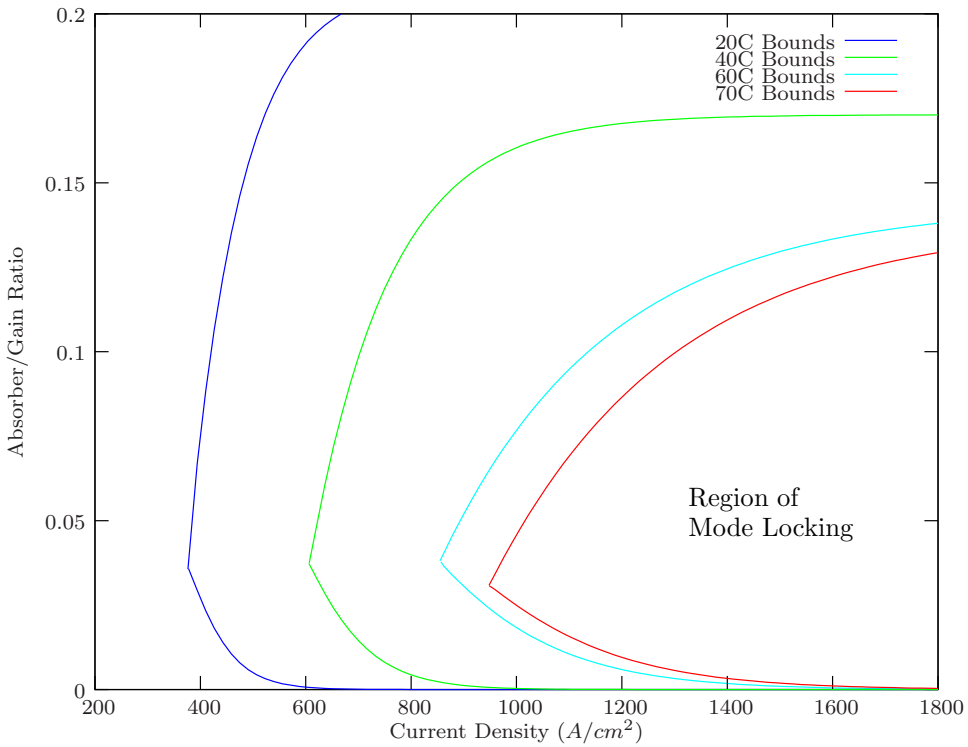

Figure 3.4: Projected mode locking map for device 967E with -3 V reverse bias on the saturable absorber

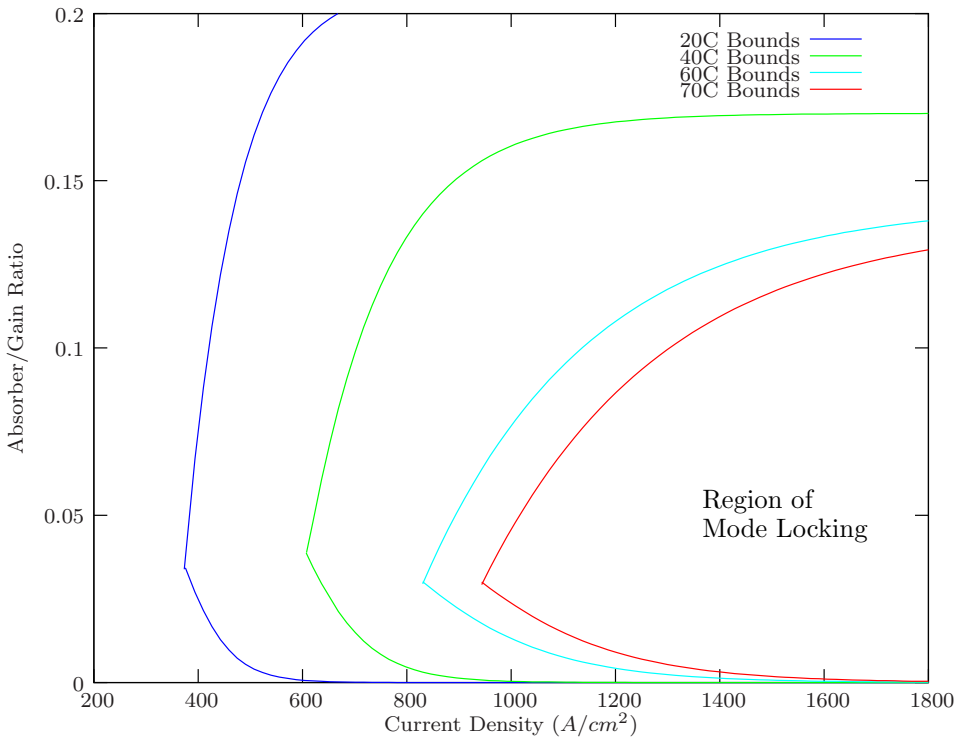

Figure 3.5: Projected mode locking map for device 967E with -4 V reverse bias on the saturable absorber

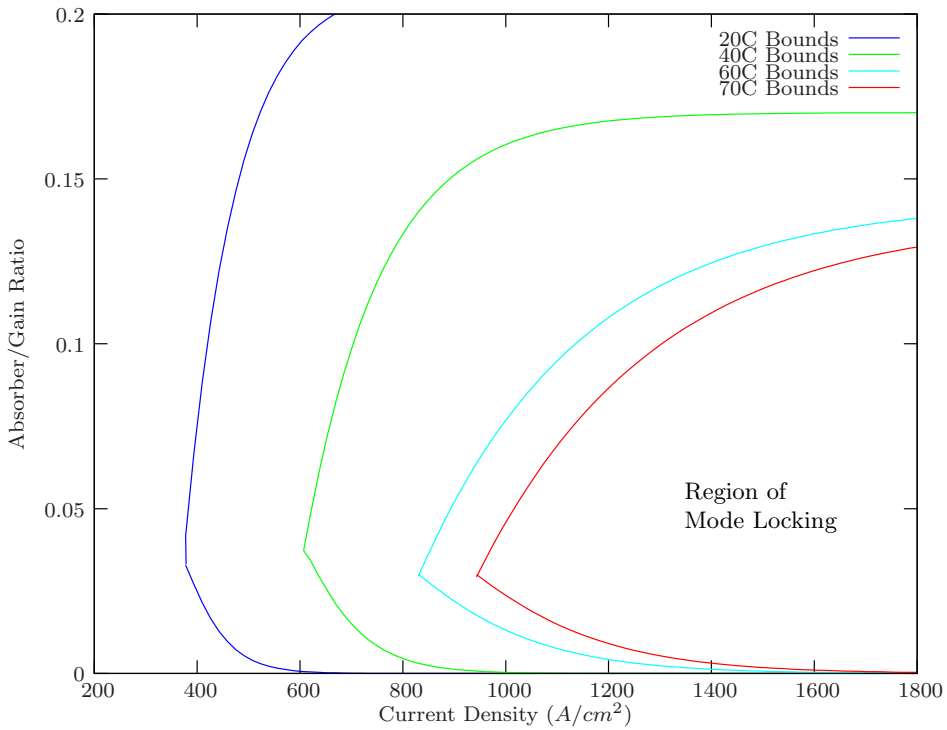

Figure 3.6: Projected mode locking map for device 967E with -5 V reverse bias on the saturable absorber

3.3 Gain Measurement in Semiconductor Lasers

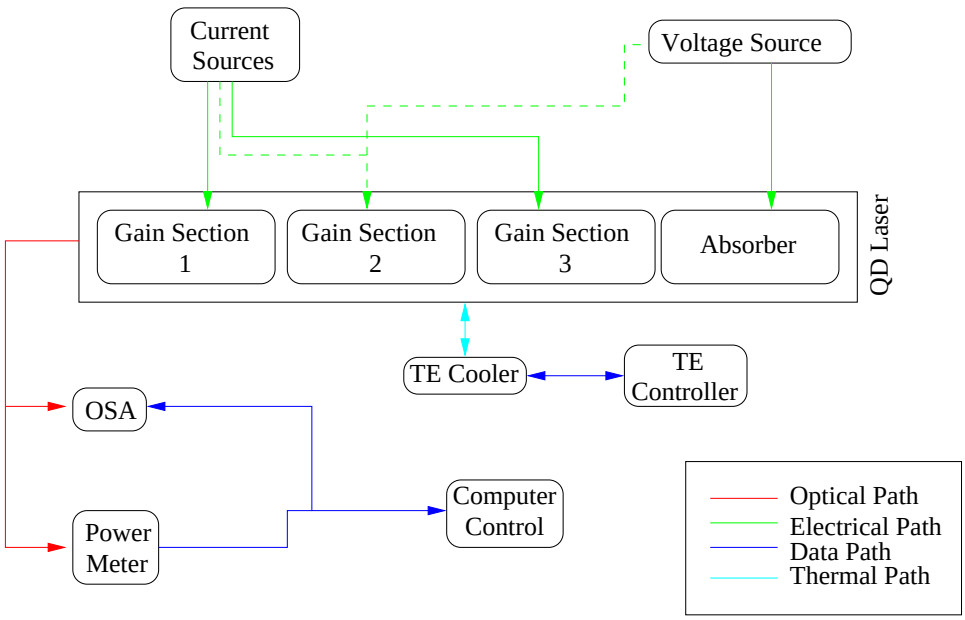

Figure 3.7: Schematic diagram of the gain measurement setup

Here, a practical method is sought that allows one to determine whether a given Mode Locked Laser (MLL) can maintain mode locking over a desired temperature range and, if not, to understand why it fails. In comparison to our recent delay differential equation model [5] and the work of Vladimirov and Turaev [6], the advantage of this analytical approach is the ability to predict functional MLL device layouts through the use of measured temperature-dependent static laser parameters measured on the actual device under investigation. Consequently, valuable insight can be gained without knowing dynamic material parameters such as the carrier lifetime or the gain/absorption recovery times of the active semiconductor material. A temperature dependent picture of the gain profile of our quantum dot laser devices is critical to the prediction of the device properties. To this end, a measurement setup was devised that has the capability to perform data sampling at the full range of temperatures from 10 C to beyond 100 C. Temperature ranges from 10 C-70 C are

accomplished through Peltier junctions (TE) alone but set points in excess of 70 C require the use of electrical heating tape to achieve. Lasers under test are mounted on a Copper heatsink with Indium solder to ensure effective thermal and electrical contact. This Copper mount is then secured onto a larger temperature controlled Copper block before measurements are performed. The limitation in test temperature is often this Indium solder which has a melting point around 130 C. Experiments that require higher temperatures must use different methods of mounting.

The system is designed with a very high thermal mass near the laser itself to maintain equilibrium temperature during each of these current measurements. The schematic diagram of the experimental setup used for gain and absorption measurements is given in figure 3.7. The meaning of the current wiring configurations will be discussed later. A typical QDMLL device that we test is comprised of multiple electrically isolated sections with dimensions of 500 μm $\times$ 3.5 μm as shown in figure 3.8. The gain sections are comprised of two device sections making the total length of each 1 mm. The remainder of the device length is used as an absorber to reduce back reflections. The effects of different biases on these remaining sections can have a dramatic effect on the measured gain as shown in figure 3.9. This variance is due to the elimination of the back reflections previously mentioned which conceal the true device gain.

Electronic control is done using a control board re-purposed from previous work at the University of New Mexico. Two current sources and a voltage source are used to stimulate the device and measurement is conducted using an integrating sphere power meter and an Agilent spectrometer. Data capture is performed via GPIB connections to a central computer. Coupling of the laser light from the Quantum Dot laser is achieved through an integrated optical head containing a small lens and isolator. This head couples the light into a fiber which is routed to the measurement equipment. The coupling lens is Anti Reflection (AR) coated to reduce back reflections.

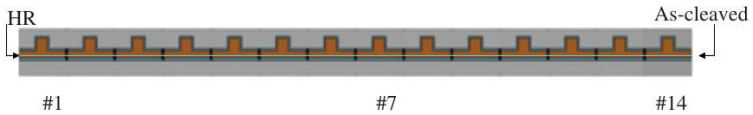

Figure 3.8: Schematic of the multi-section segmented contact amplifier used to measure the gain and loss properties of the QD DWELL active region as a function of current density coated AR/HR to reduce the lasing threshold

The theory behind the segmented contact gain measurement method is taken from the previously published work from Xin et al. [7]. Our measurement method requires single pass amplification of spontaneous emission of the gain sections shown in figure 3.7. The expression for computing the net modal gain of the laser is given in equation 3.3.

$$g = ln\left(\frac{I_3 - I_1}{I_2 - I_1} - 1\right) L^{-1} \tag{3.3}$$

Where I_{1-3} are the intensity from each of the three measurement steps and L is the length of the gain sections. Absorption measurements can be arrived at using a similar technique with equation 3.4.

$$\alpha = ln\left(\frac{I_2 - I_1}{I_4 - I_1}\right) L^{-1} \tag{3.4}$$

Where α is the absorption, I_4 is a special measurement condition where Sections 1 and 3 are biased and Section 2 has reverse bias, and the remainder of the variables follow the convention of equation 3.3. Further detail of this method can be found in the literature. Back reflection is one of the variables that provides a significant difference to the measured gain using this technique. Any back reflection at all from the opposing facet will contribute to the measured spectrum and decrease the

observed gain. This effect is clearly shown in figure 3.9. Gain compilation shown in that figure was performed on the same device at the same temperature. The difference only is in the back reflection contribution muted in the absorber in the case of the -5 V reverse bias.

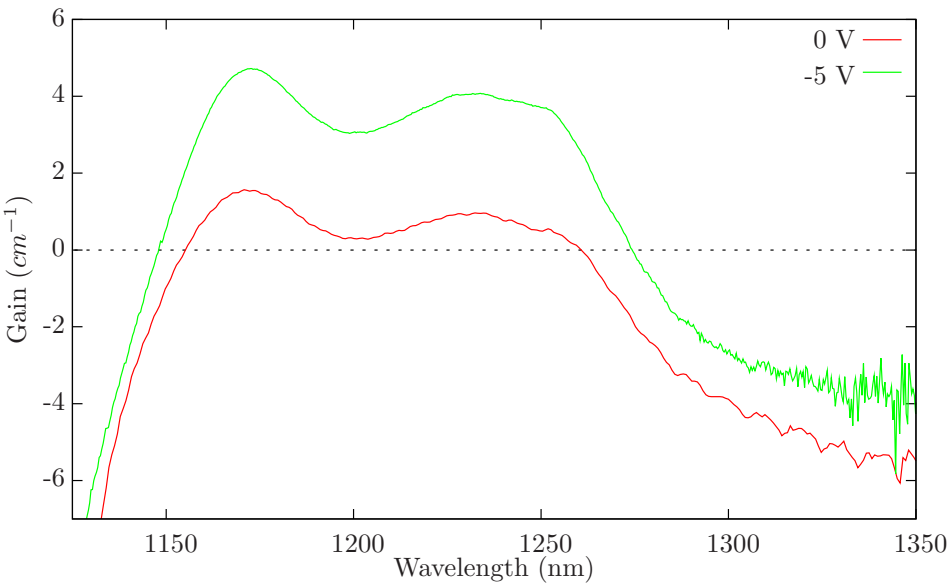

Figure 3.9: Gain measurement comparison using the segmented contact method on wafer 966 with 0V and -5V bias on unused sections at 10C

Initial assumptions that the absorber length was sufficient without reverse bias were shown to be clearly incorrect and thankfully so because revised gain values were far more promising for higher temperature operations. The double peak featured in the displayed gain curve clearly shows the ground state and the first excited state of the quantum dots. The result of this scan from a temperature range of 15 C to 40 C is shown in figure 3.10. In general, higher temperatures show decreased gain with a single outlier on the 20 C temperature test. This is attributed to errors in measurement procedure arrived at in this early stage. These values are promising because they show reasonable gain even for the highest temperature level reachable by our setup. This result was encouraging for device performance at higher temperatures.

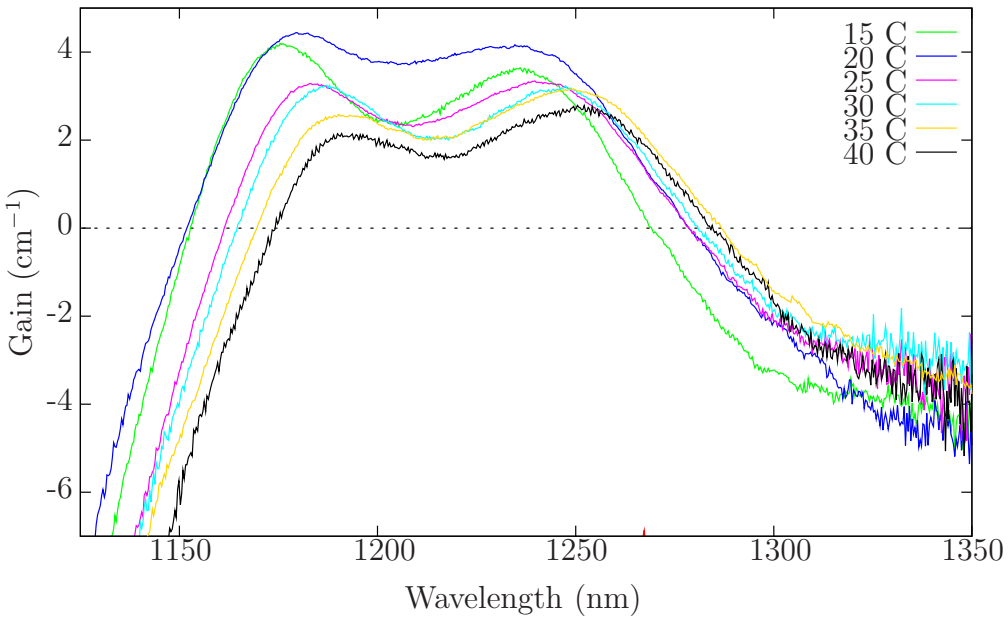

Figure 3.10: A temperature dependent gain profile of a QDMLL

An additional observation of our gain spectrum shows a clear wavelength shift as a function of temperature due to shifts in band structure [8]. These shifts are shown in table 3.1. The wavelength shift of the gain peaks in the 966 device is noticeable and linear as expected for the quantum dot devices of this type. However, this device is intended to serve in a waveguide application so this tuning range must be taken into consideration when designing the geometry of the silicon waveguide. Projected shifts in the gain peaks across the entire planned temperature range are significant. A linear fit is presented in figure 3.11.

Another interesting effect is the relative magnitude of the two gain peaks present in the laser as a function of temperature. The higher energy (excited state) peak dominates at lower temperatures but falls to a value smaller than that of the lower energy (ground state) peak as the device temperature increases. This seems to imply that we will be able to focus on the lower energy peak for larger gain as the experiment pushes into ever increasing temperature ranges.

Temperature C	First Excited State (nm)	Ground State (nm)
10	1166.28	1242.71
15	1171.16	1248.37
20	1172.16	1250.59
25	1174.69	1254.67
30	1178.88	1257.22
35	1179.65	1258.71
40	1184.32	1263.36

Table 3.1: Peak center migration

Improvement of accuracy in the gain measurement can be assured using a method called "self calibration". A laser at exactly the threshold current has a modal gain equal to the mirror losses in the cavity. Computing this threshold current and modal gain allows for the comparison with a measured gain at identical current density.

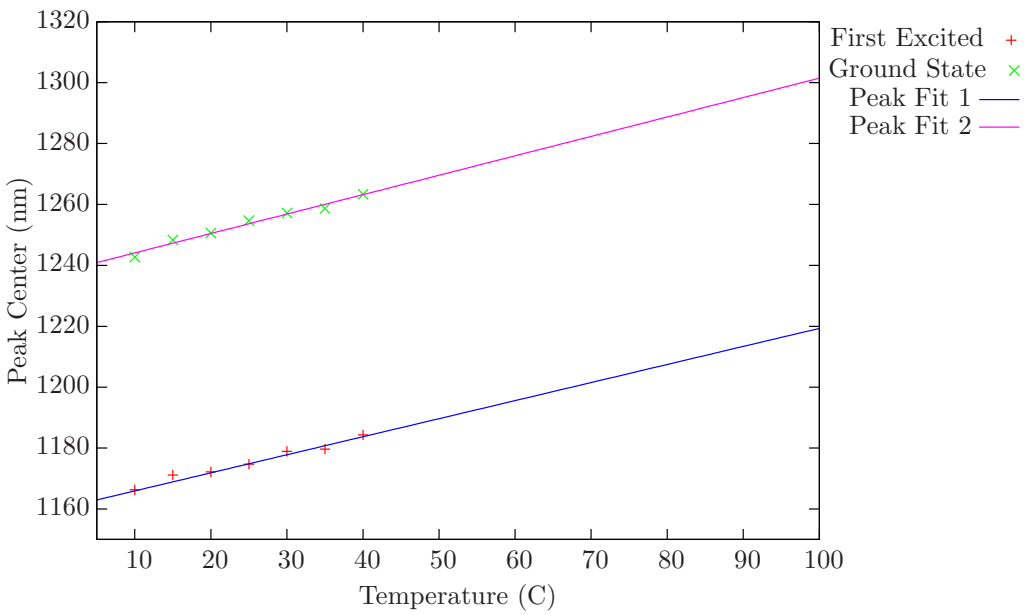

Figure 3.11: Wavelength shift of the ground and excited lasing state of the 966 wafer as a function of temperature

Threshold current measurements are quick to perform and very descriptive of device performance and are also thermally variable [9]. This is a sanity check that compares the measured gain using the segmented contact method with the threshold value.

In this chapter, it is demonstrated that having measured the modal gain and loss properties of the material system under investigation. Parameters of the QDMLL are examined as a function of temperature, wavelength, gain section current density and absorber section reverse bias. The regions of operation where mode locking is predicted are derived reliably using an analytic approach based on an expansion from previous models [2]. The static device parameters feeding the model can be readily measured using the segmented contact method [7]. The predictions of the model are found to agree very closely with an experimental characterization of the temperature-dependent mode locked operation of a two-section QDMLL. Physical insight as to why mode locking breaks down with elevated temperature is revealed in terms of the measured gain and loss. The primary aim of this work is to highlight the usefulness of this model in guiding the cavity layout for MLLs capable of operation over a wide temperature range.

3.4 Device Structure and Fabrication

Owing to their compact size, direct electrical pumping and low power consumption, monolithic MLLs have commanded serious attention as attractive sources of ultra-short optical pulses. These devices have been investigated for use in Optical Time Division Multiplexing (OTDM) communication systems [10], optical clock distribution [11], arbitrary waveform generation [12], meteorology [13], and generation of RF signals [14]. The core investigation is how to predict the fitness of QDMLLs for these purposes in more challenging environmental conditions.

Quantum Dot Mode Locked Lasers (QDMLLs) possess a number of unparalleled features over their higher dimensional counterparts (quantum well and bulk active materials); which enables the formation of short pulses with minimal timing jitter making QDMLLs especially attractive for schemes based on high bit-rate optical time division multiplexing [10, 11]. Beneficial QDMLL attributes include a broad gain bandwidth, ultrafast gain and absorption dynamics, as well as an easily saturated gain and absorption [12, 13]. These features of the QDMLL strengthen the candidacy for integration into pulsed sources for optical interconnects in next generation multi-core processor architectures among other systems. Traditional electronic interconnects based on Copper exhibit limitations as the required bandwidth increases through resistance as lines are narrowed [15], massive cables for long haul transmission [16], and other shortcomings [17]. These limitations primed Copper for replacement in long haul communications and now bolster the case for the ascension of optical systems in chip to chip interconnects.

For use in optical interconnects, ideally, QDMLLs will be situated close to the microprocessor cores and will therefore need to operate over a broad temperature range, with highs typically in the vicinity of 100 C and beyond. Furthermore, deployment in hot environments (like the tip of a wellbore) also require such thermal flexibility. It is therefore highly desirable to develop uncooled optical interconnects that can function in these high temperature ranges. Firstly, an uncooled device reduces the system size and complexity; freeing a source from constant thermal stabilization eliminates the power-hungry requirements associated with overworked Peltier coolers. Semiconductor lasers are inherently temperature sensitive with temperature-dependent effects such as the red-shifting of the lasing wavelength and the increase of the threshold current density with increasing temperature seemingly inevitable, even in systems, such as III-V QDs, where the electron-hole pairs are confined in all three dimensions [18].

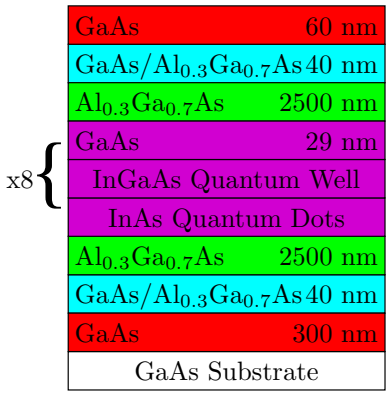

Figure 3.12: Illustration of the epitaxial structure of the 8-stack dots-in-a-well laser structure

Despite these intrinsic properties, it is possible to design the QDMLL to consistently and reliably maintain mode locking over a wide temperature range. QDMLLs have already demonstrated a wide range of operating conditions where mode locking from the dot ground state occurs (1300-nm), even at elevated temperature [19, 20]. Recently, an analytic model based on a net gain modulation phasor approach was developed to predict the expected stability of mode locking (ML) operation based on several measurable static device parameters, namely the modal gain and loss characteristics of the active region of the laser [2]. Previously this model was used as a guideline in constructing the relative lengths of the gain and absorber sections on monolithic two-section passively mode locked for room temperature operation in 1.55 μm GaInAsNSb quantum wells [3], 1.3 μ m InAs/GaAs QDs [4] and 1.58 μm InAs/InP quantum dashes [2].

The multi-layer dots-in-a-well (DWELL) laser structure used here was grown by elemental source molecular beam epitaxy (MBE) and consists of 8 stacks of dots in the active region. The layers are composed of an n-type (10^{18} cm^{-3}) 300 nm-thick GaAs buffer, an n-type lower $Al_xGa_{1-x}As$ (x=0.2) cladding layer, a GaAs core waveguide, a p-type upper cladding layer, and a p-doped (3×10^{19} cm^{-3}) 60 nm-

thick GaAs cap. The cladding layers are doped at 10^{17} cm^{-3} and are each 2μm thick. In the center of the waveguide 8 DWELL layers with 29-nm GaAs barriers were grown. QDs formed from about 2 monolayers of InAs are confined in the middle of an $In_{0.15}Ga_{0.85}As$ QW in each layer. The QDs and QW were typically grown at 500 C, as measured by an optical pyrometer. The QDs formed under these conditions have an areal density of about 3 $\times 10^{10}$ cm^{-2}, a base diameter <40 nm, and are $\approx$7 nm high. Detailed descriptions of the DWELL growth technique can be found elsewhere [21, 22].

A schematic of the 8-stack DWELL is shown in figure 3.12. The 20% Aluminum composition in the cladding layers allows for high peak power operation by reducing the optical confinement of the waveguide. In addition to this, the high current confinement of the DWELL structure simultaneously provides low threshold currents [21]. The mode locked lasers fabricated from this material are 2-section ridge-waveguide lasers with a ridge width of 3.5 μm. A multi-section device was used in characterizing the gain and loss of the active QD material and consisted of 14 500-m electrically isolated sections, shown schematically in figure 3.8. Devices were fabricated according to standard multi-section device processing [23]. After the first lithography with the ridge-waveguide-mask, the sample was etched to form 3.5 μm wide, 1.8 μm deep ridges by inductively coupled plasma (ICP) etching in BCl_3. Then a Bisbenzocylcloutene (BCB) layer was applied for isolation between the p-type metal and the etched cladding layer. After depositing Ti/Pt/Au to form the p-metal contact, an electrical isolation between the adjacent sections was provided by proton implantation, with an isolation resistance of >10 $M\Omega$. After the substrate had been thinned and polished, a Au/Ge/Ni/Au n-metal contact was deposited on the backside of the n+-GaAs substrate and annealed at 380 C for 1 minute to form the n-ohmic contact. A temperature greater than 380 C can crack the BCB. Another Ti/Au metal layer was deposited for n-side mounting, and then the sample was cleaved to form devices with a short absorber section and long gain section. In

this work, the InAs DWELL MLL had a 1-mm absorber section and a 7-mm gain section resulting in a 4.96 GHz optical pulse repetition rate in its optical output. The cleaved facet near the absorber section was High Reflectivity (HR)-coated (R 95%) to create self-colliding pulse effects in the saturable absorber for pulse narrowing. The other facet was as-cleaved (R 32%). The multi-section device was constructed with both facets as-cleaved. Both devices originated from the same section of the wafer and are therefore assumed to be nominally identical.

3.5 Mode Locking Measurements

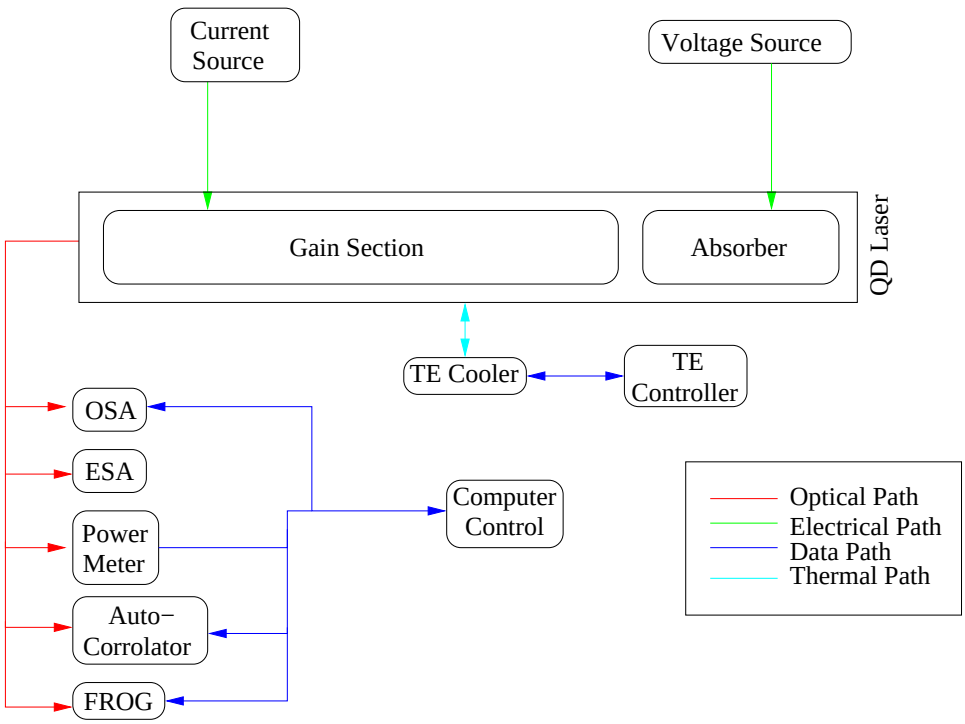

Figure 3.13: Experimental apparatus for mode locking measurements

Measurement and characterization of a mode locked laser must be done using a different technique than with the segmented contact method previously discussed. The experimental setup is diagrammed in figure 3.13 and it allows for RF, optical, and temporal investigation of the pulse itself. Characterization of our QDMLLs must extend beyond possible mode locking measured by the Electrical Spectrum Analyzer (ESA) into physical observation of the pulse train as well as the time dependent trace of the pulse itself. This setup allows us to verify models for predictive mode locking developed previously in our group [2] and expanded [24] in this chapter. The recent addition of a Frequency Resolved Optical Gating (FROG) system [25] allows for even more detailed characterization of our pulse. However, the pulse characterization and validity of mode locking was determined using autocorrelation [26] to verify the pulse

width. This method was chosen because of the relative ease when measuring pulses on the edge of mode locking compared with the more detailed FROG scans.

As before, the experimental setup is temperature controlled and able to reach set points from 30-100 C without excessive fluctuation. Coupling is achieved using the same technique as the segmented contact method, but it is easier to achieve because these devices are tested in the lasing regime rather than the amplified spontaneous emission regime required for intrinsic gain measurements. Mode locked lasers used in this test and shown schematically in figure 3.13 are comprised of two sections; one gain section and one absorber section with the relative length of the two providing a critical parameter in mode locking fitness as previously described. Gain sections are forward biased with a typical current density on the order of 1 kA/cm^2 to excite the ground state in the dots.

3.6 Presentation of Mode Locking Data

3.6.1 Recalculated Gain and Loss Curves over Temperature

Figures 3.14, 3.15, and 3.16 present the measured modal gain and total loss characteristics of the QD material. In these measurements, the current density applied to the gain section is limited to 1.6 kA/cm^2 to avoid potential damage to the device. The reverse bias on the saturable absorber section is varied from 0 to 5 V. Figures 3.14 and 3.15 show the measured total loss spectra over temperature for reverse voltage values of 0 V, 1 V, 3 V and 5 V. The total loss evaluated at the gain peak for each temperature is indicated in figures 3.14 and 3.15 by the dashed lines. The internal loss can be extracted from the long wavelength side of the total loss spectra. An averaged value of 3.3 cm^{-1} is determined here for this device over the temperature range considered. The temperature variation of the peak loss spectra displayed in

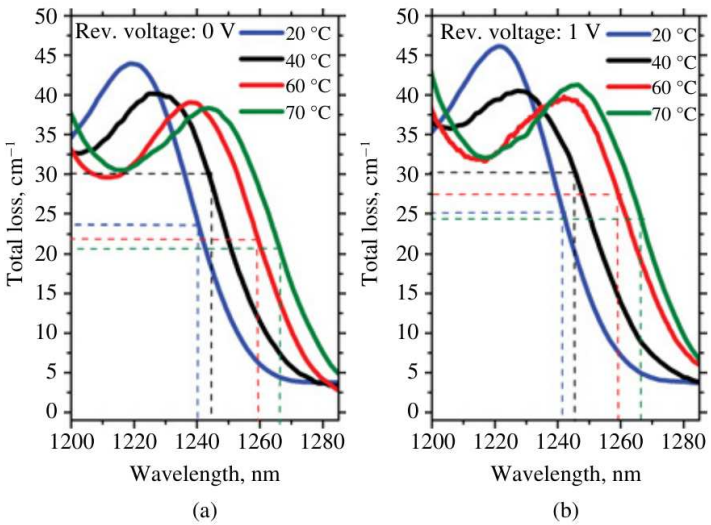

Figure 3.14: Measured temperature-dependent total loss spectra at 0 V reverse bias (a) and 1 V reverse bias (b) measured on the multi-section device using the segmented contact method. The dashed lines guide the eye to the total loss values (evaluated at the gain peak) for each temperature considered. The unsaturated absorption, a_o, is acquired by subtracting the internal loss from the total loss. [24]

figures 3.14 and 3.15 is observed to vary by as much as 4 cm^{-1} over reverse bias 0 V to 5 V at 20 C and 40 C. This variation in loss doubles at higher temperature (60 C and 70 C). The larger loss variation observed at elevated temperature can be explained as a temperature-induced enhancement of carrier sweep-out from the absorber [19]. Figure 3.16 (a) shows the measured net modal gain spectra for a range of heat sink temperatures and a constant current density of 1.4 kA/cm^2. The gain is measured up to 70 C where it was noted that the device continued to operate from the ground state QD transition. Two localized transitions are apparent in the spectra corresponding to the QD ground state (GS) and QD first excited state (ES), which appear at 1238-nm and 1174-nm at 20 C, respectively (blue plot in Figure 3.16 (a)). The ground state gain magnitude is observed to decrease from 10.4 cm^{-1} to 7.0 cm^{-1} when the temperature increases from 20 C to 70 C, a 32% degradation. The ES degrades even more substantially from 13.6 cm^{-1} at 20 C to 6.7 cm^{-1} at 70 C, a

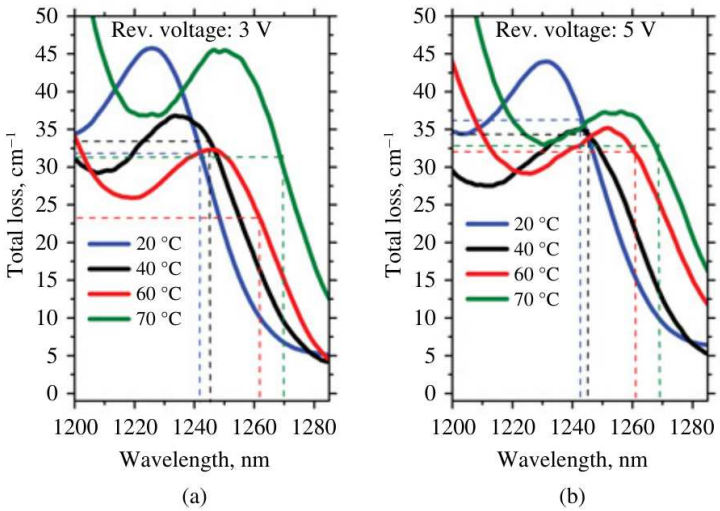

Figure 3.15: Repeat of figure 3.14 for reverse voltages of 3V (a) and 5V (b) [24]

51% degradation. This corroborates that with increasing temperature the portion of carriers occupying higher order states increases resulting in a decreased integrated radiative efficiency. It has been shown [18] that this is likely to arise from two main sources: the first is due to the temperature mediated electron-hole occupation of states that have weak transition probability, and secondly because of the increase in non-radiative recombination resulting from carrier population of these states.

The hatched region shown in figure 3.16 (a) illustrates the range of threshold gain values of the two-section QDMLL. These were calculated using equation 3.2 with $g_o = g_{th}$ and the measured unsaturated loss values (evaluated from the loss measurements of figures 3.14 and 3.15 and compiled in table 3.2). These g_{th} values cover reverse biases on the saturable absorber ranging from 0 to 5 V and current densities on the gain section ranging from 0 to 1.6 kA/ cm^2. From figure 3.16 (a), it is apparent that ML will be difficult to achieve at 70 C (green plot) since the GS gain peak lies below the lower limit of the calculated threshold gain (7 cm^{-1}). Figure 3.16(b) is a plot of the measured variation of the modal gain as a function of

Temp (C)	Reverse bias (V)	Abs. peak (nm)	a_{peak} (cm^{-1})	a_o (cm^{-1})
20	0	1219.2	44.6	20.
40	0	1227.6	41.1	26.2
60	0	1238.4	40.2	18.7
70	0	1244.4	39.8	17.7
20	1	1222.0	46.3	21.7
40	1	1228.4	40.8	28.7
60	1	1240.4	31.7	18.2
70	1	1245.0	41.4	19.7
20	3	1227.0	46.2	28.7
40	3	1235.0	37.2	31.2
60	3	1245.6	32.6	22.7
70	3	1249.6	45.8	29.7
20	5	1232.0	44.4	32.9
40	5	1242.0	41.1	31.5
60	5	1250.4	35.6	30.0
70	5	1254.0	37.5	29.7

Table 3.2: Table of measured absorption characteristics on the 967 device considering temperature and absorber reverse bias. The a_o value for unsaturated absorption was taken at the gain peak and assuming an averaged internal loss of 3.3 cm^{-1} over the temperature range considered.

current density applied to the gain section. One can readily observe the increase of J_{tr} with increasing temperature as well as the progression of the gain saturation to a less abrupt saturation with increasing current density, a signature of the increasing carrier occupation of higher order electronic states. A T_o [9] of 50 K is extracted for this device from 20 C to 70 C similar to other un-doped QD lasers [18]. An analytic expression, equation 3.5, is used to fit the measured variation of the modal gain, shown in figure 3.16 (b), as a function of current density for each of the temperatures considered, where the gain magnitude is taken at the gain peak.

Temp (C)	J_{th} at 0V,1V,3V,5V (A/cm^2)	G_{peak} (nm)	g_o at J=1.6kA/cm^2, (cm^{-1})
20	357, 387, 462, 537	1238	10.5
40	564, 616, 744, 811	1249	9.4
60	713, 792, 953 , no lasing	1261	8.3
70	No lasing	1268	7.7

Table 3.3: Threshold current density J_{th} of the two-section device, peak gain wavelength G_{peak} and modal gain value measured on the multi-section device at 1.6 kA/cm^2. No lasing was observed at 5 V and 60 C and at 70 C for current densities up to 1.6 kA/cm^2.

$$g_o(J) = g_{max}\left[1 - exp(J_{tr} - J)/b)\right] + \alpha_i \tag{3.5}$$

$$\frac{dg_o}{dJ} = \frac{g_{max}}{b} exp\left(\frac{J_{tr} - J}{b}\right) \tag{3.6}$$

where g_o and g_{max} are the modal and maximum net modal gains respectively, J_{tr} is the threshold current density, and α_i is the internal loss. The parameters b, J_{tr}, and g_{max} are adjusted for a best fit to the measured data points. The use of equation 3.5 to represent the measured gain points helps in computing a smooth differential gain, equation 3.6, which otherwise would be piecewise due to the limited number of measured data points recorded in practice. The measured absorption peaks shown in figures 3.14 and 3.15 are found to red-shift at a rate of 0.5 nm/C, thereby shifting by 25-nm between 20 C and 70 C. By contrast, the GS gain peak exhibits a stronger red-shift varying by 0.6-nm/C and thus shifting 30 nm between 20 C and 70 C. The balancing of the losses and gain are critical in establishing mode locking. Anticipating the separate variations of the gain and loss over temperature is not readily apparent. By measuring these quantities and their temperature dependence on the actual device itself, any such ambiguities can be removed. The shift of the gain peak

can be attributed to a combination of the temperature-related shift of the bandgap, bandfilling effects, and possible Coulomb related shifts . The shift of the absorption peak consists of two contributions:

- The temperature-dependent shift of the bandgap [8]
- the Stark shift [27]

The Stark shift is observed to be 12-nm (10 meV) at each temperature from 0 V to 5 V. Assuming all of the reverse voltage was applied to the active region (320-nm thick), an electric field strength up to 160 kV/cm is calculated. These values are comparable with values reported previously [27]. One should note that the gain peak is always longer in wavelength than the absorption peak. For example, inspecting table 3.2 and 3.3, the gain peak at 20 C is 1238 nm (table 3.3) whereas the absorption peak is at 1219 nm at 0 V reverse bias applied to the absorber section. When the reverse bias applied to the absorber section is increased to 5 V, the absorption peak shifts to 1232 nm. The shortest pulses are obtained when the absorption peak and gain peak overlap. This allows for the optimum trimming of the pulse, of course, provided that the gain is sufficient to overcome the total cavity losses. This becomes problematic at higher temperature where the available gain is reduced as a consequence of thermal population of non-lasing states. The measured unsaturated modal gain, the unsaturated loss (the total loss minus the internal loss) presented in this section will be used in the next section to predict the temperature sensitivity of mode locking on a two-section QDMLL based on the model discussed previously. Unlike our previously published research, no a priori knowledge of the lasing wavelength is assumed [2, 3].

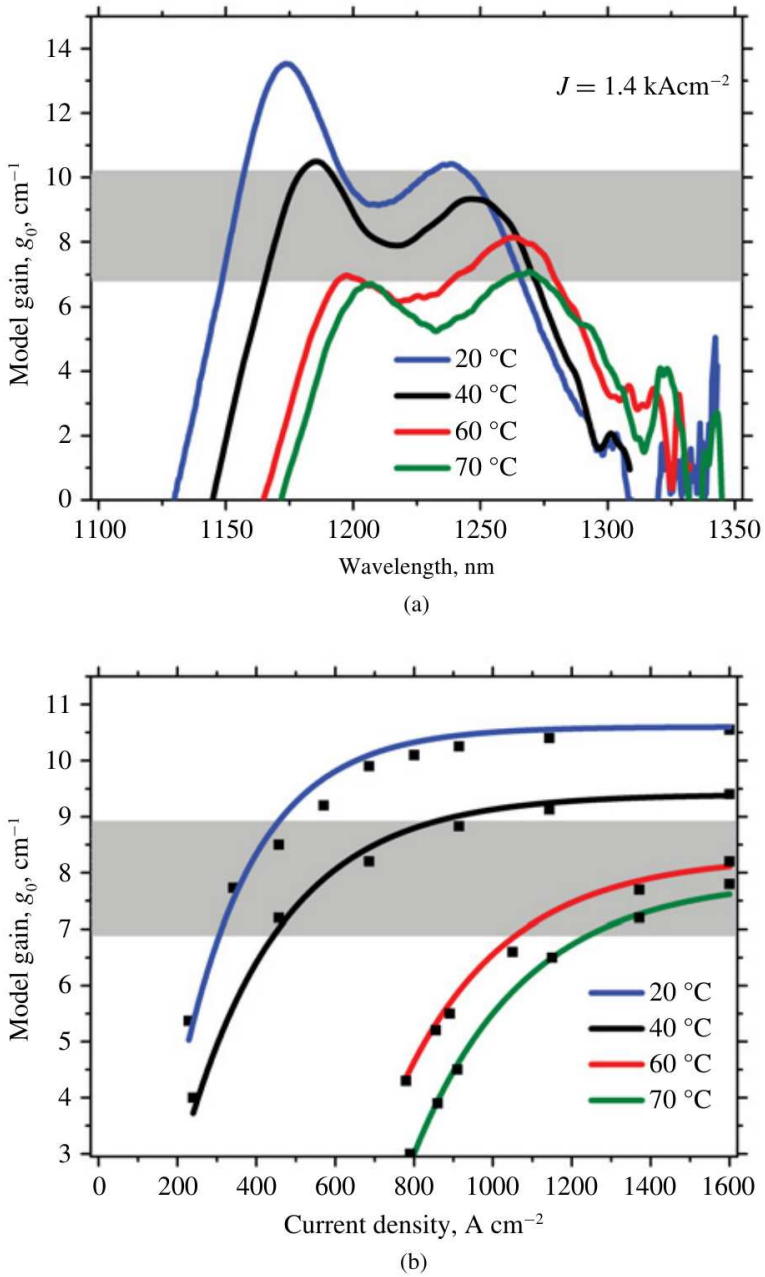

Figure 3.16: Measured modal gain spectra of the 967 in both (a) wavelength and (b) applied current density fit by equation 3.5. The hatched area illustrates the range of threshold gain values covered in this study. [24]

3.6.2 Modeled Temperature-Dependent Mode Locking Stability

In this section, the measured gain and loss properties (summarized in tables 3.2 and 3.3) are used in conjunction with equations 3.1 and 3.2 to predict the expected impact of temperature on the ability of the QDMLL to mode lock. The results are presented in figure 3.17 where the boundaries between hatched and white areas represent the extreme boundary for the onset of mode locking. Stable mode locking without self-pulsation is predicted to exist within the individual contours for each temperature considered [1]. The upper bound of each contour is determined by equation 3.2 whereas equation 3.1 describes the lower bound of these maps. The dashed black line is a guide for the eye illustrating the absorber to gain length ratio of the two-section QDMLL characterized in this projection represents a value of $L_a/L_g = 0.14$. The open symbols denote the measured threshold current density values of the two-section device. Figure 3.17 (a) displays one such set of contours when 0V is applied to the saturable absorber as a function of the ratio L_a/L_g and the gain section current density, J. Specifically, figure 3.17 (b) is a repeat of (a), but using the values compiled in table 3.2 for 1 V reverse bias applied to the absorber. Likewise, figure 3.17 (c) is a repeat of (a) but using the values compiled in table 3.2 for 3 V reverse bias applied to the absorber section. Note that the mode locking boundary at 60 C (red) is beginning to break down and (d) uses the values compiled in table 3.2 for 5 V reverse bias applied to the absorber section. Note that mode locking at 60 C cannot be achieved for the two-section cavity geometry of the device used in this work but is predicted to be possible for shorter L_a/L_g ratios. Figures 3.17 (a)-(d) predict stable mode locking at 20 C and 40 C for the full range of absorber reverse bias values considered (0 V-5 V). The upper bounds of the maps follow the saturation of $g_0(J)$. The model also predicts that the device will not mode lock at 70 C and that mode locking will shut down at 60 C for absorber bias values greater

than 3 V (examine figure 3.17 (c) and (d)).

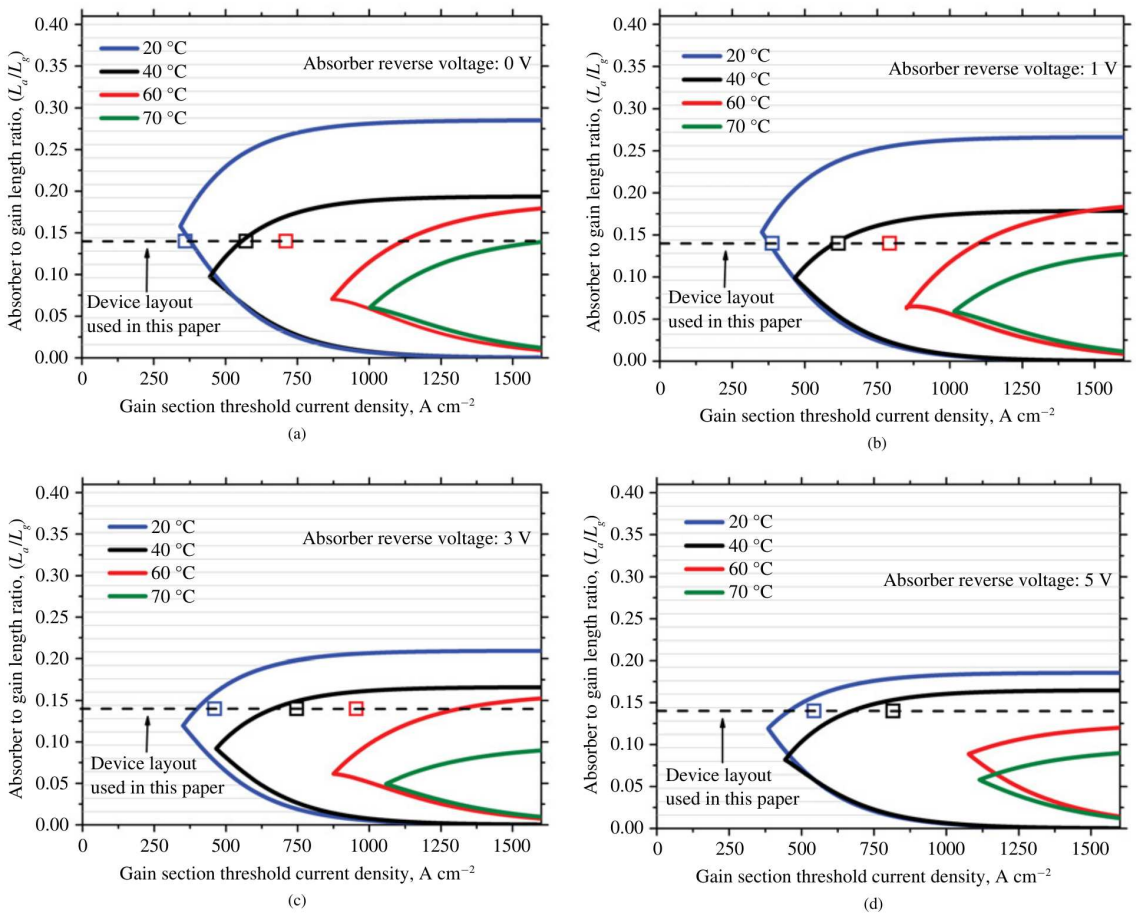

Figure 3.17: (a) Calculated mode locking stability maps with observed threshold current in the two section test device denoted by the colorized boxes for (a) 0 (b) 1 (c) 3 (d) 5 V reverse bias on the absorber [24]

Mode locking in the regions above the upper parts of the boundaries does not occur because the laser cannot operate given the magnitude of the losses present. Note that the gain per unit length is considerably less than the absorption per unit length, typically a factor of 4 difference, as shown in tables 3.2 and 3.3. One should realize that the tendency for the lower bounds of the maps to approach vanishingly small absorber lengths is an artifact of the gain saturation model used, equation

3.5, and arises from the gain saturating completely and consequently approaching a zero differential gain. However, in practice, the differential gain will never be zero due to the existence of excited dot states as well as the higher energy states surrounding the dots. Including this mechanism in equation 3.5 would ensure that the differential gain could never reach zero. However, there is some physical meaning to the absorber length becoming very small. In that case, the laser will switch to excited state operation. This behavior has been observed elsewhere [28].

For each temperature tested in figure 3.17, the intersection of the lower and upper bound represents the cavity geometry permitting the lowest threshold current density. It is clear that the device geometry (L_a/L_g=0.14) is optimized for 20 C operation (open square close to intersection of lower and upper bound (blue)). Physically, this occurs because the available gain cannot overcome the cavity losses. In contrast to the 20-40 C, predictions, the fact that the measured threshold current at 60 C (open red symbol in figure 3.17) does not fall within the boundary of the 60 C contour (red plot) is a tell-tale sign that the mode locking will not be as stable as that observed at cooler temperatures. The underlying physical reasons for this behavior will be discussed in more detail later in terms of the measured gain and loss presented in tables 3.2 and 3.3.

With increasing temperature, the contours in figure 3.17 close up and shift towards lower L_a/L_g ratios as a result of the degradation in g_0 (see figure 3.16). The plots in figure 3.17 predict that there exists a range of cavity layouts that permit mode locking over the 20-70 C temperature range investigated. In fact, figure 3.17 is pointing towards shorter absorber sections to compensate for the temperature mediated deterioration of g_o in order to permit broader temperature insensitivity. For example, an L_a/L_g ratio of 0.075 (figure 3.17) is predicted to ensure mode locking from 20 C to 70 C and 0-5 V. Next, the temperature performance of the QDMLL is characterized experimentally to validate the predictions of the model presented here.

3.6.3 Observed Temperature-Dependent Mode Locking Stability

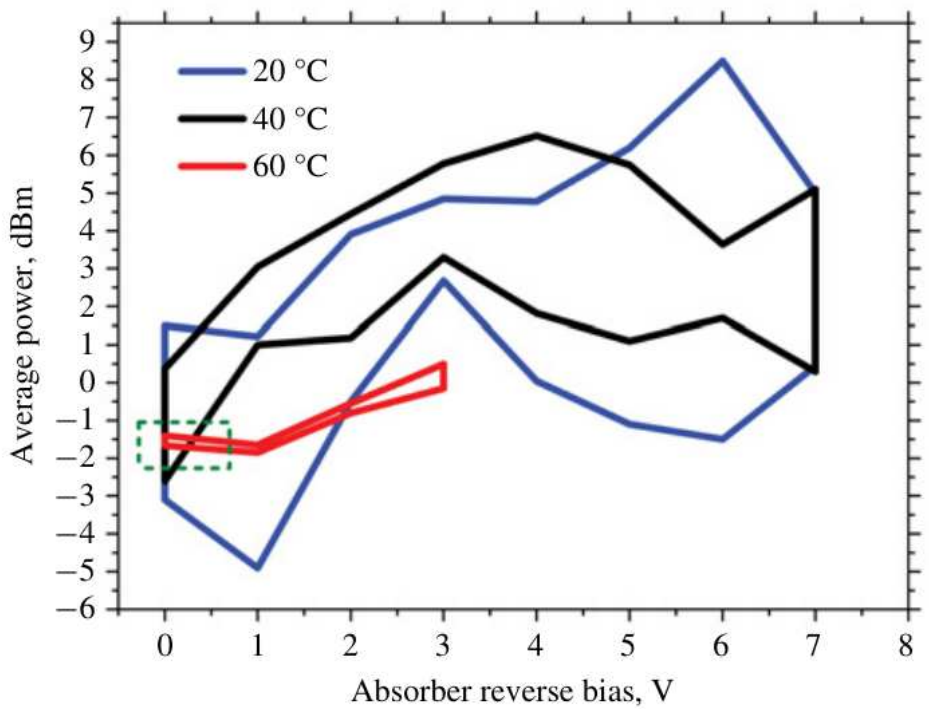

Figure 3.18: Measured stability map for the two-section QD laser under investigation showing the operating regions where stable mode locking occurs at three different ambient temperatures. The contours define regions of stable mode locking where the pulses generated were measured by autocorrelation to be no more than 15 ps FWHM in duration (chosen to allow a reasonable comparison to the modeled stability maps). The area circled by the dashed green line indicates the common operating point for all temperatures. [24]

To substantiate the predictions of the model in the previous section, this section concentrates on measuring the impact of temperature on the mode locking stability of the two-section passively mode locked QD laser fabricated from the same material used in the gain and loss characterization. An RF spectral analysis and an autocorrelator are relied upon to characterize the mode locking. Specifically, we identify

stable mode locking when at least two harmonics with 15-20 dB extinction ratio are obtained from the RF spectrum analyzer. The pulse-width was retrieved from auto-correlation measurements assuming a Gaussian pulse shape. The measured ability of the device to mode lock over temperature for a range of absorber reverse bias values is presented in figure 3.18. To facilitate a comparison to the modeling presented in the previous section, the maps in figure 3.18 define the pulse width observed before the mode locking broke down. Typically, this is observed to occur for pulse widths in the range of 15 ps (ML stability rapidly degrades for durations greater than these values). These pulse width trends are observed consistently over the entire temperature range considered. In fact, this is the shortest pulse width at 60 C for absorber reverse bias voltages between 0 V and 3 V, resulting in the thin contour (red plot in figure 3.18). Thus, this can be considered a reasonable assumption to the sinusoidal modulation for which the modeling of the previous section is based. In comparing the modeled and measured ML maps, it should be stressed that the model does not predict pulse widths but rather gives an indication of whether mode locking is likely to be achieved or not. Such predictions of pulse width can be reached using a Delayed Differential Equation (DDE) model [29].

Between 20 C and 40 C, the device exhibits stable mode locking over a wide range of operating conditions; however, the performance at 60 C deteriorates dramatically and mode locking was not observed beyond 3 V absorber reverse bias at this temperature (see figure 3.18). The device did not mode lock at 70 C for the range of current densities used. The tendency, at elevated temperature, for the device not to mode lock at higher absorber reverse voltages (compare 60 C (red contour) and 20 C (black contour) maps in figure 3.18) has been reported previously [19, 20] and is attributed to the increasing sweep out of carriers from the saturable absorber as the temperature increases. The agreement between the measured and calculated ML stability is rather close, highlighting the accuracy and effectiveness of the approach. Tan et al studied the effect of absorber length on ML operation in a QW system find-

ing that at high temperatures a shorter absorber section is required to maintain ML [30]. This result is in agreement with our findings in a QDMLL and highlights the idea that the variation of the modal gain is more sensitive to temperature than the absorption. Figure 3.16 portrays this idea more clearly where it can be observed that the modal gain is reduced by 25% when the ambient temperature is raised from 20 C to 70 C. By contrast, the absorption magnitude at the gain peak can be manipulated by the application of a reverse bias.

From the predictions of the model presented in section V, the broadest range of operating parameters where stable mode locking is maintained occurs for temperatures cooler than 60 C. Indeed this is where the shortest pulses are measured, typically in the range of 3-10 ps. The pulses measured at 60 C were generally much broader in duration, 15 ps. The quality of the pulses can be attributed to the temperature-dependent walk-off of the absorption and gain peaks. From the measurements presented in this work (refer to tables 3.2 and 3.3) at 20 C and 0 V reverse bias, there is a 19-nm difference in the absorption and gain peaks. This is reduced at 5 V reverse bias down to 6-nm. At 40 C the gain-absorption peak separation contracts from an initial 21.4-nm at 0 V to 7.0-nm at 5 V. Conversely, at 60 C the separation between the absorption peak and gain peak is 23-nm at 0 V reverse bias on the absorber and 11-nm at 5 V reverse bias. From tables 3.2 and 3.3, it is seen that this result means that the magnitude of the unsaturated loss at the gain peak ranges from a_o=18.2-22.7 cm^{-1} at 60 C. These values compare to a_o=26.2-31.7 cm^{-1} at 40 C and a_o=20-28.7 cm^{-1} at 20 C for reverse bias values of 0-3 V. At 5 V, a_o rose to 32.9 cm^{-1}, 31.5 cm^{-1} and 30.0 cm^{-1} at 20 C, 40 C and 60 C, respectively. The shortest pulses and widest range of operation were observed at 20 C and 40 C at 5V and beyond since the saturable absorber can trim pulses more effectively. By the same argument that adequate absorption is needed, it may be that the loss at 60 C between 0 V and 3V is insufficient to generate stable mode locking, hence resulting in the observation of broad pulses in the time domain. It may also explain why mode

locking at 60 C was only observed at a significant current density increment above threshold, about 200-300 A/cm^2, in stark contrast to cooler temperatures (predicted in figure 3.17). The mode locking observed at 60 C in this work is stable only over a very narrow range of operating parameters, see red plot in figure 3.18. Mode locking at 60 C with a larger range of operating parameters in a two-section monolithic passively mode locked laser with a p-doped InAs/GaAs DWELL active region structure has been reported [19] where the L_a/L_g ratio was 0.11. A recent study on two-section QD passively MLLs has demonstrated that there exists an optimum L_a/L_g ratio to obtain the shortest pulses at room temperature [31]. Clearly, there is an optimum layout to simultaneously allow for mode locking over a sizable temperature span while not compromising the pulse width.

3.7 Concluding Remarks and Extensions of the Technique

In summary, an analytic formalism to map the temperature dependent mode locking stability of monolithic two-section passively MLLs was presented. The method, based on a microwave photonics perspective, has the advantage that all of the quantities appearing in the equations can be measured on the device under investigation. The model assumes a sinusoidal modulation of the net gain and hence the generated light intensity and, therefore, represents the boundary before the onset of passive mode locking in a semiconductor laser. The scheme requires measurement of the gain and loss of the device over wavelength, current density, and a given temperature range. Using this information in the model determines the range of device layouts where ML can be achieved (absorber to gain section length ratios) for that range of temperatures. The validity of the model over temperature was confirmed by using the measured gain and loss characteristics of an 8-stack InAs/GaAs DWELL

QD material in the model and then comparing to the measured characterization of the mode locking performance of a two-section MLL fabricated from the same QD material.

The failure to mode lock at higher temperatures is shown to occur not only as a consequence of the deterioration of the modal gain with temperature but also because of the different shifts associated with the gain and absorption peaks with varying temperature and absorber reverse bias, resulting in a "walk off" effect between the two peaks. In the spirit of practicality, the model provides a quantification of the necessary cavity layouts which can permit mode locking over a wide temperature range. Although the device used in this work failed to ML beyond 60 C, the modeling clearly indicates that by reducing the absorber length, effectively reducing the threshold condition, will enable ML beyond 60 C. Ultimately, fabricating QD materials with a higher T_o and more temperature resistant gain magnitude should allow for wider maps as presented in figure 3.17 and extend the operation where stable mode locking can be achieved. Based on the best published QD laser performance over temperature and recorded observation, realizing 100 C ML operation is a realistic acquisition [32, 33]. The approach presented here should not only motivate the design of more temperature resistant gain media but should also effectively guide the optimization of current QD technologies in terms of p-doping and number of stacked QD layers. Indeed, it should prove to be an invaluable tool for the design of next generation devices capable of operation over broad temperature excursions.

Beyond this, one can also use these techniques to examine the effects that any process that degrades device gain has upon mode locking operation. Degradation of gain values due to temperature variation, damage to emitting facets or coatings, damage to metalization layers and nonuniform pumping, or finally to waveguide damage itself are all considerable in this model. Using the balance between the lasing threshold in equation 3.2 and the mode locking inequality 3.1 we can incorporate and

quantify effects without changing the mathematics needed for our predictions. This insight propelled investigation into the effects of other types of gain degradation effects on QDMLLs.

References for Chapter 3

[1] K. Lau and J. Paslaski, "Condition for short pulse generation in ultrahigh frequency mode-locking of semiconductor lasers," *Photonics Technology Letters, IEEE*, vol. 3, pp. 974–976, Aug. 1991.

[2] C. Y. Lin, Y. C. Xin, Y. Li, F. L. Chiragh, and L. F. Lester, "Cavity design and characteristics of monolithic long-wavelength InAs/InP quantum dash passively mode-locked lasers," *Optics express*, vol. 17, pp. 19739–19748, Oct. 2009.

[3] Y.-C. Xin, C.-Y. Lin, Y. Li, H. Bae, H. Yuen, M. Wistey, J. Harris, S. Bank, and L. Lester, "Monolithic 1.55 μm GaInNAsSb quantum well passively modelocked lasers," *Electronics Letters*, vol. 44, no. 9, p. 581, 2008.

[4] F. Grillot, C.-Y. Lin, N. A. Naderi, M. Pochet, and L. F. Lester, "Optical feedback instabilities in a monolithic InAs/GaAs quantum dot passively mode-locked laser," *Applied Physics Letters*, vol. 94, no. 15, p. 153503, 2009.

[5] N. Usechak, L. Lester, D. Kane, and V. Kovanis, "Modeling and Direct Electric-Field Measurements of Passively Mode-Locked Quantum-Dot Lasers," *IEEE Journal of Selected Topics in Quantum Electronics*, vol. 15, no. 3, pp. 653–660, 2009.

[6] A. G. Vladimirov and D. Turaev, "Model for passive mode locking in semiconductor lasers," *Physical Review A*, vol. 72, pp. 033808+, Sept. 2005.

[7] Y. C. Xin, Y. Li, A. Martinez, T. J. Rotter, H. Su, L. Zhang, A. L. Gray, S. Luong, K. Sun, Z. Zou, J. Zilko, P. M. Varangis, L. F. Lester, and S. Member, "Optical gain and absorption of quantum dots measured using an alternative segmented contact method," *Quantum Electronics, IEEE Journal of*, vol. 42, pp. 725–732, July 2006.

[8] I. Vurgaftman, J. R. Meyer, and Mohan, "Band parameters for {III}–V compound semiconductors and their alloys," *Journal of Applied Physics*, vol. 89, no. 11, pp. 5815–5875, 2001.

[9] J. Pankove, "Temperature dependence of emission efficiency and lasing threshold in laser diodes," *IEEE Journal of Quantum Electronics*, vol. 4, pp. 119–122, Apr. 1968.

[10] G. Keeler, B. Nelson, D. Agarwal, C. Debaes, N. Helman, A. Bhatnagar, and D. Miller, "The benefits of ultrashort optical pulses in optically interconnected systems," *IEEE Journal of Selected Topics in Quantum Electronics*, vol. 9, pp. 477–485, Mar. 2003.

[11] D. Miller, "Rationale and challenges for optical interconnects to electronic chips," *Proceedings of the IEEE*, vol. 88, pp. 728–749, June 2000.

[12] M. G. Thompson, A. R. Rae, M. Xia, R. V. Penty, and I. H. White, "InGaAs Quantum-Dot Mode-Locked Laser Diodes," *Selected Topics in Quantum Electronics, IEEE Journal of*, vol. 15, pp. 661–672, May 2009.

[13] M. Kuntz, G. Fiol, M. Lammlin, D. Bimberg, M. G. Thompson, K. T. Tan, C. Marinelli, R. V. Penty, I. H. White, V. M. Ustinov, a. E. Zhukov, Y. M. Shernyakov, and a. R. Kovsh, "35 GHz mode-locking of 1.3 μm quantum dot lasers," *Applied Physics Letters*, vol. 85, no. 5, p. 843, 2004.

[14] C. Y. Lin, Y. C. Xin, J. H. Kim, C. G. Christodoulou, and L. F. Lester, "Compact Optical Generation of Microwave Signals Using a Monolithic Quantum Dot Passively {Mode-Locked} Laser," *IEEE Photonics Journal*, vol. 1, pp. 236–244, Oct. 2009.

[15] D. Miller and H. Ozaktas, "Limit to the Bit-Rate Capacity of Electrical Interconnects from the Aspect Ratio of the System Architecture," *Journal of Parallel and Distributed Computing*, vol. 41, pp. 42–52, Feb. 1997.

[16] A. Shacham, K. Bergman, and L. P. Carloni, "Photonic Networks-on-Chip for Future Generations of Chip Multiprocessors," *IEEE Transactions on Computers*, vol. 57, pp. 1246–1260, Sept. 2008.

[17] J. Meindl, "Interconnect opportunities for gigascale integration," *IEEE Micro*, vol. 23, pp. 28–35, May 2003.

[18] M. Crowley, I. Marko, N. Masse, A. Andreev, S. Tomic, S. Sweeney, E. O'Reilly, and A. Adams, "The Importance of Recombination via Excited States in InAs/GaAs 1.3 μm Quantum-Dot Lasers," *IEEE Journal of Selected Topics in Quantum Electronics*, vol. 15, no. 3, pp. 799–807, 2009.

[19] G. Fiol, C. Meuer, H. Schmeckebier, D. Arsenijevic, S. Liebich, M. Laemmlin, M. Kuntz, and D. Bimberg, "Quantum-Dot Semiconductor Mode-Locked Lasers and Amplifiers at 40 GHz," *IEEE Journal of Quantum Electronics*, vol. 45, pp. 1429–1435, Nov. 2009.

[20] M. a. Cataluna, D. B. Malins, A. G. Iglesias, W. Sibbett, A. Miller, E. U. Rafailov, and A. Gomez-Iglesias, "Temperature dependence of electroabsorption dynamics in an {InAs} quantum-dot saturable absorber at 1.3 mu m and its impact on mode-locked quantum-dot lasers," *Applied Physics Letters*, vol. 97, no. 12, pp. 121110+, 2010.

[21] G. T. Liu, K. J. Malloy, A. Stintz, H. Li, and L. F. Lester, "Extremely low room-temperature threshold current density diode lasers using {InAs} dots in {$In_{0.15}Ga_{0.85}As$} quantum well," *Electronics Letters*, vol. 35, pp. 1163–1165, July 1999.

[22] A. Stintz, G. T. Liu, H. Li, L. F. Lester, and K. J. Malloy, "Low-threshold current density 1.3-μm InAs quantum-dot lasers with the dots-in-a-well (DWELL) structure," *Photonics Technology Letters, IEEE*, vol. 12, pp. 591–593, Aug. 2002.

[23] Y. C. Xin, Y. Li, V. Kovanis, A. L. Gray, L. Zhang, and L. F. Lester, "Reconfigurable quantum dot monolithic multisectionpassive mode-locked lasers," *Opt. Express*, vol. 15, pp. 7623–7633, June 2007.

[24] M. T. Crowley, D. Murrell, N. Patel, M. Breivik, C.-Y. Lin, Y. Li, B.-O. Fimland, and L. F. Lester, "Analytical Modeling of the Temperature Performance of Monolithic Passively {Mode-Locked} Quantum Dot Lasers," *IEEE Journal of Quantum Electronics*, vol. 47, p. 1059, Feb. 2011.

[25] D. Kane and R. Trebino, "Characterization of arbitrary femtosecond pulses using frequency-resolved optical gating," *IEEE Journal of Quantum Electronics*, vol. 29, pp. 571–579, Feb. 1993.

[26] Z. Yasa and N. Amer, "A rapid-scanning autocorrelation scheme for continuous monitoring of picosecond laser pulses," *Optics communications*, vol. 36, pp. 406–408, Mar. 1981.

[27] P. Fry, I. Itskevich, D. Mowbray, M. Skolnick, J. Finley, J. Barker, E. O'Reilly, L. Wilson, I. Larkin, P. Maksym, M. Hopkinson, M. Al-Khafaji, J. David, A. Cullis, G. Hill, and J. Clark, "Inverted Electron-Hole Alignment in InAs-GaAs Self-Assembled Quantum Dots," *Physical Review Letters*, vol. 84, pp. 733–736, Jan. 2000.

[28] M. Cataluna, E. Rafailov, A. McRobbie, W. Sibbett, D. Livshits, and A. Kovsh, "Stable mode-locked operation up to 80 ^{o}C from an InGaAs quantum-dot laser," *IEEE Photonics Technology Letters*, vol. 18, pp. 1500–1502, July 2006.

[29] R. Raghunathan, M. T. Crowley, F. Grillot, S. D. Mukherjee, N. G. Usechak, V. Kovanis, and L. F. Lester, "Delay differential equation-based modeling of passively mode-locked quantum dot lasers using measured gain and loss spectra," in *Proc. of SPIE Vol 8255* (B. Witzigmann, M. Osinski, F. Henneberger, and Y. Arakawa, eds.), p. 82551K, Feb. 2012.

[30] W. K. Tan, H. Y. Wong, A. E. Kelly, M. Sorel, J. H. Marsh, and A. C. Bryce, "Passive modelocking of InGaAsP/InP laser diode over wide operating temperature range," *Electronics Letters*, vol. 41, no. 25, pp. 1380+, 2005.

[31] A. R. Rae, M. G. Thompson, A. R. Kovsh, R. V. Penty, and I. H. White, "InGaAsGaAs Quantum-Dot Mode-Locked Laser Diodes: Optimization of the Laser Geometry for Subpicosecond Pulse Generation," *IEEE Photonics Technology Letters*, vol. 21, pp. 307–309, Mar. 2009.

[32] V. Tokranov, M. Yakimov, A. Katsnelson, M. Lamberti, and S. Oktyabrsky, "Enhanced thermal stability of laser diodes with shape-engineered quantum dot medium," *Applied Physics Letters*, vol. 83, no. 5, pp. 833–835, 2003.

[33] J. K. Mee, M. T. Crowley, D. Murrell, R. Raghunathan, L. F. Lester, and S. Member, "Temperature Performance of Monolithic Passively Mode-Locked Quantum Dot Lasers: Experiments and Analytical Modeling," *Selected Topics in Quantum Electronics, IEEE Journal of*, vol. 19, p. 1101110, July 2013.

Chapter 4

Radiation Hardness Studies

4.1 Motivation

Impediments on the gain profiles of Quantum Dot Gain Media occur from other causes beyond the temperature variations described in previous chapters. Permanent reduction in a device's gain profile can also occur as a result of physical damage to the material itself. System durability is the enduring focus of any design engineer that seeks to meet the bandwidth demand challenges in the future with semiconductor optoelectronics. New control and communications systems that use photonics to relieve the crushing bandwidth demands must be robust enough to survive the extreme environments where they are expected to function. The outer reaches of our atmosphere and beyond comprise the harshest environments known. Demonstrated device fitness in the harshness of orbit and deep space provide a natural proving ground for demanding terrestrial applications as well. The versatility of examination using the gain and loss values as well as complimentary measurements for unprocessed material are of great value. These examinations allow for us to extend our predictive models previously used to characterize temperature impediments to mode

locking performance. Thus, we can use our methods to predict the susceptibility of an entirely different type of physical damage, damage due to ionizing radiation.

Extremes of ionizing radiation do not reflect the only environmental challenge orbital vehicles must face. Temperature variations are extreme between the sides of the spacecraft illuminated by sunlight and those left shaded; thus, the performance characterizations already done have a dual use. The reliability of devices over temperature ranges is of particular interest in any durability study. Furthermore, thermal challenges are not so alien to us here within the atmosphere and many [1] techniques from radiators to Peltier electric regulators have been developed to manage them. In space, many of these solutions are effective and require one currency to function: power. Energy generated by a spacecraft is preciously finite and any savings in power allowed by wider envelopes of temperature operation are a welcome addition to any systems engineer tasked with power balancing. The Quantum Dot Mode Locked Laser (QDMLL) has shown exceptional resilience in regard to temperature operation. Devices under test have been operated at temperatures exceeding 100C [2] and their power efficiency increases as their temperature cools. This "wall plug efficiency" is a direct measure of the conversion from input electrical energy to output optical photons. Reliability in these two extrema of temperature and ionizing radiation make the QDMLL ideally suited for operation aboard an orbiting vehicle as part of a communications system.

The thrust of this research was to determine the damaging effects of ionizing radiation on Quantum Dot laser gain material. Literature searches before local testing began showed that quantum dots are exceptionally hardened to radiation of many types. Our investigation focused on the most difficult radiation to shield from: high energy Gamma Rays. Charged particle illumination has been demonstrated to have more effect on quantum dot media from Leon [3] and Cavaco [4] to cite a few. Other groups have examined high energy photon irradiation of functional

devices [5] and have shown additional durability. However, our investigation focuses on vulnerability of the gain media to radiation. The dots in the device are directly probed with our measurement technique which does not consider extensive damage in the laser waveguide itself. We can thus claim that our investigation focuses on the dots rather than the material they are embedded in.

4.1.1 Radiation Hazards in Earth Orbit

Exposure to ionizing radiation is a constant threat beyond the confines of Earth's atmosphere. Much effort has been devoted to mapping the magnitude and geography of these threats in orbit by groups from around the world. Direct experimental measurements aboard manned fights at lower altitude and geostationary satellites have been performed for years. Experimental data from a geostationary satellite using radiation sensitive transistors characterized the yearly dose measured in 2003 [6]. This is the orbit that a communications satellite would most likely inhabit. Bhat's experiment on the GSAT-2 orbiter employed a series of radiation sensitive elements with Aluminum shielding varying from less than 1 mm in thickness to that approaching 1 cm. Their calculated yearly radiation dose for moderate shielding was less than 1 krad per year. Radiation caused by solar activity follows a cyclic pattern with spurts of activity resulting from sunspots and flares. This pattern has been well studied also which means that we can compare solar ferocity from 2003 when GSAT-2 to potential maximas. Examination of solar activity for that time period [7] reveals that 2003 was a moderate year for solar radiation sources. Thus, the measurements on the GSAT-2 craft provide an excellent baseline for anticipating what our devices could be expected to see in space. We use these average values for radiation exposure to develop a test scheme over a range of irradiation sources and durations to appropriately simulate orbital environments.

However, average radiation dose is only part of the hazards vehicles must contend with. The cyclic solar pattern has been well studied; therefore, we can compare solar ferocity from 2003 when GSAT-2 flew to potential maximas. One must carefully consider the solar periodicity when predicting baseline radiation expectations for maximum accuracy over time. Examination of solar activity for that time period as shown in Reitz [7] reveals that 2003 was a moderate year for solar radiation sources on the trailing end of sunspot cycle 23. Therefore, we are even more confident in our baseline numbers for analysis as this sampling year was not at either extrema of the Sun's output. It is important to note that levels of radiation flux vary not only with altitude but also with latitude across the globe. The configuration of the Van Allen belts shunt captured charged particles which would increase the effective radiation dose in polar orbits. This study focuses on resilience to ionizing radiation rather than focusing on charged particle effects. Further studies [3, 8] into charged particle irradiation on the quantum confined media have shown resilience, but it is important to note that any bombardment by charged particles onto a doped semiconductor will have device effects beyond that of lattice dislocations through shifts in the doping levels. Charged particles are hindered by far less shielding than is required to attenuate high energy photons by a similar fraction. Thus, we assume that the craft that would hold our test devices would carry at least this minimal shielding for the orbital inclination chosen for the mission.

4.1.2 Investigation Methods

The investigation into the radiation hardness of quantum confined media began with Photoluminescence (PL) characterization of gain material samples and ended with irradiation of functioning quantum dot devices. A linear accelerator, ^{137}Cs, and ^{60}Co were used as Gamma Ray sources over the course of the experiment. Previous discussions of the gain and loss methods to project device effectiveness rely on an active

laser or processed gain material. The substitution of PL data for the unprocessed gain material is a measure of the same physical effects but cannot be couched in our oscillator mathematics. However, both PL and the traditional gain/loss curves are related to each other and the insights of both are valuable. The investigations of PL changes as the samples went through irradiation sessions relied on common baselines taken before the material was stressed. Care was taken to ensure that the PL measurement setup was calibrated consistently across each measurement run by using a control sample before the test sample was measured. Analysis of the PL peaks' Full Width Half Max (FWHM), peak height, and integrated intensity provide the points of comparison needed to determine the extent of damage incurred through illumination runs. We search for dramatic changes in any of the three previous PL measurement avenues which would provide evidence of degradation from our experiments. We also look for recovery in PL intensity as a function of time after irradiation to see if there is any "relaxing" effect after the Quantum Dots are exposed. In practice, we saw very little changes in PL measurements. Any changes in the PL effect were largely dwarfed by the variance of the PL values caused by variances in the MBE growth itself rather than from subsequent damage. The processed laser materials were examined using the segmented contact method in the case of multisection device and mode locking threshold conditions in the case of the two section laser. The segmented contact method [9] and a single run of the process used to create a mode locked map [10] provide quantitative benchmarks for testing.

4.1.3 Photoluminescence as a Qualitative Measurement

Closer examination of our experimental setup for PL measurement has prompted us to expand our research technique to achieve finer quantitative observations. Alignment of the stage and mirrors to collect the emitted light is highly variable. Use of a calibrated sample to normalize the results is problematic because the setup needs

to be changed again for integration of the genuine experimental devices. Thus, the measured PL peak intensities vary widely. Our efforts with PL focused on determining the radiation hardness of the unprocessed gain material. Many groups have studied high energy gamma irradiation on quantum dot lasers [5, 8, 11] and more have examined similar devices under particle irradiation [8, 12, 3]. All of these tests were performed on active devices examining only the aggregate effect of the damage on the laser's light curve and threshold values. The data taken by those groups told us only that some part of the device is responsible for the degraded performance and did not examine the mode locking characteristics. Examination of the health of the gain media in this work allows us to make more proper investigation into what part of the laser structure is breaking due to higher radiation susceptibility. Identification of susceptible elements to irradiation and subsequent strengthening of those elements could be most useful for mission endurance.

Investigation of unprocessed quantum dot material is a twofold process involving either microscopy or optical methods. Photoluminescence is an excellent technique for determining the health of a sample after irradiation [13]. The PL measurement setup that we used is diagrammed in figure 4.1 and is a traditional apparatus for free space measurements of this kind. The light source is an electrically pumped HeNe laser operating at the fundamental lasing wavelength of 632.8 nm at a power of less than 5 W. This power and wavelength is sufficient to excite PL in the sample, which has a bandgap in the range of mid-infrared. Background light is eliminated through the use of a Lock-In amplifier synchronized to a rotating beam chopper in the HeNe beamline. A band pass filter restricts the linewidth of the HeNe to its fundamental line only. Collected PL light is separated from the exciting beam through the use of another filter in the monochromator. The monochromator is computer controlled allowing for stepped scans of the PL spectrum using the attached photodiode detector. Data is collected after the Lock-In amplifier has integrated out the noise of the signal caused by background light.

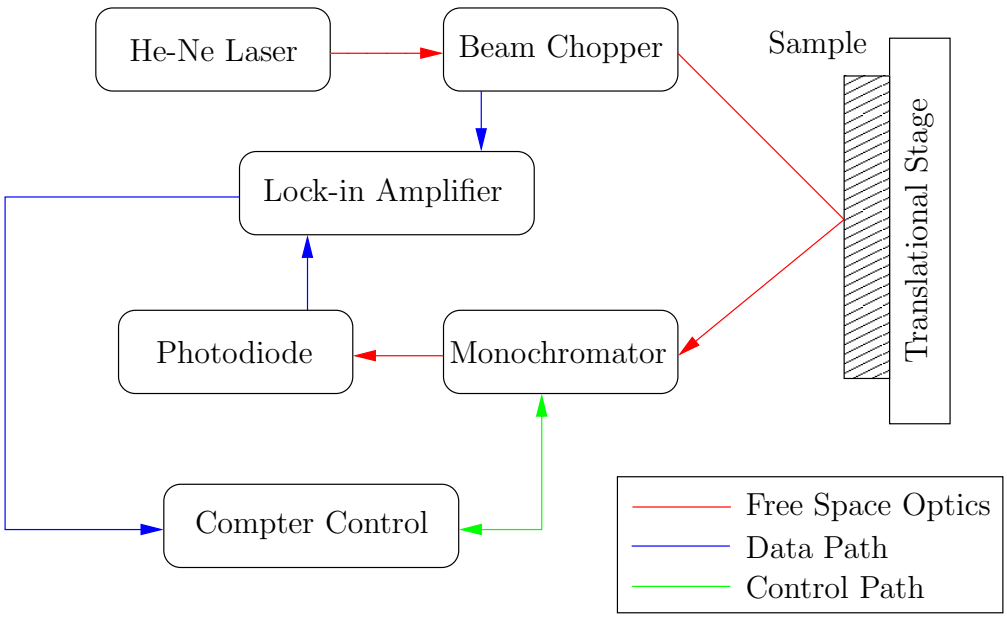

Figure 4.1: Schematic diagram of the Photoluminescence Setup

This PL setup is designed using freespace optical components through its entire length which implies frequent alignment is necessary. These alignment changes are most important for the collecting mirrors near the Sample's translational stage. Care is taken to ensure the configuration settings are as close as possible between each measurement by examining pre-set points on a control sample before testing the experimental sample. PL measurements are qualitative because of the delicate nature of their alignment. Our setup can rate PL as "strong" or "weak" but cannot make definitive comparison across many measurements taken many months apart. However, they can illustrate large changes conducted over the course.

The PL setup was a freespace arrangement so alignment after each of the measurements to measure repeated spots was vital. Initial measurements used a full quarter wafer with a matrix of 9 points dispersed throughout as diagrammed in figure 4.2. These were all defined relative to the edges and were reached through translation stages on the mounting fixture. The visible HeNe spot was used as a

guide in the experiments. The initial desire for a higher number of measurement points dispersed on the quarter wafer was arrived at because of the assumption that the wafer itself was homogeneous. This turned out not to be the case at all as the thickness of the epitaxial layer is radially symmetric and varies from the center to the wafer's edge. Thus, the resolution in two dimensions was unnecessary and a new measurement scheme was devised for subsequent unprocessed gain media tests.

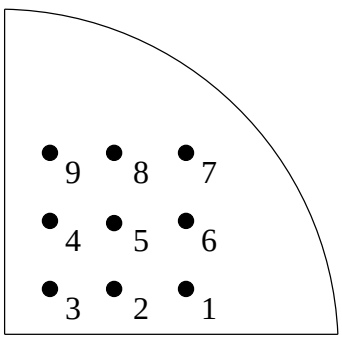

Figure 4.2: PL measurement points for the quarter wafers

Exploiting the radial symmetry of MBE growth is simple enough if you can cleave a fragment of the wafer along the radial direction. The edge sections of the quarter wafers were cleaved following the schematic in figure 4.3.

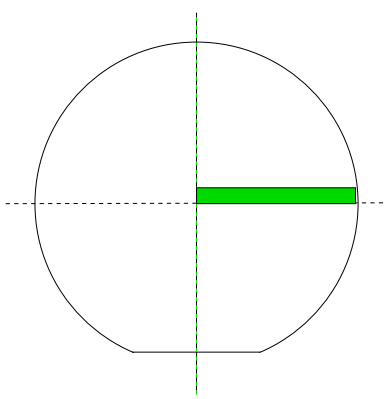

Figure 4.3: Schematic diagram of a test geometry exploiting the radial symmetry of MBE growth with an example radial test bar highlighted

This new arrangement allows for one axis restriction and simple references of distances from the edge. It also produces more beautiful plots because the baseline PL values are continuous along a curve relative to the thickness of the dot layer. Alignment is also easier as errant calibrations are more obvious. However, even with these adjustments PL is something that can be used only as a broad hint of the behavior of the quantum media under irradiation. More detailed study is best performed in the more controlled environment of a lasing cavity.

4.2 Material Studies

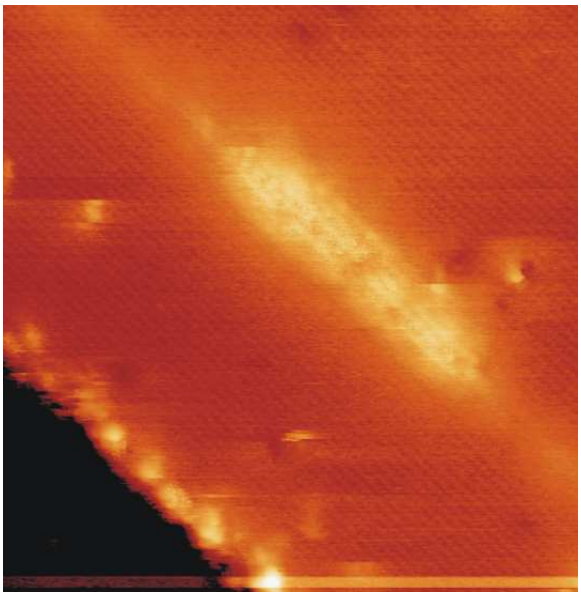

Figure 4.4: X-STM scan of a QD layer

Quantum Dot Material is unique in its epitaxial structure. The source of the optical gain from these quantum heterostructures relies on many individual dots rather than a single continuous layer. Irradiation damage from high energy photons typically cause crystal dislocations which can cause the heterostructure to inherit

defects that can destroy the device. Quantum dots are energetically isolated from the surrounding region inside of the band gap material and damage to an individual dot does not significantly factor into the net production of billions more. Therefore, this investigation examines the durability of the QDMLL for use in extreme environments where ionizing radiation is a prolific threat. These QDMLLs [14, 15] are fabricated using Dots in a Well (DWELL) epitaxial structures which utilizes the unique properties of 2D and 3D Quantum Structures [15] to achieve low threshold current density in an exceptionally durable gain medium [12]. QDMLLs are well suited to mode-locking because of the very high differential gain resulting from their 0D quantum geometry [16]. As previously referenced, these QDMLLs are remarkably resilient to decreases in device gain as a function of temperature [17]. We show that the devices tested continue to perform well even after being dosed with sufficient ionizing radiation to simulate a long mission at geostationary altitudes. The QDMLL is an exceptionally radiation hardened device with potential application for use in optical back planes of on orbit vehicles. A microscopic cross section of the quantum dots themselves on a similar device is shown in figure 4.4.

The experiment itself includes three samples that are made from unprocessed material.

- QW 1076 (Quantum Well)
  - Chosen for its 1D quantum structure
- ZLG 246.2 (InAs Dots)
  - Chosen for its 0D quantum structure
- R10-106 (InAs Dash on InP)
  - Chosen for the different radiation cross section of InP

And two devices that are fully processed laser waveguides. Both devices were from the 788 series. A multisection device for characterizing gain and loss (multisection) and a two section (device 4) for characterizing mode locking conditions. The unprocessed gain material was evaluated using photoluminescence and the lasers were evaluated using the segmented contact method or simple mode locking threshold characteristics in the case of the two section device.

4.3 Unprocessed Gain Material Studies

These are the initial studies conducted to determine the resilience of the QD gain structures to ionizing radiation before we went forward with the laser irradiation later. We used 3 sources of ionizing radiation, a linear accelerator, a ^{137}Cs source, and a ^{60}Cs source. The total irradiation sessions for the unprocessed material are summarized in table 4.1. The susceptibility of all the component elements in our test material to gamma irradiation is shown in figure 4.5. This table also includes the irradiation values for the 788 series lasers discussed later in the chapter as a reference.

Session	1	2	3	4	5
Source	^{173}Cs	0.605 MeV $h\nu$	15 MeV $h\nu$	^{60}Co	^{60}Co
	krad	krad	krad	Mrad	Mrad
ZLG 246.2	316.16	12.69	311	1.5	-
QW1076	-	-	-	1.5	-
R10-106	-	-	-	1.5	-
788	-	-	-	-	2.2

Table 4.1: Total radiation dose for all samples

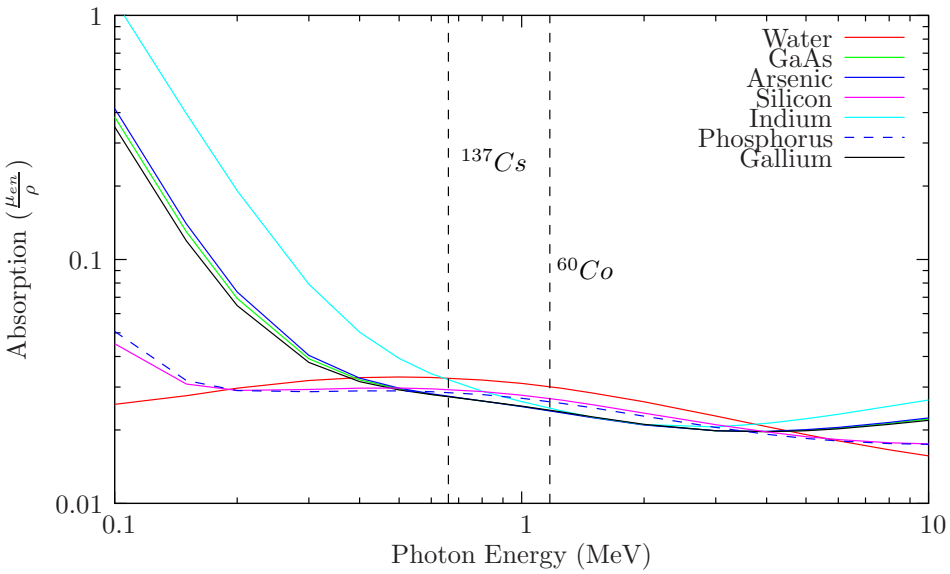

Figure 4.5: Absorption profiles for various elements in the test materials [18]

4.3.1 Initial Irradiation Trials with InAs Dots

The first attempt at measurement of the InAs quantum dot gain media (ZLG 246.2) was to examine quarter sections of a single 2 inch wafer. One wafer was to act as a control sample while each of the others was designated for a particular type of radiation treatment. Measurement points were defined relative to the inner corner of the wafer as shown in figure 4.2. These points were probed and positioned using the micrometers on the translation stage. Typical PL measurements are shown in figure 4.6. The first observation one can make from this data is that the dot concentration and properties are not uniform across the entire surface of the quarter as a result of the growing process by MBE. As mentioned earlier, this was an attempt to survey the variance in the growth process but was ultimately an extra restraint that would have been unnecessary with a more thoughtful cleave.

A local ^{137}Cs source at the University of New Mexico Cancer Research Center was used to provide the initial irradiation of the quarter wafer to look for possible

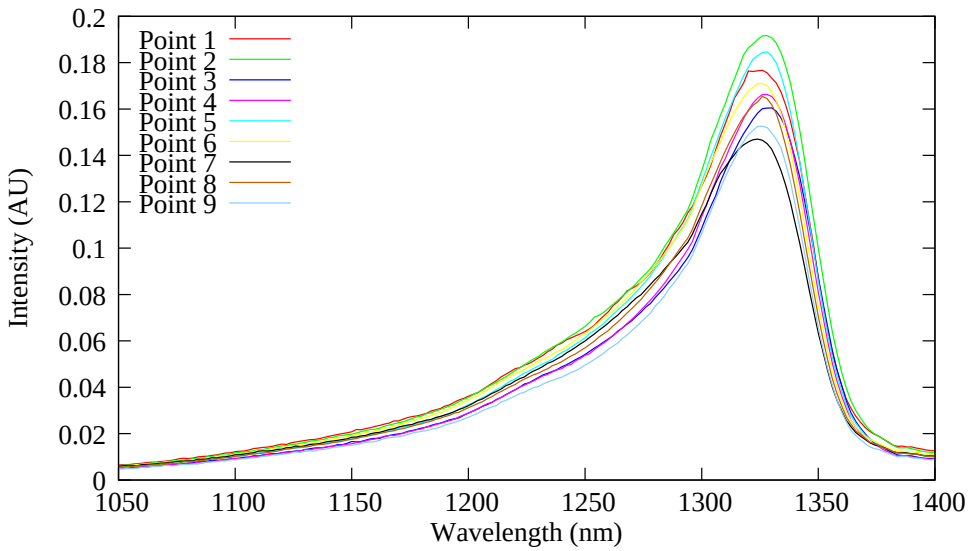

Figure 4.6: PL peak for the ZLG 246.2 InAs Dot sample

damage. This initial run did not yield any significant change in the PL spectra both immediately after exposure and several days afterwards. Problems in making consistent measurements at each of the prescribed points were considered and a new test sample geometry was devised. The failure of the long exposure of the ^{137}Cs to cause any measurable change in the Quantum Dots attest to the radiation hardness of this material but also highlighted that we needed to search for a more damaging source of radiation to stress our samples further. Thus, we elected to try very high energy irradiation to see if a short burst at that level would have any effect. The problems we encountered reliably probing the quarter wafer for PL measurements directed us to change the test sample geometry. Cleaving a rectangular bar from the wafer as shown in figure 4.3 allowed us to make more consistent measurements in only one free dimension which exploited the radial symmetry of the MBE growth itself. These samples were mounted on glass slides for ease of transport and measurement. We gained access to a linear accelerator that could produce photon streams of high energy and intensity. We irradiated the sample with 15 MeV photons for a brief period of time. PL measurements of the wafer bar were taken before and after the

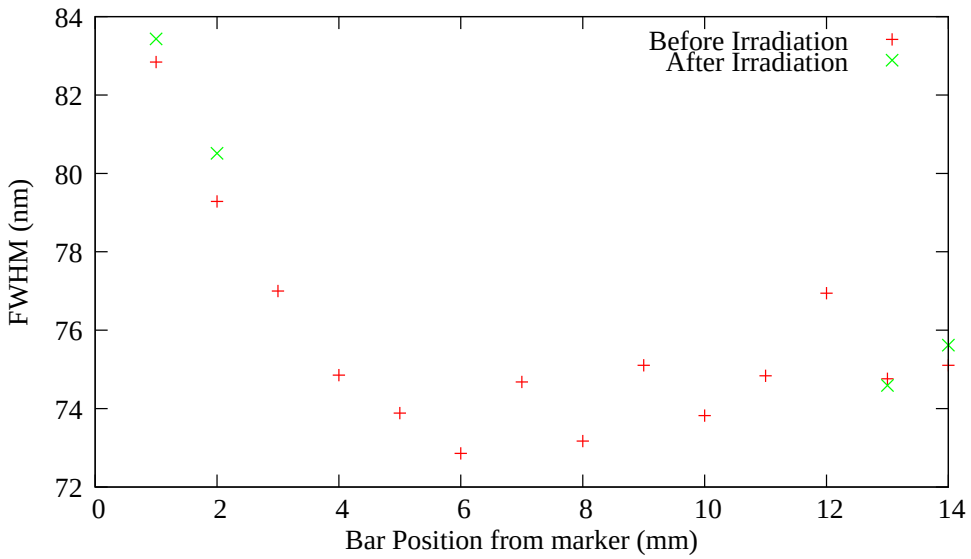

Figure 4.7: FWHM of PL before and after second irradiation of ZLG 246.2

irradiation session. The full width half max of the sample's PL peak is shown in figure 4.7 and the change in max intensity is shown in figure 4.8. The distance on the horizontal axis of both plots represents the distance from a standardized mark proceeding outwards from the original wafer center. s

The results are clear that the irradiation even with a photon energy orders of magnitude higher than our first radiation source is insufficient to cause damage to the quantum dot gain media in a way measurable by PL. These results are even further evidence of radiation hardness of the Quantum Dot Material. However, these inferences need to be further examined with additional radiation sources and targets. We lay out these processes in the next section.

4.3.2 ^{60}Co Irradiation Session with Broader Samples

It was clear that higher energy and larger irradiation doses individually didn't achieve any significant damage on our samples. Thus, we elected to pursue a higher energy

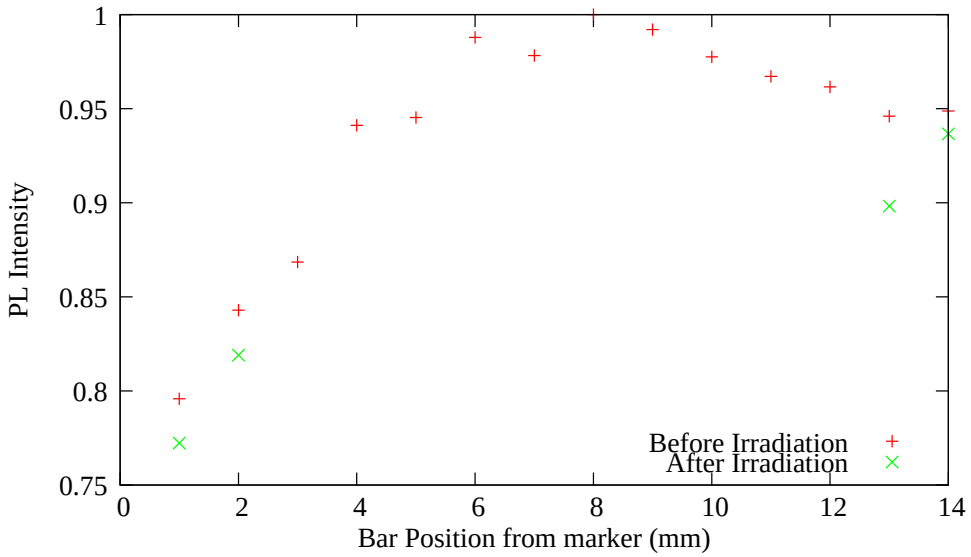

Figure 4.8: Max intensity of PL before and after second irradiation of ZLG 246.2

source that could provide a much larger dose in a short time. The hope was to shock the devices with a large amount of energy very quickly and observe the result before any relaxation effect could be observed. We gained access to the ^{60}Co source at Kirtland Air Force Base for a large scale irradiation of three samples of varying material composition. Specifically, we incorporated the InAs Dashes on InP as well as Quantum Well devices as mentioned earlier in the material description.

All of the samples were mounted on microscope slides for ease of handling. The irradiation chamber setup is shown in figure 4.9 with the radioactive source contained within a 4" diameter cylindrical dust cover. The source is raised from the shielding below the testing table and rests inside the dust cover when the irradiation is in progress. All of the samples were positioned around the dust cover 0.8 cm from the edge of that lip. Calibration for radiation dose rate was done at that distance immediately before the irradiation run to ensure uniformity. We measured a dose in excess of 100 Rad/s with the rad unit being measured for silicon absorption. The irradiation target for this run was 1.5 MRad, which took about 2 hours at the

measured irradiation rate. The sample was set to automatically retract when the target times were reached so that the desired dose could be reached precisely. The Air Force Research Laboratory's facilities were invaluable in this effort allowing for a large radiation dose in a small time. However, the examination of the data did not show significant changes to the PL profiles on the samples which implies that even the larger dose was shrugged off by these measured samples. The measured data for this irradiation session is presented in figures 4.10-4.15

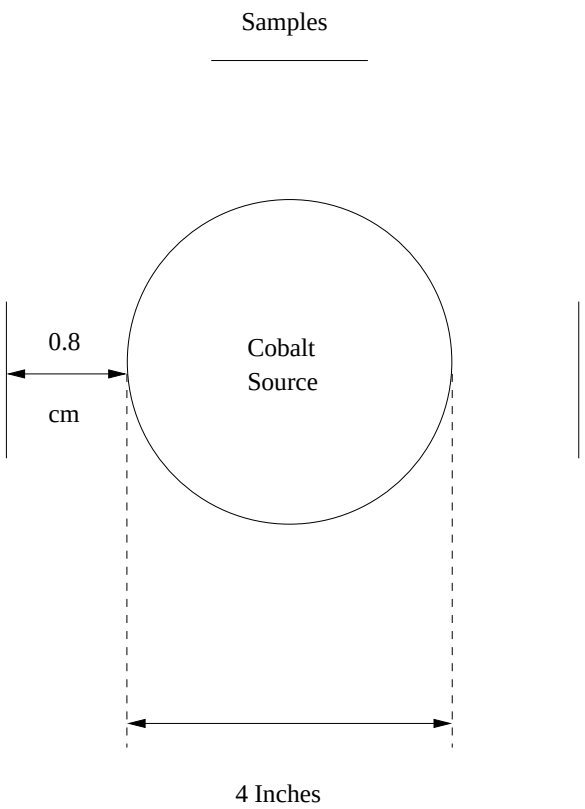

Figure 4.9: Schematic diagram of the ^{60}Co irradiator

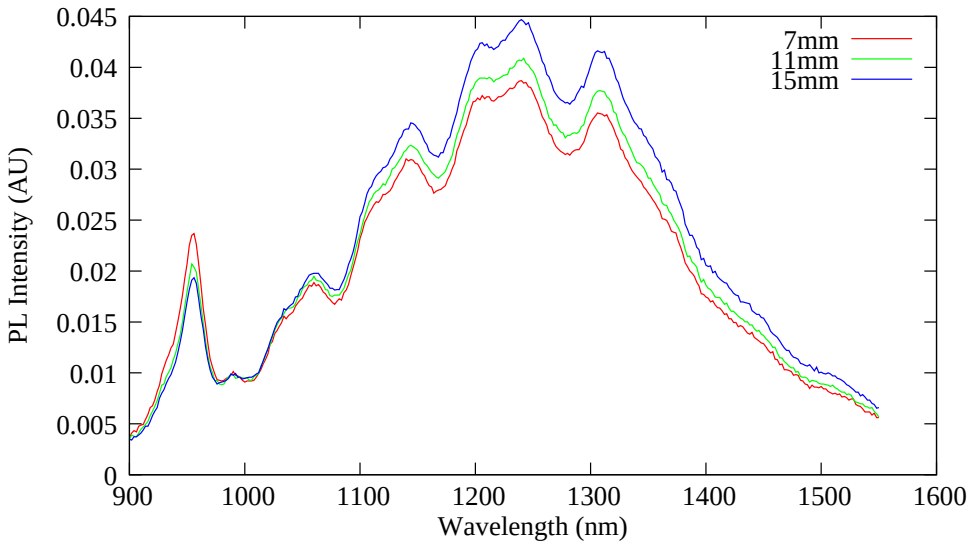

Figure 4.10: Quantum Wells before irradiation

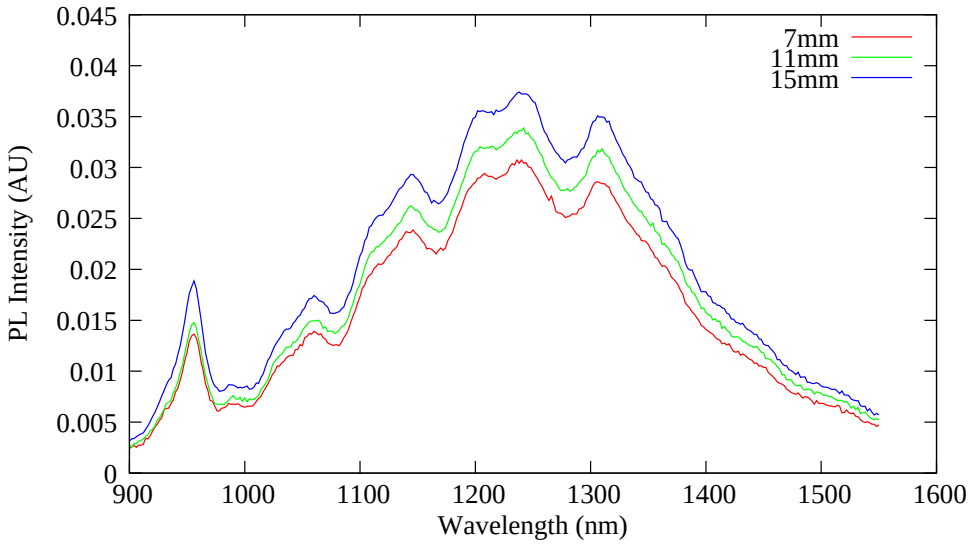

Figure 4.11: Quantum Wells after irradiation

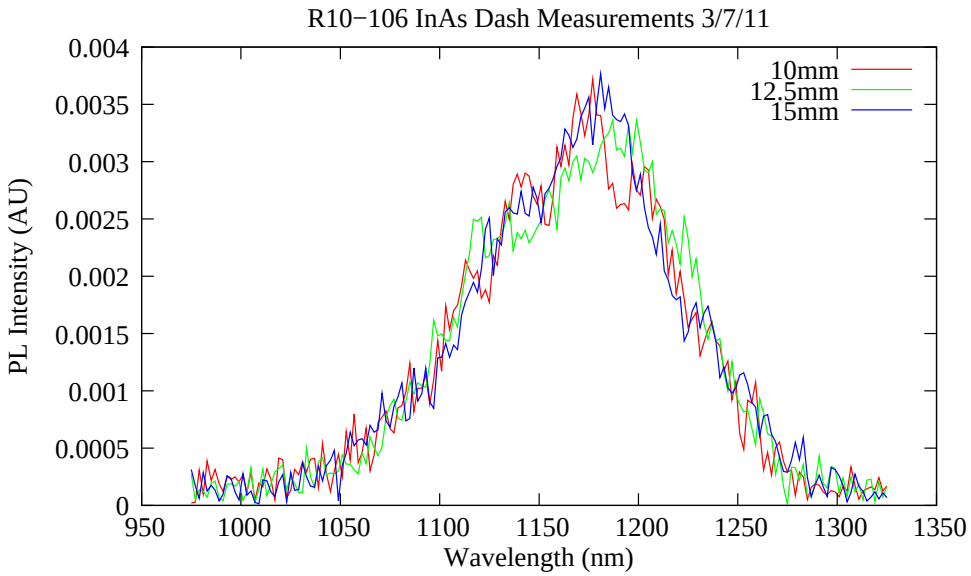

Figure 4.12: InAs Dashes before irradiation

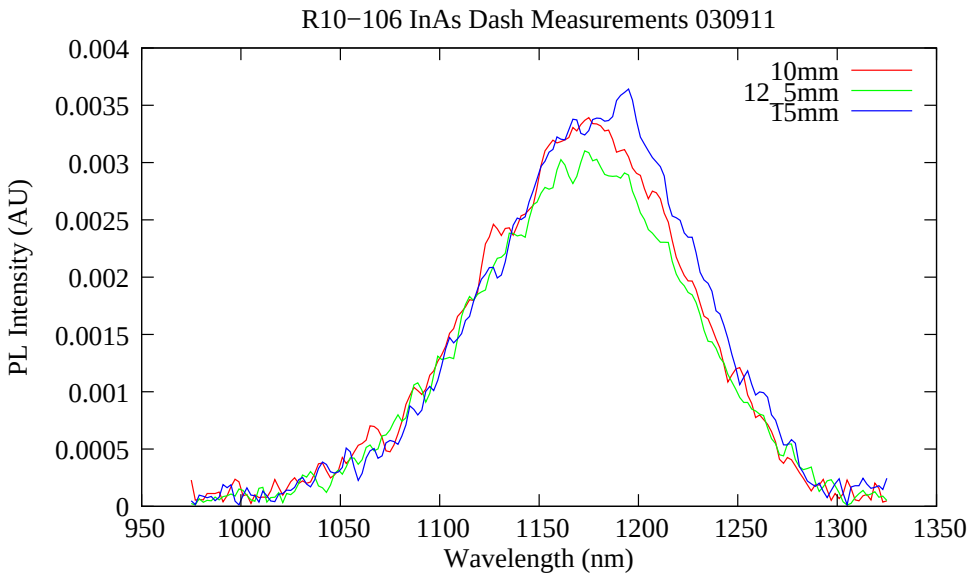

Figure 4.13: InAs Dashes after irradiation

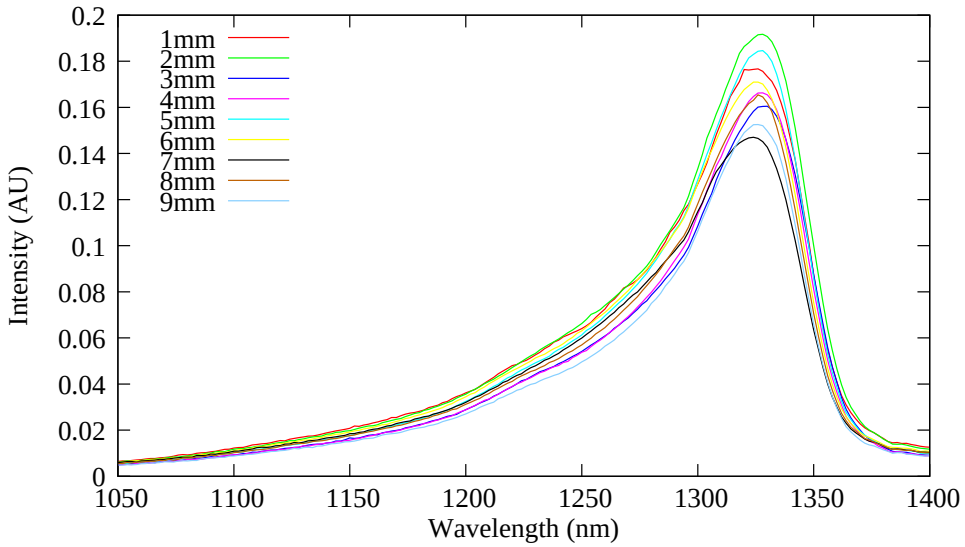

Figure 4.14: InAs Dots before irradiation

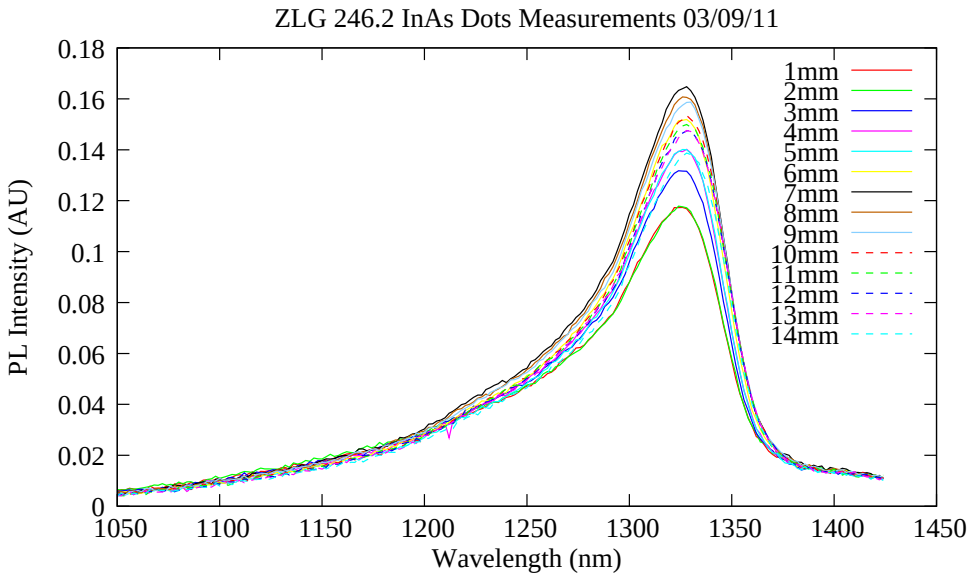

Figure 4.15: InAs Dots after irradiation

4.4 QDMLL Laser Irradiation

The initial studies with the three types of quantum epitaxial structures that were unprocessed showed little susceptibility to gamma irradiation of any kind. This is encouraging. Exposure to sessions of irradiation that far exceeds the parameters in any orbital mission leaving little doubt to the fitness of these materials to serve in an orbital capacity. This confidence gave us the confidence to commence the same gamma irradiation experiments on actual QDMLLs. We predicted, based on observation of the unprocessed material and the physical configuration of the quantum dot media, that the lasers themselves would behave similarly.

4.4.1 Device Characterization Methods

The fundamental method of analysis used in this study is the comparison of device modal gain, which can be used to predict device operation as well as mode locking conditions. The laser used in this test has been examined for its device modal gain as well as the pulse characteristics at various bias conditions. These benchmarks are achieved using the segmented contact method [16], and the damage behavior is modeled based on temperature performance estimates [12]. These tests were performed again after the irradiation session and the results recorded. Temperature variation tests using the segmented contact method produce data that can be used in predictive models.

A temperature dependent picture of the gain profile of our quantum dot laser devices is critical to our prediction of the device properties. To this end, a measurement setup was devised that has the planned capability to perform data sampling at the full range of temperatures required for this work. This setup is capable of temperature ranges from 10C to 40C. The system is designed with a very high thermal mass near the laser itself to maintain equilibrium temperature during each of

these current measurements. The schematic diagram of the experimental setup is given in figure 4.16. The device is comprised of 11 electrical isolated sections with dimensions of 0.5 mm x 0.0035 mm. The gain sections are comprised of two device sections making the total length of each 1mm. The remainder of the device length is used as an absorber to reduce back reflections.

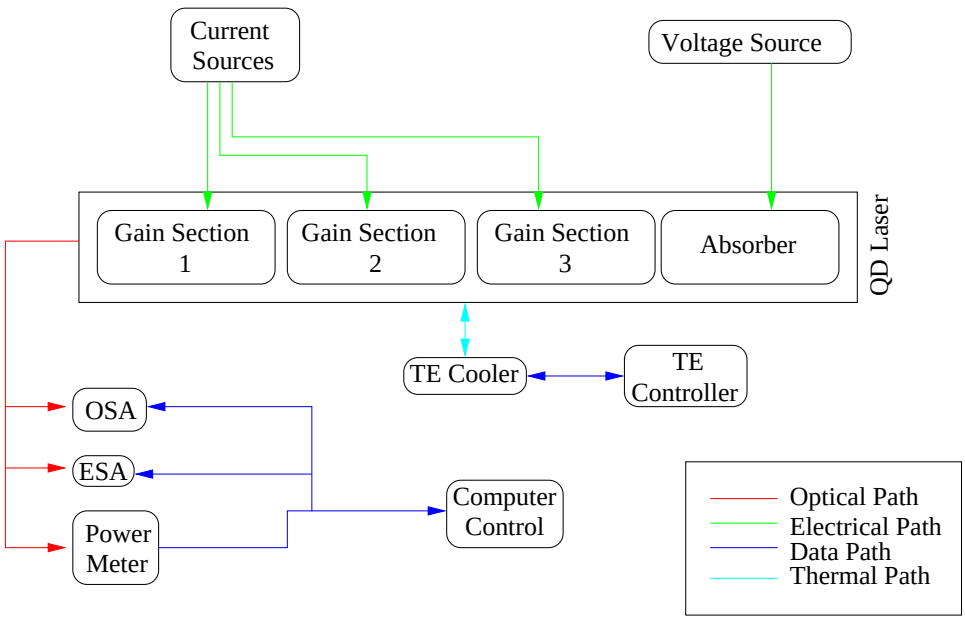

Figure 4.16: Segmented contact measurement setup for measurement of laser gain

Electronic control was done using an electronic control board re-purposed from previous work at UNM. Two current sources and a voltage source are used to stimulate the device and measurement was conducted using an integrating sphere power meter and an Agilent spectrometer. Data capture was performed via GPIB connections to a central computer. Coupling of the laser light from the Quantum Dot laser is achieved through an integrated optical head containing a small lens and isolator. This head couples the light into a fiber which is routed to the measurement equipment. The coupling lens was optically coated to reduce back reflections.

The theory behind the segmented contact gain measurement method is taken from the previously published work [9]. Our measurement method requires single pass amplification of spontaneous emission of the gain sections shown in figure 4.16. The expression for computing the net modal gain of the laser is given in the following equation 4.1.

$$g = L^{-1} ln \left(\frac{I_3 - I_1}{I_2 - I_1} - 1 \right) \tag{4.1}$$

Where I indicates the intensity from each of the three measurement steps and L is the length of the gain sections. Absorption measurements can be arrived at using a similar technique with the following expression 4.2.

$$a = L^{-1} ln \left(\frac{I_2 - I_1}{I_4 - I_1} \right) \tag{4.2}$$

Where the variables follow the convention. Further detail of this method can be found in the literature and in the method chapter of this dissertation. We can now proceed to the results as a function of temperature or radiation damage by looking at differences. The last piece of information that can be gleaned about the laser is the value of the internal loss of the cavity. The convergence point for the gain measurement data at longer wavelength is a representation of the internal loss of the cavity in cm^{-1}. This is a measure of the loss in the optical waveguide as an aggregate of all scattering and provides an excellent method for assessing viability.

4.4.2 Irradiation and Experimental Methods

Previous experiments with Quantum Dot Lasers operating in CW have shown that they can operate while under gamma irradiation even after exposures as high as 120

Mrad [5]. Work with the gain material had shown resilience up to 1.5 Mrad as well. This provides an excellent backstop for our test because such dosages are well beyond what is proposed in this investigation. On orbit exposure observed at geostationary altitude averages about 3.4 krad per year [6]. One must also consider the effect of periodic solar flares that would increase the radiation dosage. Worst case estimates for dosages on orbit have been calculated from historical events. Expectations for the largest feasible solar events could add an additional 1.5 krad for a satellite in the most susceptible polar orbits [19]. Two devices were selected for irradiation. First was a device selected because of its usefulness to gain profile measurements using the segmented contact method. The second device is a working laser that can be used to test the effect of irradiation on the mode-locking pulses of the laser itself. Characterization of both devices used in the irradiation test was completed to provide a baseline temperature and electrical response. One irradiation session of 2.2 MRads from a ^{60}Co source has been performed, which would correspond to an average flight duration of several centuries. This provides an excellent reliability standard for integration into any system and provides an exceptionally high ceiling for radiation bursts. These bursts of radiation from solar events or of cosmic origin can greatly exceed the average exposure values. Analysis of the gain and loss curves of the diagnostic devices after the irradiation will provide us with the metrics that we can gauge the overall effect of the radiation damage. The testing facility was the ^{60}Co irradiation facility at the Air Force Research Laboratory in Albuquerque, NM. This highly energetic source allowed us to examine the behavior of the device after a significant radiation dose. Verification of mode locked operation after the irradiation set is satisfactory to confirm the hardness of the device. Mode-locked operation is verified through the use of a high speed digitizing oscilloscope and an optical autocorrelator. Further characterization of the thermal characteristics of the lasers themselves allowed us to determine a full range of the mode locking capability even after irradiation far beyond what would be expected in an operational flight.

4.4.3 QDMLL Irradiation Results

Characterization of the two lasers used in the study began with a gain and loss measurement characterization across a broad temperature range over the entire emission bandwidth. The multisection laser was used for this purpose because its evenly divided sections allowed for the execution of the segmented contact method as previously discussed. The following matrix sampling ranges were assessed for the fitness of the laser. Its gain and loss data was taken for 20,40,60,80,100,110, and 120 C. These net modal gain plots are shown in figure 4.17. This determines the absolute gain profile as the laser warms. The gain curve of the laser becomes informative in the full range of mode locking possibilities.

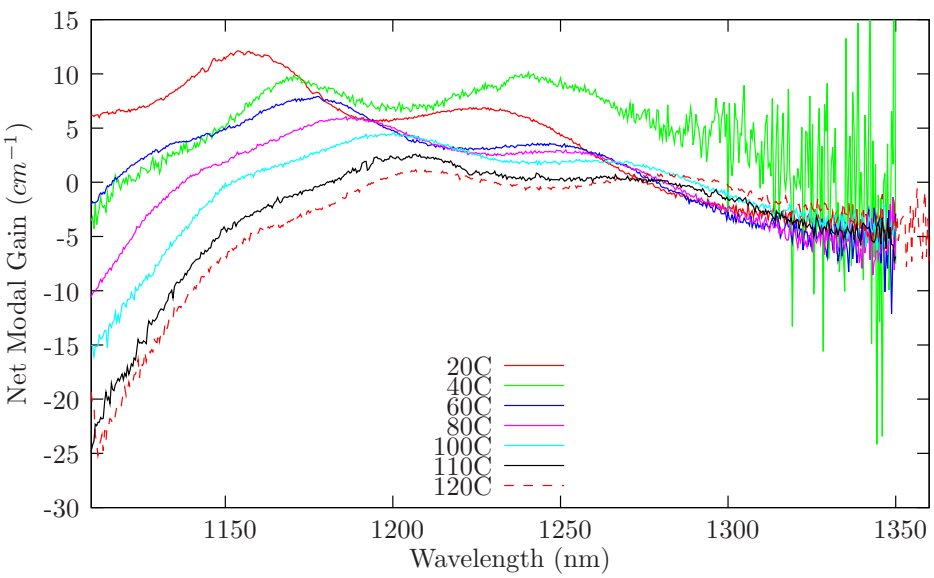

Figure 4.17: Gain profile measurements at constant current density over temperature for the 788 Multisection

The information presented in figure 4.17 provides the basic operation characteristics of the laser which we can use to extract the idealized mode locking regimes. Using the following expressions [20, 21], we show the predicted range of mode locking.

$$\frac{L_a}{L_g} > \left(\frac{\frac{dg_o}{dJ}}{\frac{dg_o}{dJ}|_{g_o=0}} \right)^2 \frac{g_o(J)}{a_o} \tag{4.3}$$

$$\frac{L_a}{L_g} = \frac{g_o(J) - \alpha_m - \alpha_i}{a_o + \alpha_m + \alpha_i} \tag{4.4}$$

Where J is current density, L are length measurements, g is the gain value, and α are the absorption values of the laser. The former expression defines the minimum mode locking condition which provides a lower bound to the operational current density of the laser. The second equation is the lasing threshold condition which determines the upper bound of the absorption values permissible for the laser to operate. This is all framed in terms of the absorber and gain length ratios which consider the physical length of the two parts on the laser itself. The results of these computations are then plotted graphically into a series of concentric curves. The regions within these curves are current and device configurations deemed suitable for mode locking operations. Detailed analysis of lasers with multiple examples of the absorber/gain length ratio has proven this model to be robust in its predictions [22].

The expected mode locking range for our device from the multisection prediction is shown in figure 4.18. The enclosed regions of the curve again indicate regions of expected mode locking. Plotted lines indicating different hypothetical devices with varying absorber lengths help illustrate that a single device can operate in a mode locking regime over a wide temperature range. Explicitly, a laser configuration can exhibit mode locking operation for a wider temperature range the more enclosed regions are traversed by the horizontal line representing it.

We then turned our attention to the second device under test which was a more traditional 2 section laser. We developed a measurement scheme to sample the laser

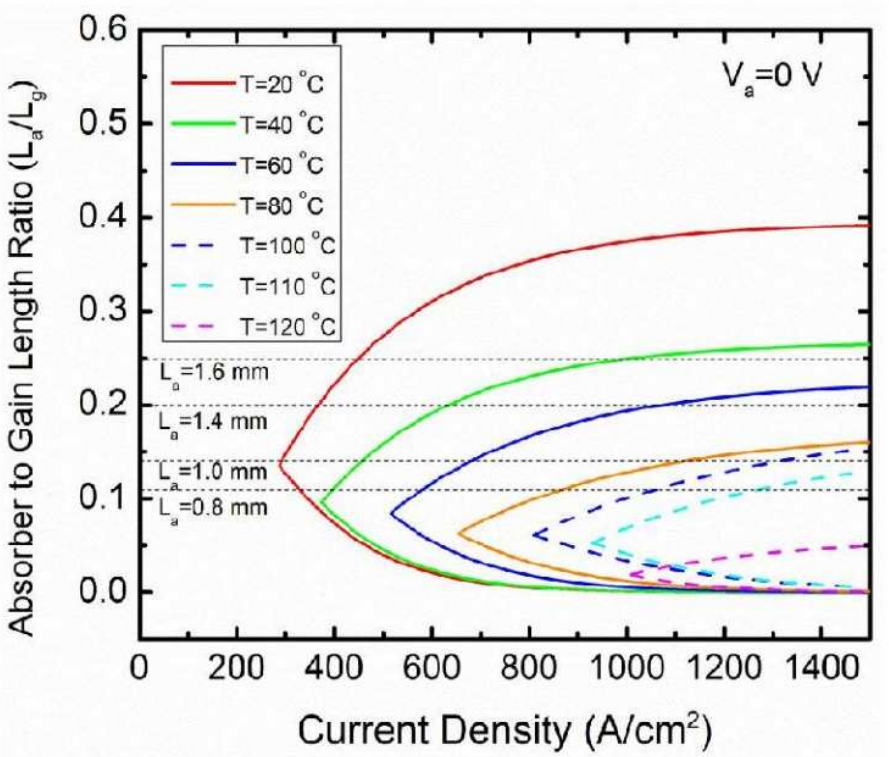

Figure 4.18: Predicted mode locking range for the QDMLL [22]

over a wide range of biasing parameters to examine the boundaries of mode locking. We found excellent agreement with the model and verified that our QDMLLs can operate over a broad range of conditions as shown in figure 4.19.

Post irradiation measurements of these lasers were done selectively rather than attempt to reproduce the entire map. As expected, the laser continued to be able to mode lock even after bombardment with 2.2 MRads of ionizing radiation from a ^{60}Co source. Further investigation is required over a longer irradiation period to determine the precise failure condition of these lasers.

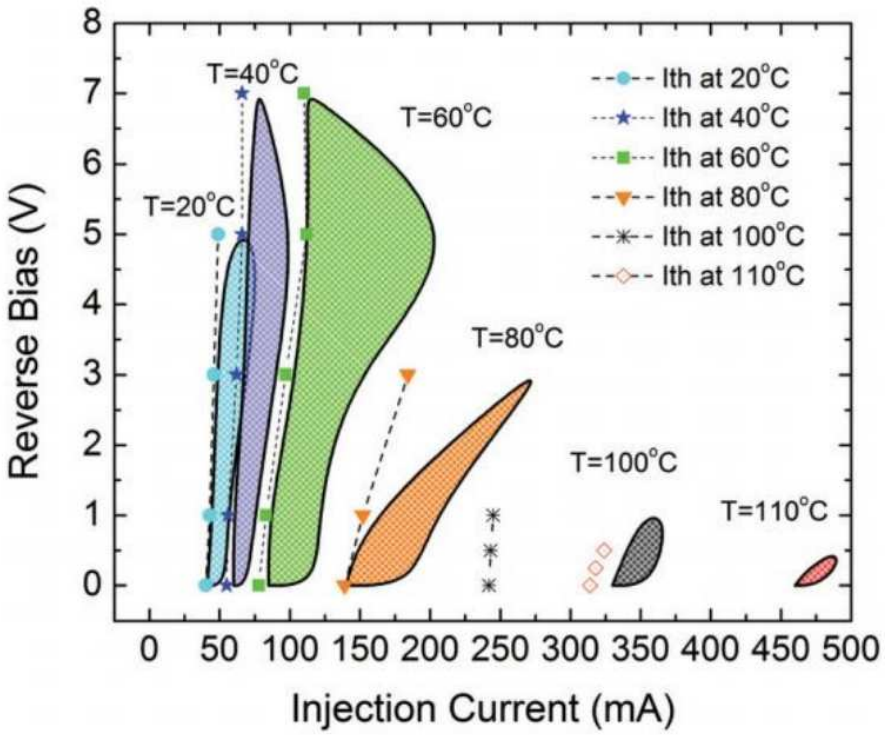

Figure 4.19: Observed mode locking for the QDMLL [22]

4.5 Conclusions

In short, irradiation of Quantum Dot Gain Material both in unprocessed form and in working devices must be massive to produce detrimental effects in either PL curves or Mode Locking criteria. None of our experiments with irradiation levels across a range of ionization energies with total doses exceeding all that would be expected for an extended orbital mission produced significant degradation to device performance. This result is a reinforcement of previous work that dealt only with lasing threshold degradation as a function of applied radiation dose. We suspect that the partitioned nature of the gain material, consisting of many quantum dots, is less susceptible to radiation damage as destruction of a few of these dots does not significantly impact the performance of the device as a whole. Broad scale analysis of these parameters

provides us the baseline for comparison to evaluate the health of these devices after the irradiation set was completed [22, 17]. Initial device testing has shown that mode locking is possible after the irradiation, but the extent of the damage has not yet been quantified because the lasers were not tremendously harmed by the irradiation set. This technology provides excellent promise for integration into systems that operate in environments of high radiation hazards and wider temperature conditions. The durability benefit is compounded by the compact size and low mass of these devices and the equipment necessary to control them. These devices are remarkably radiation hard and deserve further investigation for integration into next generation communications systems in extreme environments. This conclusion is drawn from the observation of the predictions of the gain and loss measurements that provide the basis for our device characterization showing this method can be used to characterize degradation in performance caused by factors other than simple thermal variation.

References for Chapter 4

[1] X. Liu, M. H. Hu, C. G. Caneau, R. Bhat, and C.-e. Zah, "Thermal management strategies for high power semiconductor pump lasers," *Components and Packaging Technologies, IEEE Transactions on*, vol. 29, pp. 268–276, June 2006.

[2] J. K. Mee, M. T. Crowley, N. Patel, D. Murrell, R. Raghunathan, A. Aboketaf, A. Elshaari, S. F. Preble, P. Ampadu, and L. F. Lester, "110 C operation of monolithic quantum dot passively mode-locked lasers," in *Semiconductor Laser Conference (ISLC), 2012 23rd IEEE International*, pp. 68–69, AFRL/RVSE, Kirtland AFB, NM, USA, IEEE, Oct. 2012.

[3] R. Leon, G. M. Swift, B. Magness, W. A. Taylor, Y. S. Tang, K. L. Wang, P. Dowd, and Y. H. Zhang, "Changes in luminescence emission induced by proton irradiation: InGaAs/GaAs quantum wells and quantum dots," *Applied Physics Letters*, vol. 76, no. 15, pp. 2074–2076, 2000.

[4] A. Cavaco, N. A. Sobolev, M. C. Carmo, F. Guffarth, H. Born, R. Heitz, A. Hoffmann, and D. Bimberg, "Carrier dynamics in particle-irradiated InGaAs/GaAs quantum dots," *phys. stat. sol. (c)*, vol. 0, no. 4, pp. 1177–1180, 2003.

[5] J. W. Mares, J. Harben, A. V. Thompson, D. W. Schoenfeld, and W. V. Schoenfeld, "Gamma Radiation Induced Degradation of Operating Quantum Dot Lasers," *IEEE Transactions on Nuclear Science*, vol. 55, pp. 763–768, Apr. 2008.

[6] B. R. Bhat, N. Upadhyaya, and R. Kulkarni, "Total radiation dose at geostationary orbit," *IEEE Transactions on Nuclear Science*, vol. 52, pp. 530–534, Apr. 2005.

[7] G. Reitz and G. R. Ã, "Characteristic of the radiation field in low earth orbit and in deep space," *Zeitschrift für Medizinische Physik*, vol. 18, pp. 233–243, Dec. 2008.

[8] M. Van Uffelen, J. Mols, A. Goussarov, C. Neumeyr, M. Ortsiefer, and F. Berghmans, "Comparison of gamma and proton-induced radiation damage in long-wavelength VCSELs," in *2007 9th European Conference on Radiation and Its Effects on Components and Systems*, pp. 1–4, IEEE, Sept. 2007.

[9] Y. C. Xin, Y. Li, A. Martinez, T. J. Rotter, H. Su, L. Zhang, A. L. Gray, S. Luong, K. Sun, Z. Zou, J. Zilko, P. M. Varangis, L. F. Lester, and S. Member, "Optical gain and absorption of quantum dots measured using an alternative segmented contact method," *Quantum Electronics, IEEE Journal of*, vol. 42, pp. 725–732, July 2006.

[10] K. Brown, B. Wysocki, M. Fanto, J. Malowicki, V. Kovanis, and L. Lester, "Control over spectral content via differential pumping of a monolithic passively mode-locked quantum dot laser," *Proceedings of SPIE*, vol. 6572, pp. 65720A+, May 2007.

[11] Y. P. Zhou, G. L. Chang, J. Q. Zhou, J. Ma, and L. Y. Tan, "Gamma-ray irradiation effects on distributed-feedback laser diodes," *Journal of Russian Laser Research*, vol. 30, pp. 164–171, Mar. 2009.

[12] N. A. Sobolev, A. Cavaco, M. C. Carmo, M. Grundmann, F. Heinrichsdorff, and D. Bimberg, "Enhanced Radiation Hardness of InAs/GaAs Quantum Dot Structures," *phys. stat. sol. (b)*, vol. 224, no. 1, pp. 93–96, 2001.

[13] F. Guffarth, R. Heitz, M. Geller, C. Kapteyn, H. Born, R. Sellin, A. Hoffmann, D. Bimberg, N. a. Sobolev, and M. C. Carmo, "Radiation hardness of InGaAs/GaAs quantum dots," *Applied Physics Letters*, vol. 82, no. 12, pp. 1941–1943, 2003.

[14] Y.-C. C. Y. Xin, A. Stintz, H. Cao, L. Zhang, A. L. Gray, S. R. Bank, M. Osinski, J. Harris, and L. F. Lester, "Monolithic passively mode-locked lasers using quantum-dot or quantum-well materials grown on GaAs substrates (Proceedings Paper)," in *Integrated Optoelectronic Devices 2007* (M. Osinski, F. Henneberger, and Y. Arakawa, eds.), vol. 6468, International Society for Optics and Photonics, Mar. 2007.

[15] A. Stintz, G. T. Liu, H. Li, L. F. Lester, and K. J. Malloy, "Low-threshold current density 1.3-μm InAs quantum-dot lasers with the dots-in-a-well (DWELL) structure," *Photonics Technology Letters, IEEE*, vol. 12, pp. 591–593, Aug. 2002.

[16] G. T. Liu, A. Stintz, H. Li, T. C. Newell, A. L. Gray, P. M. Varangis, K. J. Malloy, and L. F. Lester, "The influence of quantum-well composition on the performance of quantum dot lasers using InAs/InGaAs dots-in-a-well (DWELL)

structures," *Quantum Electronics, IEEE Journal of*, vol. 36, pp. 1272–1279, Nov. 2000.

[17] D. Murrell, M. T. Crowley, M. Breivik, R. Raghunathan, A. Aboketaf, A. Elshaari, S. F. Preble, B. O. Fimland, and L. F. Lester, "Design of uncooled high-bandwidth ultra-low energy per bit quantum dot laser transmitters for chip to chip optical interconnects," in *2012 Optical Interconnects Conference*, (Santa Fe, NM), pp. 72–73, IEEE, May 2012.

[18] J. H. Hubbell and S. M. Seltzer, "NIST: X-Ray Mass Coefficients," 1996.

[19] L. W. Townsend, J. L. Hoff, and D. L. Stephens, "Hypothetical worst case solar particle event doses in LE0," in *2004 IEEE Aerospace Conference Proceedings (IEEE Cat. No.04TH8720)*, vol. 1, pp. 589–595, Dept. of Nucl. Eng., Tennessee Univ., Knoxville, TN, USA, IEEE, Mar. 2004.

[20] C. Y. Lin, Y. C. Xin, Y. Li, F. L. Chiragh, and L. F. Lester, "Cavity design and characteristics of monolithic long-wavelength InAs/InP quantum dash passively mode-locked lasers," *Optics express*, vol. 17, pp. 19739–19748, Oct. 2009.

[21] M. T. Crowley, D. Murrell, N. Patel, M. Breivik, C.-Y. Lin, Y. Li, B.-O. Fimland, and L. F. Lester, "Analytical Modeling of the Temperature Performance of Monolithic Passively {Mode-Locked} Quantum Dot Lasers," *IEEE Journal of Quantum Electronics*, vol. 47, p. 1059, Feb. 2011.

[22] J. K. Mee, M. T. Crowley, D. Murrell, R. Raghunathan, L. F. Lester, and S. Member, "Temperature Performance of Monolithic Passively Mode-Locked Quantum Dot Lasers: Experiments and Analytical Modeling," *Selected Topics in Quantum Electronics, IEEE Journal of*, vol. 19, p. 1101110, July 2013.

Chapter 5

Examination of Higher Repetition Rates in QDMLLs

5.1 Introduction

The fundamental repetition rate of a Quantum Dot Mode Locked Laser (QDMLL) follows the same relation as any other edge emitting device as shown in equation 5.1.

$$\nu = \frac{c}{2nL} \tag{5.1}$$

Where ν is the repetition rate, c is the speed of light, n is the optical index of the material (typically 3.4 for GaAs) [1], and L is the length of the cavity. One cannot simply reduce the cavity length L without limit to increase the repetition rate. Limits in modal gain for ultrashort cavities will inhibit lasing. However, it is also possible to excite higher order harmonics that are integer multiples [2] of the fundamental rate defined in equation 5.1. Efforts to increase the base repetition rate of QDMLLs have grown ever more urgent as industrial communication standards

[3] begin to approach the 100 GHz threshold. Reporting of subsequent records and new approaches to higher base repetition rates have been remarkable, but mostly iterative. In this study, I present an analytical method to approximate the maximum repetition rate of QDMLLs using their cavity configuration and gain profiles as the variable parameters. Specifically, I examine the often neglected differential gain as a function of carrier density to gain insight into the fundamental limitations of device repetition rate regardless of cavity geometry. These analytical methods can be used to forecast the potential of existing QDMLL devices and inform the design of next generation devices.

Additionally, I examine values of maximum possible repetition rates using an alternative derivation of previous models reported in our research group [4]. The intention here is to examine the physical parameters and try to define ballpark limits analytically; then efforts can be focused on elements of the laser design that could be used to increase the repetition rate upper limits. These two approaches using ratioed methods and numerical evaluation provide insight into how fast the QDMLLs can operate.

5.2 Upper Limits of the Repetition Rates

New interpretations of the evolved phasor mode locking model [5] are investigated in order to project the maximum performance of QDMLL lasers under test. First, the device (internally identified as wafer 789) is characterized for gain and loss values and examined with two different methods of analysis. One method focuses on evaluating device potential based on physical parameters and the other based on the absorption contrast. Both methods report similar values for higher limits of repetition rates.

5.2.1 Gain Characteristics of Quantum Confined Media

Laser gain materials that exhibit quantum confinement provide unique properties that are beneficial [6] to passive mode locking. The fast gain recovery time, low threshold current density, and high differential gain are boons to stable pulsation. Stricter quantum confinement as exhibited in Quantum Dots provide the greatest enhancements due to their density of state profile. Quantum dashes and quantum wells also exhibit these desirable mode locking qualities but to a lesser degree. Our template for investigation is a QDMLL that utilizes 6 layers of InAs/InGaAs Quantum Dot gain media with a Dots-in-a-Well (DWELL) configuration. The device has 11 sections, a total device length of 5.5 mm, and a width of 3.5 μm. Unsaturated gain and loss values were measured using the segmented contact method [7]. These gain values are illustrated in figure 5.1 and the absorption values are noted for our calculations. The device measured for this study also has reported values for its maximum repetition rate [2].

$$f(x) = a - b\, e^{c\, x} \tag{5.2}$$

The emission peak for the ground state is identified as 1243.1 nm and the excited state at 1154.4 nm. The gain profiles for both the ground and excited state were fit with equation 5.2. The fitting results using nonlinear least squares methods for the ground and excited state are shown in table 5.1. These parameters were fit to the original data collected and will produce a curve with units of cm^{-1} vs current per section. A translation factor is applied to transform the applied current value into a current density of A/cm^2. The information from the gain profiles in figure 5.1 and the subsequent measurement of the unsaturated absorption allows us to provide experimental backing to our evaluation of equations 5.9, 5.10, and 5.12 derived later. The explicit values for the constants used are given in table 5.2. The

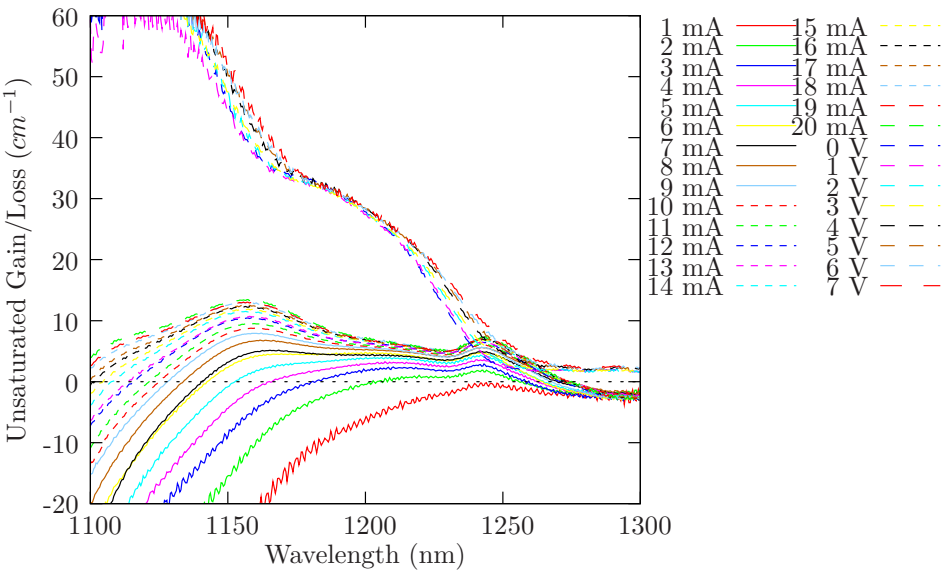

Figure 5.1: Measured Gain and Loss values for the QDMLL under investigation

baseline value used for the differential absorption is on the order of $10^{-15}\ cm^2$ as previously reported for comparable devices [8]. This physical measurement provides experimental grounding to my theoretical examination.

Variable	Value	Uncertainty	% Error
Ground State			
a	7.218	± 0.130	(1.8%)
b	9.037	± 0.284	(3.14%)
c	-0.210	± 0.015	(6.93%)
Excited State			
a	12.298	± 0.464	(3.77%)
b	49.062	± 1.731	(3.53%)
c	-0.283	± 0.017	(6.03%)

Table 5.1: Fitting parameters for the gain function $f(x) = a - b\,Exp[c\,x]$ applied to the 789 device measurements

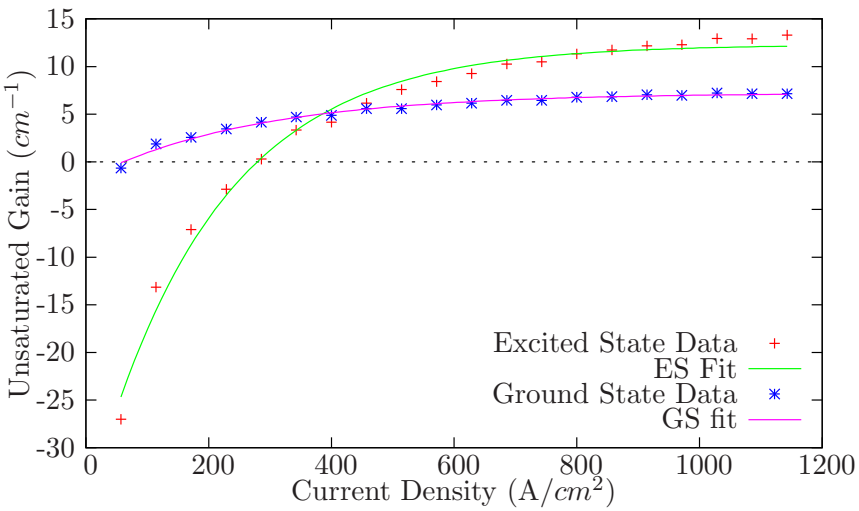

Figure 5.2: Gain curves of the 789 device for the ground and excited state with fits

Figure 5.2 illustrates the data graphically. From this fit, we can quickly calculate the differential gain. Quick analysis shows that transparency occurs at a current density of 61.04 A/cm^2 for the ground state and 279.35 A/cm^2 for the excited state.

5.2.2 Max Repetition Rate Derivations

Analysis of the maximum repetition rate phasor expressions in previous work [4] warranted a second look at the theoretical source material previously derived in Lau's work on the subject [5]. This provides the basis for equation 5.3.

$$\left(G_a^2 a_o \frac{L_a}{L} - G_g^2 g_o \frac{L_g}{L}\right) \frac{S_o^2}{2\Omega_{MLL}^2} > \alpha_i \tag{5.3}$$

$$Repetition\ Rate = \frac{v_g}{2L} = \Omega_{MLL} \tag{5.4}$$

$$\frac{\Gamma P}{\alpha_m v_g h\nu W dL} = S_o \tag{5.5}$$

$$v_g \frac{dx_o}{dn} = G_x \tag{5.6}$$

Where the MLL repetition rate is given by equation 5.4, the photon constant S_o is defined in equation 5.5, and the differential gain/absorption contribution G_x is given generally by equation 5.6. Additionally, a_o is the unsaturated absorption, g_o is the unsaturated gain, L_g is the length of the gain section, L_a is the length of the absorber section, L is the device length, v_g is the device group velocity, α_m is the mirror loss, α_i is the internal loss, W is the thickness of the active region, d is the width of the device, Γ is the optical confinement factor, P is the peak pulse power, and ν is the emission frequency.

This entire model is derived based on a sinusoidal approximation with the gain and absorption contrast illustrated on the LHS of equation 5.3 features prominently in the argument of the exponential oscillation that projects the pulsewidth. Lau's model [5] claims that mode locking collapses if the gain and absorption contrast is equal to zero. This is due to a collapse of oscillation as the argument of the oscillating exponential becomes a real number. Thus, the model fails to oscillate. The addition of the internal loss as a supplemental restriction [4] of the mode locking in equation 5.3 provides an another constraint beyond the theoretical limits.

Now we revisit the assumption that the unsaturated gain is much less than the saturated absorption and that differential absorption is approximately equal to the differential gain when evaluated at transparency. Thus, equation 5.3 is rearranged to equation 5.7

$$\sqrt{\left(G_g^2\big|_{g_o=0} a_o \frac{L_a}{L}\right) \frac{S_o^2}{2\alpha_i}} > \Omega_{MLL} \tag{5.7}$$

The measurement of the carrier density of the laser itself is difficult to accomplish directly so I perform a substitution to use the differential current density which can be more readily measured. Performing the substitution in equation 5.8 results in equation 5.9.

$$v_g \frac{dg}{dn} = v_g \frac{dg}{dJ} \frac{q\eta_i W}{\tau} = G_g \tag{5.8}$$

$$\sqrt{\left(\frac{dg}{dJ}\Big|_{g_o=0} \frac{q\eta_i}{\tau}\right)^2 \left(\frac{\Gamma P}{\alpha_m h\nu dL}\right)^2 \frac{a_o L_a}{2L\alpha_i}} > \Omega_{MLL} \tag{5.9}$$

Where η_i is the injection efficiency, q is the elementary charge, and τ is the carrier lifetime. Interestingly, the dominant parameter that determines the maximum repetition rate is the peak power of the pulse itself. This observation corresponds with experimental measurements showing that the higher repetition rate lasers all have higher pulse power either as a result of additional gain or shorter pulse width. Using equation 5.9, I examine previously reported cases [2] exploring cavity geometries that divide the laser into active gain sections, passive waveguide sections, and absorbing sections. Then, I project the max repetition rate based on the constants in table 5.2 using equation 5.9 which represents the best case mode locking scenario.

ν	$\frac{c}{1243 \times 10^{-9}}$ Hz
W	2.16×10^{-6} cm
L	5.5×10^{-1} cm
α_m	0.51 (mirror losses)
Γ	0.074 (optical confinement factor)
d	3.5×10^{-4} cm
τ	10^{-11} s
α_i	2 cm^{-1}
η_i	0.8 (injection efficiency)
h	6.626×10^{-34} J.s
q	1.602×10^{-19} q
c	3×10^8 m/s

Table 5.2: Evaluative parameters for the numerical max rep rate computation

I then evaluate the projected maximum repetition rate for each of the 4 reported cases [2] for this device. The dedicated absorber section and the passive section are

all included in the absorber length to provide a more generous upper bound in the theory. The differential gain was evaluated at the transparency condition, which occurs at 61 A/cm^2, and the unsaturated absorption was given a value of 4 cm^{-1}. The specific absorber length and peak power values are evaluated uniquely for each of the four cases. The max repetition rate values include the length of the passive waveguide with the absorber length in the calculation. Additionally, I examine the worst case scenario where the assumption that the gain term of equation 5.13 is much smaller than the absorption term is relaxed resulting in equation 5.10.

$$\sqrt{\left(\frac{\Gamma P}{\alpha_m h\nu dL}\right)^2\left(\left(\frac{dg}{dJ}\Big|_{g_o=0}\frac{q\eta_i}{\tau}\right)^2\frac{a_o L_a}{2L\alpha_i}-\left(\frac{dg}{dJ}\Big|_{g_o=sat}\frac{q\eta_i}{\tau}\right)^2\frac{g_o L_g}{2L\alpha_i}\right)} > \Omega_{MLL} \quad (5.10)$$

The absorber section length in this worst case evaluation considers only the section of the device that is reverse biased and the passive sections are neglected from the calculation entirely. The biasing conditions of the gain section are taken to be at gain saturation. This implies that the differential gain is small with respect to the differential absorption and the gain is at a maximum. The final projections are given in table 5.3.

Configuration	$A_{0.5}G_{5.0}$	$A_{0.5}P_{0.5}G_{4.5}$	$A_{0.5}P_{1.0}G_{4.0}$	$A_{0.5}G_{4.0}P_{1.0}$
Absorber Length (cm)	0.05	0.1	0.15	0.15
Peak Power (W)	0.150	0.166	0.202	0.224
Max Rep Rate (GHz)	72.61	113.64	169.37	187.81
Worst case (GHz)	71.98	79.73	97.10	107.68

Table 5.3: Projections for max repetition rate

Discussion of the Carrier Lifetime

An interesting observation in the numerical computation of maximum repetition rates was the contribution of the order of magnitude of the carrier lifetime τ listed in table 5.2. All of the work in our research group based upon the analysis of absorption contrast in mode locking [4] has been arranged in such a way that the carrier lifetime term has canceled in the final expression. Clearly, equations 5.9 and 5.10 both scale inversely with τ. Traditional interpretation of the carrier lifetime in early iterations of this investigation scaled τ to be a ns effect on the order of 10^{-9} s. This produced maximum repetition rates of MHz which are contradicted by experiment [2] where even the fundamental repetition rates are higher. Other parameters in table 5.2 seemed to have solid foundations and the model [5] has been used to great effect in the prediction of mode locking operation over a wide range of parameters [9, 10, 11]. Thus, suspicion turned to the carrier lifetime and I began a literature search to find more investigation in similar devices. Previous work in QD detectors [12] has shown carrier lifetimes on the order of 10^{-11} at reverse bias values similar to the operating points. Integrating this faster value for τ produces more physical results in agreement with experiment and thus provides a good argument for the revision of the carrier lifetime. Further study into the carrier dynamics within QDMLLs under operation is warranted to further refine these values.

5.2.3 Ratioed Repetition Rate Derivations

The model used to predict the maximum repetition rate of a QDMLL configuration utilizes a sinusoidal mechanism for pulse creation [5] which allows for the prediction of output as a function of a laser's gain profile [4] in two section devices. The full

expression of the mode locking condition is given in equation 5.13.

$$\left[\left(v_g\frac{da_o}{dn}\right)^2 a_o\frac{L_a}{L} - \left(v_g\frac{dg}{dn}\right)^2 g_o\frac{L_g}{L}\right]\frac{S_o^2}{2\Omega_{MLL}^2} > \alpha_i \tag{5.11}$$

Where the repetition rate $\Omega_{MLL} = v_g/2L$ and S_o is the cavity photon density defined in equation 5.5. Additionally, a_o is the unsaturated absorption, g_o is the unsaturated gain, L_g is the length of the gain section, L_a is the length of the absorber section, L is the device length, v_g is the device group velocity, α_i is the internal loss, d is the thickness of the active region, and W is the lateral mode width. From here we follow the assumption that the $\frac{dg}{dn}$ contribution to equation 5.11 is small compared to $\frac{da_o}{dn}$. This condition holds well when the gain section of a QDMLL is biased into saturation. Thus, we can neglect the second term in the brackets of equation 5.11. Rearranging, we arrive at an inequality in equation 5.12 that relates the observed maximum repetition rate to the physical parameters of a QDMLL.

$$\Omega_{MLL} < \sqrt{\frac{L_a}{2L}}\frac{da_o}{dn}\left(\frac{\Gamma P}{\alpha_m h\nu LWd}\right)\sqrt{\frac{a_o}{\alpha_i}} \tag{5.12}$$

Evaluation of equation 5.12 using the differential absorption with respect to carrier density is troublesome because of the difficulty in experimentally measuring this parameter. Thus, we approach it from a different perspective using the observed maximum repetition rate of a QDMLL at constant power as our baseline.

5.2.4 Analysis of Absorption Ratio Method

Equation 5.12 offers insight into how basic device parameters can be leveraged to overcome limitations to achieving higher repetition rates. As an illustrative example, we study the experimentally observed trends in mode-locking stability for one of the devices characterized in [2]. As seen from figure 5.4a of this reference, 7th

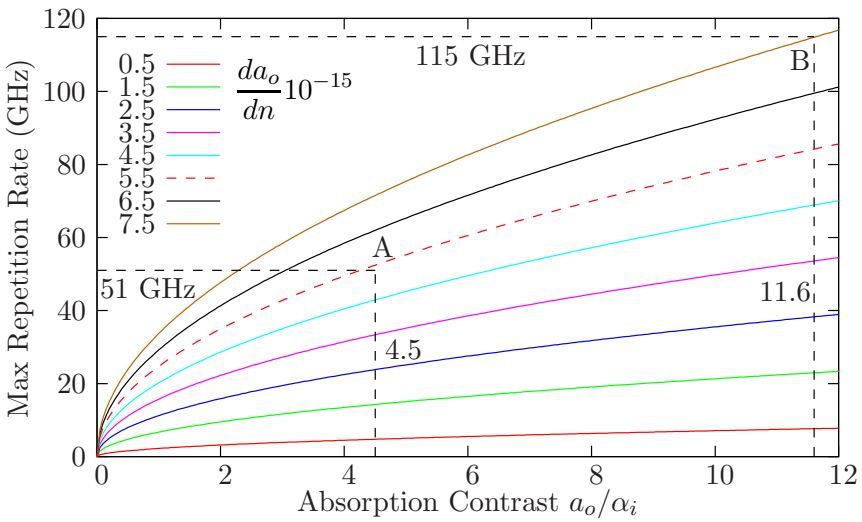

Figure 5.3: Projected repetition rate parameter space for a QDMLL when the differential absorption and the absorption contrast are allowed to vary

harmonic mode locking achieved pulses of width 6 ps and peak power of 70 mW, with a repetition rate of 50.7 GHz. However, figure 5.4b shows incomplete mode locking at a repetition rate of 115 GHz. In order to obtain an understanding of the causes underlying this trend, as well as to get a sense of the parameters that could be manipulated to achieve stable mode-locking, the maximum possible repetition rate in equation 5.12 can be plotted as a function of the unsaturated absorption-to-internal loss contrast ratio. The family of curves spans a range of differential absorption values that are typical of such devices [8]. From the gain and absorption spectra shown in figure 5.1 and constants in table 5.2 the contrast ratio is shown to be 4.5 (point A in figure 5.3). From the family of curves shown, this corresponds to a differential absorption of $5.5 \times 10^{-15} cm^2$. A careful examination of the curves in figure 5.3 shows that if the operating point A were shifted upward to correspond to a higher differential absorption value, higher repetition rates could be achieved without raising the value of the unsaturated absorption. One such technique involves the use of strong optical injection and has been recently shown to accomplish a

50X differential gain enhancement in a quantum dash laser [8]. Next, we consider the case of incomplete mode locking shown in figure 5.4b of [2]. A glance at the curves shown in figure 5.3 (point B) reveals that a repetition rate of 115 GHz lies on the outer edge of the parameter-space comprising differential absorption values typical for such devices. In fact, the contrast ratio for this case can be seen to be 11.6, corresponding to an unsaturated absorption of 23.2 cm^{-1}. Such high values of unsaturated absorption are indicative of a high degree of losses in the cavity, so that the absorber bias could not be raised beyond 0V due to limitations in device gain. The combination of the buildup of intracavity noise, along with the slow absorber recovery owing to a 0V bias leads to incomplete pulse trimming, with significant levels of background noise between pulses. This is manifest as the incomplete mode-locking seen in figure 5.4b of reference [2].

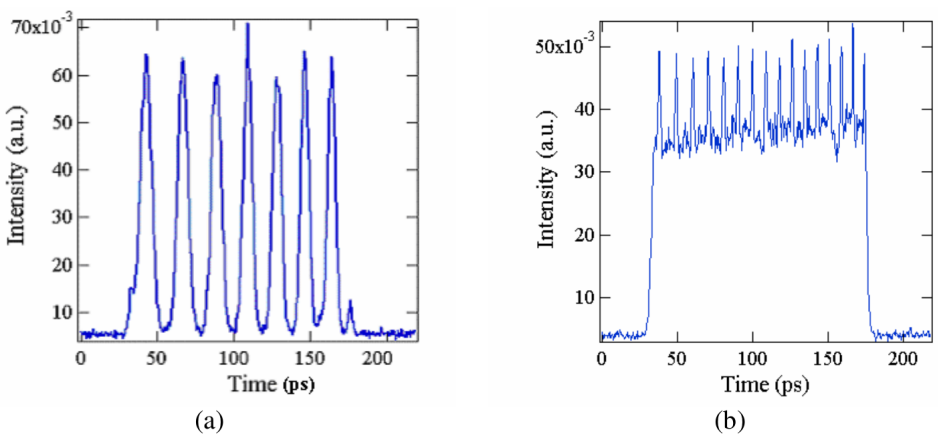

Figure 5.4: Previously reported QDMLL output pulses showing mode locking repetition rates of (a) 50.7 GHz and pulsation at (b) 115 GHz [2]

5.3 Higher Repetition Rates through Gain Contrast

Pursuit of higher repetition rates in pulsed laser sources continues at a feverish pace [13] as demands in communication systems grow ever faster. QDMLLs continue to be a strong candidate for this effort. A common approach to increasing the base repetition rate of the QDMLLs relies on shortening the cavity length. However, lasing threshold conditions become more difficult to satisfy as cavities get shorter due to limited gain from the QDs. Harmonic mode locking [2] and variance of the absorber position [14] can increase the repetition rate of QDMLLs but are still stunted by gain limits. I propose a new approach that takes advantage of the very high differential gain contrast of QD material to achieve mode locking in a two section gain lever. The proposed device is pictured schematically in figure 5.5. I introduce a "control" section that is forward biased below the Continuous Wave (CW) laser threshold current density and above the transparency condition. The differential gain contrast between the gain section and the control section provide the necessary mode shaping to achieve mode locking. I present an analysis of measured QD gain material data that reveals regions where pulsing is predicted in our gain lever differential biasing scheme. I call this device the gain lever QDMLL. The advantages of this approach are that shorter cavities and higher repetition rates are possible by eliminating the need for absorber sections.

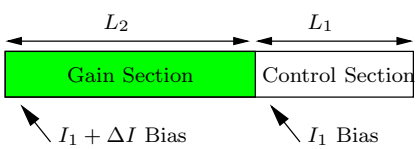

Figure 5.5: A schematic diagram of the gain lever showing the gain section, control section, and the appropriate biases

5.3.1 QD Gain Characteristics

The QD gain material used to bound our model utilizes 6 layers of InAs/InGaAs Quantum Dot gain media with a Dots-in-a-Well (DWELL) [15] configuration. Unsaturated gain values were measured using the segmented contact method for both the ground and first excited state of the dots. The modeled device uses a control section length of 0.25 cm and a gain section of 0.35 cm. The control section in the described configuration is too long for this Quantum Dot laser to achieve threshold when used as a traditional saturable absorber. The limitation would be further compounded when multiple absorbers are used to achieve harmonic mode locking. The gain lever QDMLL is not subject to either of these limitations.

5.3.2 Gain Values and Derivation

The analytical model used to predict the pulsed operation of the gain lever QDMLL method utilizes a sinusoidal mechanism for pulse creation [5], which allows for the prediction of output as a function of a laser's gain profile [4] in two section devices.

$$\left(G_a^2 a_o \frac{L_a}{L} - G_g^2 g_o \frac{L_g}{L}\right) \frac{S_o^2}{2\omega^2} > \alpha_i \tag{5.13}$$

$$v_g \frac{dx}{dn} = v_g \frac{dx}{dJ} \frac{q\eta_i d}{\tau} = G_x \tag{5.14}$$

Where the repetition rate $\omega = v_g/2L$, S_o is the cavity photon density defined in equation 5.5, and the differential gain/absorption contribution G_x is given generally by equation 5.14. Additionally, a_o is the unsaturated absorption, g_o is the unsaturated gain, L_g is the length of the gain section, L_a is the length of the absorber section, L is the device length, v_g is the device group velocity, α_m is the mirror loss, α_i is the internal loss, d is the thickness of the active region, W is the width of the device, Γ

is the optical confinement factor, P is the peak pulse power, and ν is the emission frequency, η_i is the injection efficiency, and τ is the carrier recombination lifetime.

The measured data from the segmented contact method for a range of current densities were assessed at the ground state (1243.1 nm) and excited state (1154.4 nm) peaks. These points were then fit to an exponential curve and plotted in figure 5.6 with their differential profiles as well.

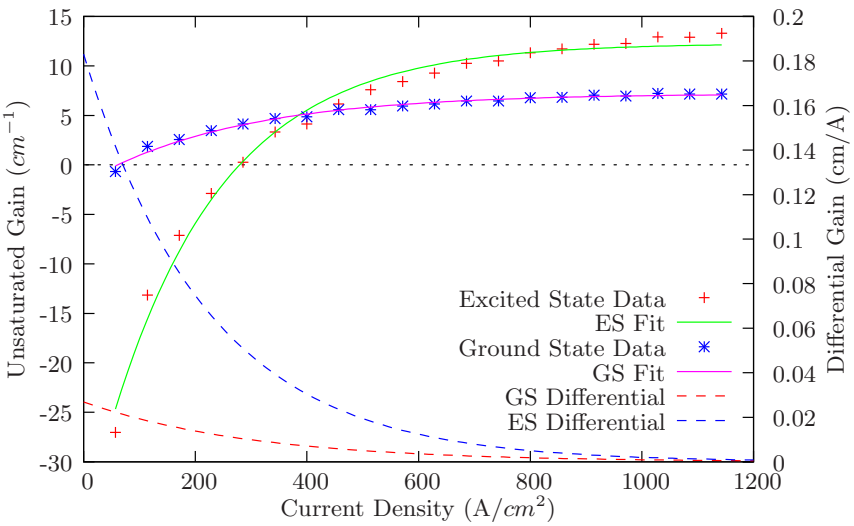

Figure 5.6: Peak emission gain as a function of applied current density for both the ground and excited states a 6 stack InAs/InGaAs DWELL at 20C

I then cast equation 5.11 to suit two forward biased sections by enforcing the condition that an effective DC offset equal to the mirror loss can serve as the absorption term so long as the control section is biased below the threshold condition. Next, I define the second section as biased by some current density Δ above the control section and arrive at the resulting inequality in equation 5.15.

$$\left(\frac{S_o q \eta_i dL}{\tau}\right)^2 \left[\left(\frac{dg_1}{dJ}\right)^2 (\alpha_m - g_1)\frac{L_1}{L} - \left(\frac{dg_{1+\Delta}}{dJ}\right)^2 (g_{1+\Delta} - \alpha_m)\frac{L_2}{L}\right] - (\alpha_m + \alpha_i) > 0 \quad (5.15)$$

The mirror loss and internal loss are enforced as necessary in the mode locking condition. Thus, we can expect to achieve pulsing when equation 5.15 is satisfied and the device is operating such that the net gain exceeds the cavity losses from all sources as configured in figure 5.5. Both the excited and ground state projections are given for the quantum dot but the excited state predictions assume that the ground state has been suppressed using a frequency selection method with the results shown in figure 5.7.

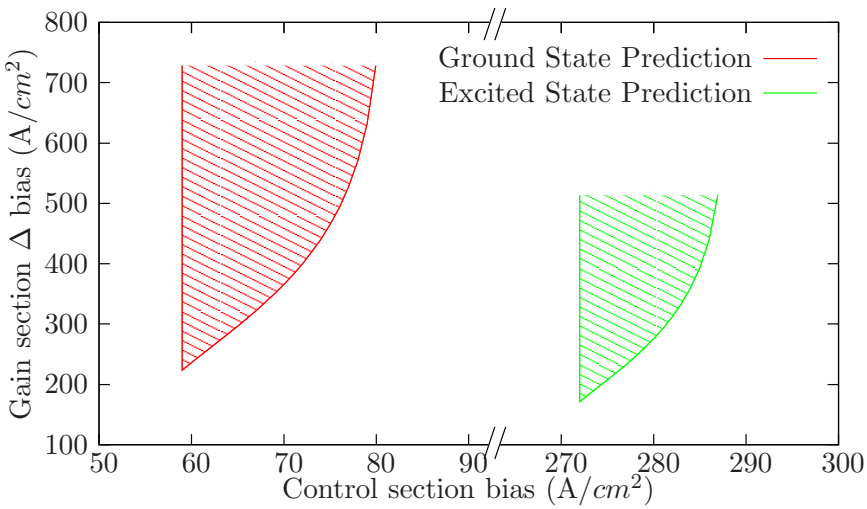

Figure 5.7: Projected pulsing regions for the 6 stack DWELL plotted as a function of the control section bias (I_1) and the differential bias of the gain section (ΔI)

5.3.3 Analysis of the Differential Gain Method

The model shows that it is possible to achieve pulsing in the gain lever QDMLL when one section, the control, is biased above transparency and below the current density that satisfies the CW threshold condition when uniformly pumped. Thus, it allows for pulsing to occur in configurations that would normally suppress CW lasing. The shaded regions in figure 5.7 indicate areas of expected mode locking and are bounded by the control section's current bias limits. Excited state pulsing is expected to begin at a lower current differential Δ than is necessary for the ground state because of the superior differential gain contrast offered in the excited state. The upper bound for the pulsing occurs at gain saturation when the differential gain values become small. A smaller projected area of operation for the excited state occurs because there is a smaller current space before saturation than in the ground state. The observation that the excited state requires a smaller gain differential to pulse provides insight into previous results that have reported single section pulsation in similar devices [16]. This model elucidates how the effects of gain contrast as a result of series resistance along a laser diode or differential pumping might induce mode locking even in single section devices.

5.4 Investigation of Differential Gain Method

Examination of mode locking behavior of the QDMLL in forward bias for both the control and the gain sections of a device following the template illustrated in figure 5.5 has not been studied before. The previous section examines the potential mode locking when both sections are biased to contribute to device gain. Characterization of any diode from solar cell, to lasers, or to any other exotic structures that exhibit nonlinear current and voltage relations are performed using a traditional Current/Voltage curve method with the region depicted in figure 5.8. This figure

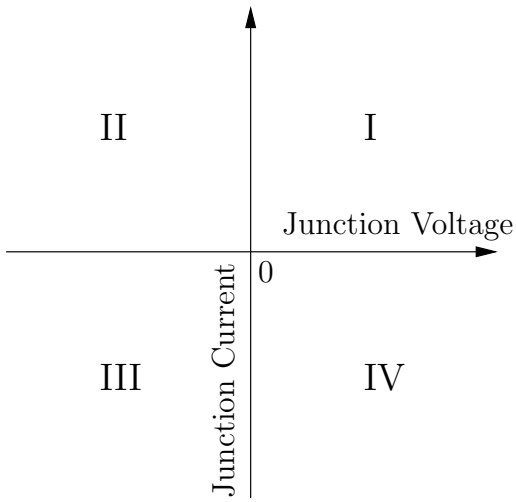

Figure 5.8: Definition of quadrants and axes for diode characterization

illustrates the classic current (I) and voltage (V) parameter space and defines the quadrants of device operation (I-IV in figure 5.8. This analysis employs electrical contacts such that the positive voltage terminal is connected to the p-type side of a semiconductor and the negative voltage terminal is connected to the n-type side. Thus, quadrants I and IV define device operation while in the forward bias condition while quadrants II and III define the reverse bias operation.

Traditional gain sections examined in this dissertation exclusively operate in quadrant I in the measurement scheme depicted in figure 5.8. These sections draw current to produce light and are operated in forward bias. Absorber sections, by contrast, are typically operated in quadrant III under reverse bias where carriers are extracted electrically in order to provide the saturable absorption [17] effect. The experimental investigation in this section examines a pair of butterfly packaged two-section QDMLLs of differing vintages. Both have absorber to gain length section ratios of near 0.1 and operate with a base repetition rate of 5 GHz. Additionally, they are both coupled into polarization maintaining fiber. The older generation (wafer 414G AH3) and the newer generation (Innolume MML-1260-BF-5GHz) were

operated with both sections in forward bias to characterize the effect upon the pulse quality. The predictive model for the two section QD Gain Lever does not forecast mode locking because of the small differential gain contrast allowed by such a large difference between the section lengths in both devices. However, the onset of mode locking from the net gain modulation phasor approach [5] does predict that the laser will continue to mode lock into quadrant IV so long as the product of the differential absorption term in equation 5.11 exceeds the value of the differential gain term. This provides fertile ground for experimentation into new regimes of mode locking previously unaddressed.

5.4.1 Experimental Setup

Modifications to our experimental setups were needed in order to reliably probe the operation of the two packaged QDMLLs (414g AH3 and the Innolume MML-1260-BF-5GHz) in quadrant IV as shown in figure 5.8. This is the regime that Solar Cells operate in and is typically characterized by a sourcemeter like the Kiethley 2400 series models. In this case, I had to improvise a two part solution that first examines quadrant IV in detail and then allows for the continuous sweep from quadrant IV to I. The precision measurement of quadrant IV was conducted using the experimental setup shown in figure 5.9.

In this setup, the two section device has a gain section bias applied using a dedicated current source so that it is biased well above the lasing threshold. The absorber section requires more dedicated attention as rewiring is required when transitioning from quadrants III, IV, and I. A digital multimeter is placed in parallel with the absorber circuit so that a common metric for the voltage across all devices can be accomplished. Quadrant III is wired so that only the voltage source provides the reverse bias to the absorber section which is the traditional treatment for this type

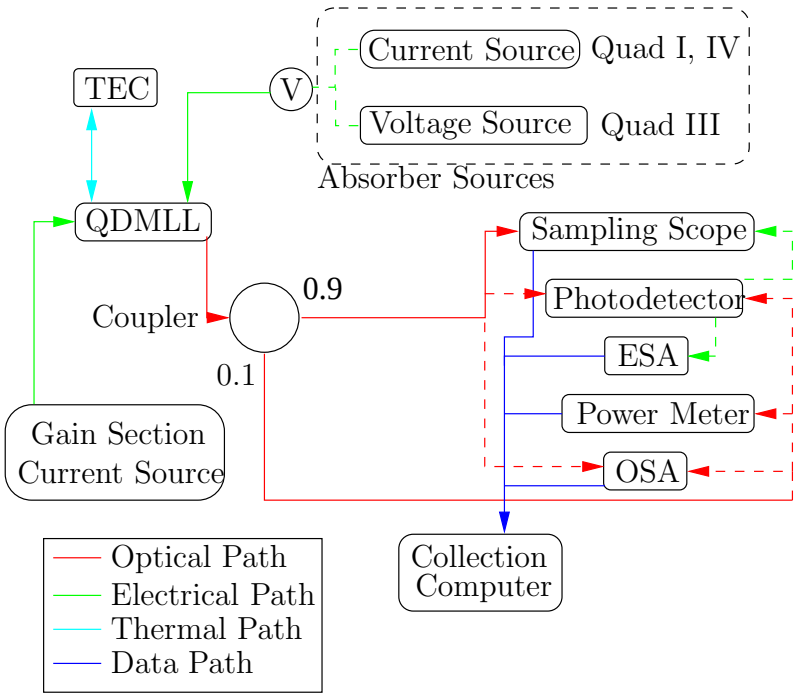

Figure 5.9: Experimental setup for absorber characterization in quadrants III and IV

of device configuration. Transitioning to quadrant IV requires that the constant current source be wired in such a way that the negative current post (current sink) is connected to the p-type side of the laser. This is so that the current sourced from the absorber section itself can be handled by the sink contact. This method can trace out the Current/Voltage profile in quadrant IV. It can characterize the open circuit voltage quite well but the short circuit current measurement can be difficult because the low current differential observed as one changes the voltage on the threshold of quadrants III and IV can cause the constant current source to loose voltage lock and run away.

Biasing quadrant I using the experimental setup in figure 5.9 requires that the current source be wired so that the positive terminal is connected to the p-type side of the absorber section. This essentially turns the laser into a gain lever device

proposed in previous sections. The differential contrast between the two sections can be explored to identify mode locking. However, the transition between quadrants III, IV, and I are not continuous in this setup even though we have exceptional current bias control. Therefore, mode locking measurements characterizing behaviors in transition regions could not be observed with this setup. However, each region was closely monitored using the measurement suite of five instruments in the lower right hand corner of figure 5.9. Temporal pulse characterization is accomplished using a high speed scope triggered by a 45 GHz photodetector. The output of the laser is run through a fiber splitter where the 10% of the power would be sent to the photodetector and 90% would be sent to the high speed scope for better pulse resolution.

Threshold characterization measurements were performed using the fiber optic power meter and was informative in determining the bias set point for the gain section. Spectral characterization of the pulse was performed using a high resolution Optical Spectral Analyzer which provided insight into the number of modes excited for each of the bias points in the measurement. Expanding the setup to cover the transitions between each of the quadrants required the replacement of the constant current source with a second voltage source wired in anti-series with the other absorber source as shown in figure 5.10.

The anti-series configuration allows for the two voltage sources to provide biases in both the forward and reverse case. Additionally, this configuration can sink current produced by the absorber section in quadrants III and IV as well as provide current in quadrant I. The digital multimeter was left in parallel with the absorber circuit to measure the effective voltage across the junction. The limitations of the equipment used (Agilent E3610A series voltage sources) meant that there was not fine control in the voltage biasing points. The trade off in resolution was acceptable when examining transitional effects to the mode locking pulse train.

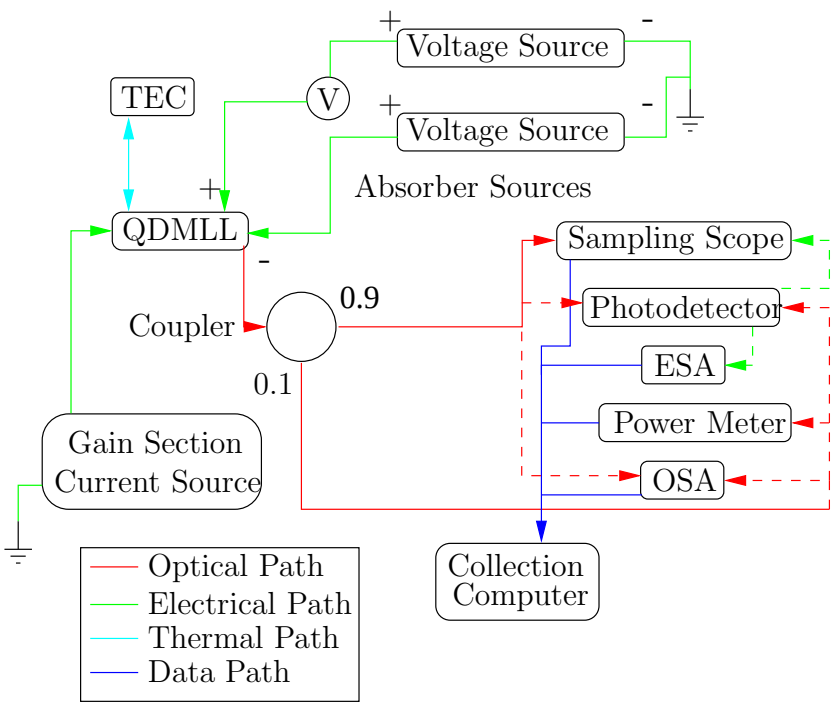

Figure 5.10: Experimental setup for absorber characterization continuously across all quadrants

5.4.2 Device Baseline Measurements

I began with a traditional light curve measurement for both packaged devices to determine threshold conditions and where the bias points should be in saturation. The temperature controller maintained the devices at 30 C and the absorber section was held at 0 V bias by an external source. The gain section current was then ramped while the output optical power was collected from the fiber power meter to produce figure 5.11.

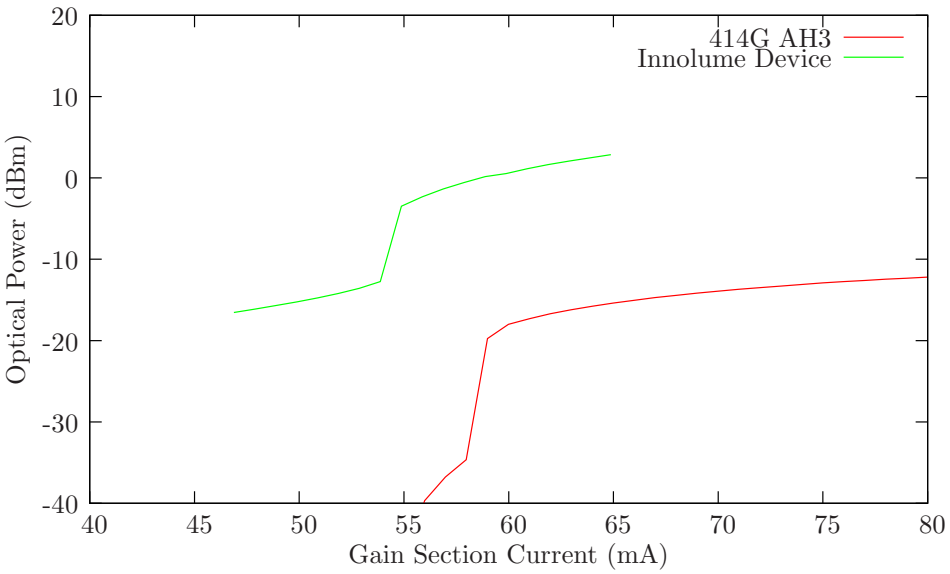

Figure 5.11: Measured optical threshold curves for lasers 414G AH3 and the Innolume packaged device

The bias point of the 414G device for the remaining measurements was set to 90 mA on the gain section to ensure the device was far from threshold. Likewise, the Innolume device was forward biased at 70 mA on its gain section in order to achieve the same effect. Both devices also retained their 30 C setpoint for the remainder of the tests.

Next, I proceeded to use the experimental setup from figure 5.9 to determine the short circuit current and the open circuit voltage for each of the device's absorber sections at the gain section bias previously selected for each. Measurements within quadrant IV produce curves like the one in figure 5.12 which shows the response for the 414G AH3. Parameters of the diode can be extracted and the functional parameters can be analyzed for device health. Interestingly, it also shows the extracted power from the absorber section which can provide insight into other experiments dealing with RF generation from compact laser sources [18, 19, 20].

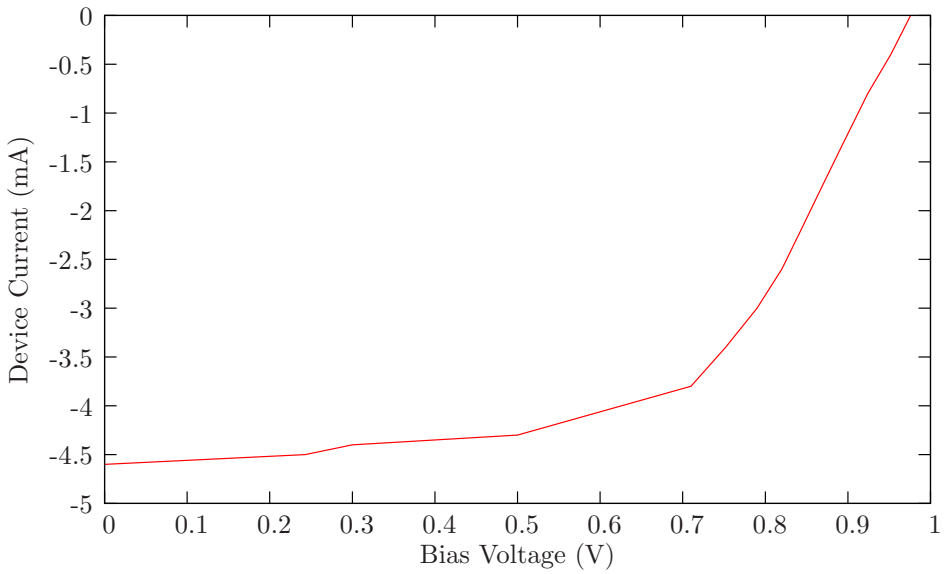

Figure 5.12: Measured absorber diode curve for the 414g AH3 laser with 90 mA gain section bias

The resulting tabulated values for both devices in this study are shown in table 5.4.

Device Name	Gain Section Bias (mA)	I_{sc} (mA)	V_{oc} (V)
414G	90	-4.6	0.976
Innolume	70	-3.0	1.096

Table 5.4: Absorber parameters for the lasers under test

These set points provide effective boundaries for the operation of both devices in quadrant IV. From here, I switch to the second experimental setup depicted in figure 5.10 in order to perform mode locking characterization to determine the effect of a forward biased absorber on the tested devices.

5.4.3 Mode Locking Under Forward Bias

Examination of mode locking was performed using the experimental setup shown in figure 5.10 utilizing a high speed sampling scope to resolve the pulse train and a high speed photodetector to trigger the waveform. Both the 414G AH3 laser and the Innolume device were tested to determine how far into the forward bias regime mode locking could be observed. The threshold for mode locking was a triggering condition on the high speed scope. The observed pulse waveform would collapse if the signal from the 45 GHz high speed photodetector became too small for the high speed sampling scope to interpret. This equipment limitation provides a convenient threshold point to compare between both of the devices under test. As before, the bias conditions listed in table 5.4 are preserved and the laser is held at 30 C through the use of a temperature controller.

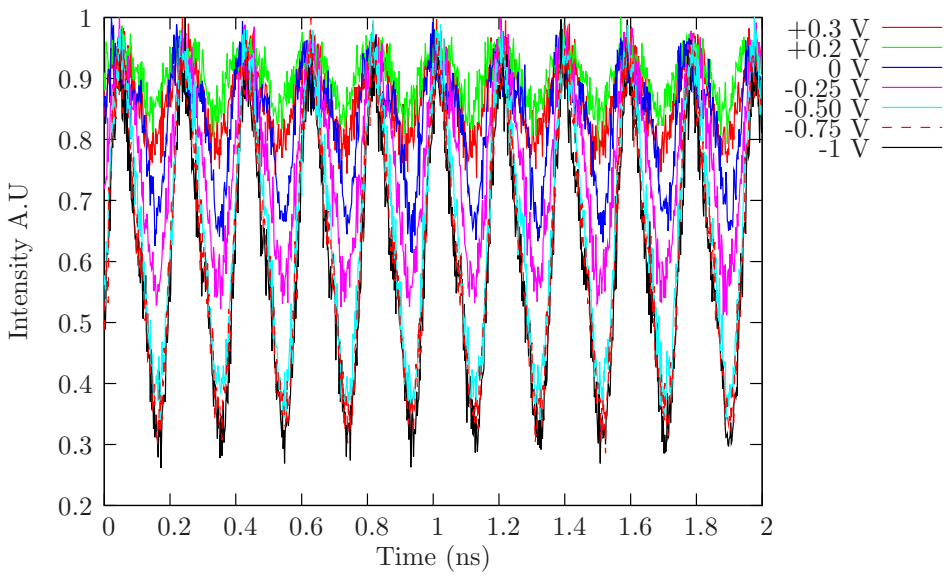

Figure 5.13: Pulse profiles from 90 mA gain section bias for the 414G device 3 laser at 30C for each absorber bias point

The examination of the 414G packaged device utilized 90 mA gain section bias and varied the absorber voltage to investigate the effects of bias on the pulse quality.

The absorber voltage sweep beings at -1 V bias and is raised incrementally until the last observed pulse train appears in figure 5.13. Mode locking for this older generation device broke down at 0.3 V forward bias which is less than half of the recorded open circuit voltage reported in table 5.4. The pulse amplitude of the device tested decreased as the forward bias was increased until the 0.3 V cutoff point was reached. Further examination of this device was performed by biasing the absorber into quadrant I, but the gain lever effect never manifested. This is due to small size of the absorber section relative to the gain section. The differential gain mode locking model proposed earlier in this chapter requires that the second section be larger than in the example 414G device in order to function. This experimental process was similarly performed on the newer generation Innolume device.

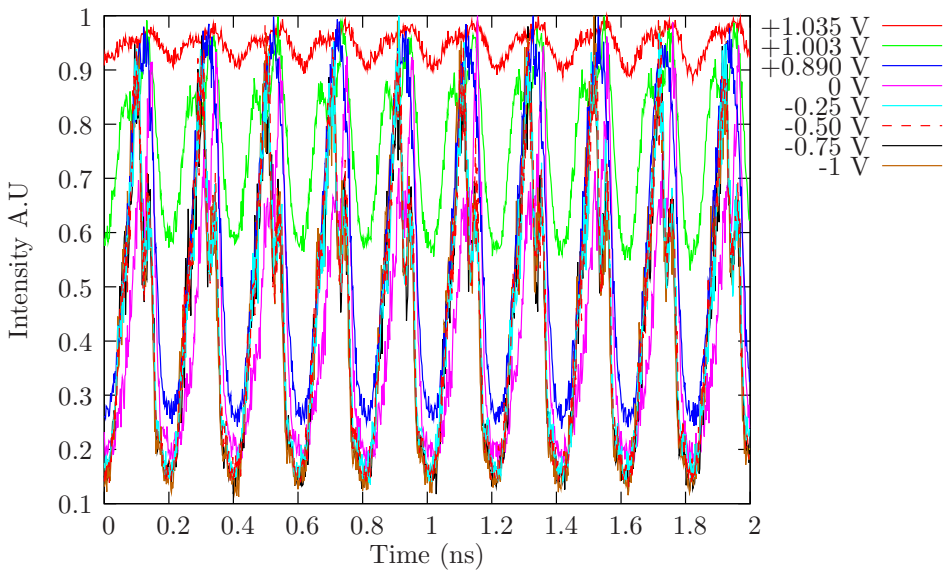

Figure 5.14: Pulse profiles from 70 mA gain section bias for the Innolume device at 30C for each absorber bias point

The Innolume device was examined with a gain section bias of 70 mA and with a voltage sweep along the absorber section following the biasing conventions illustrated in table 5.13. The resulting pulse train for each of the biasing conditions is shown in

figure 5.14. The absorber section sweep begins as before with 1 V reverse bias and continues until the pulses are no longer detectable at 1.035 V forward bias. This is a much larger range on the newer generation Innolume device and gets fractionally closer to the open circuit voltage than the 414G did. However, as before, exploring the absorber bias conditions in quadrant I did not produce a mode locking regime for the same reason as the 414G.

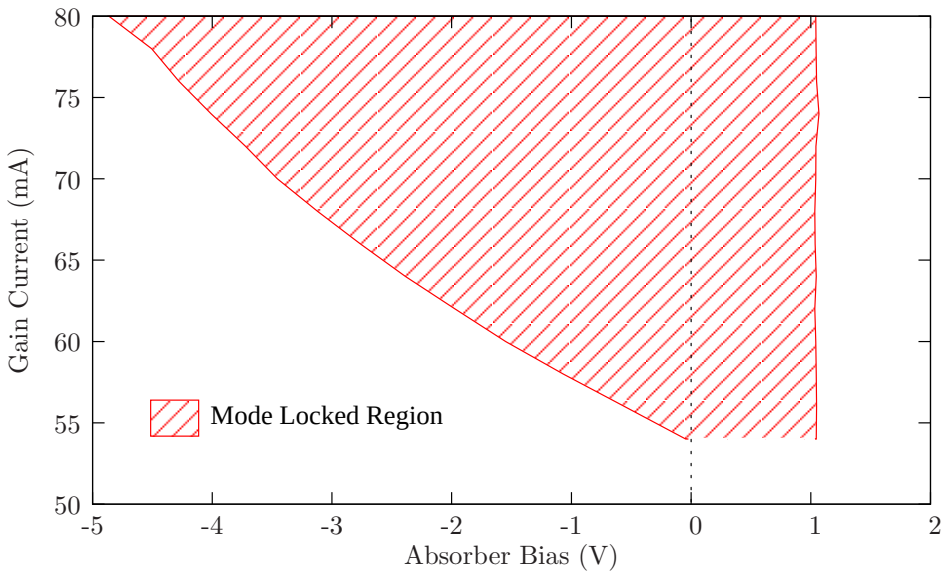

Figure 5.15: Observed regions of mode locking on the Innolume packaged device as a function of gain section current bias and absorber bias at 30 C

The Innolume's relatively high upper forward bias limit for mode locking observed in figure 5.14 than the 414G device was intriguing in the difference. An experimental map of mode locking following the same parameters as before was produced in figure 5.15 by varying both the gain section bias and the absorber bias to locate the boundaries of pulsed operation. Interestingly, the threshold for mode locking in the forward bias seems to be a constant fraction of the open circuit voltage regardless of the gain section current during this test. The mode locking region expands in reverse bias as the gain section current increases which has been previously observed

in mode locking maps [21]. The observation of this physical constraint in the forward bias regime provides additional insight into the operation of these lasers.

5.5 Remarks on Novel Geometries

The examinations in this chapter provide road maps for operating QDMLLs to achieve ever higher repetition rates. Either through cavity design, device layout, or material composition, the versatility of this technology is clear. Work remains to be done on devices that have more easily configurable cavities in order to examine the differential gain methods to achieve mode locking but I have shown that mode locking is observed in the forward biased condition which is a regime that has been previously neglected in other maps. The analytical projections made here allow for insightful design and experiment to reduce number of iterations needed as ever faster pulse sources are developed.

References for Chapter 5

[1] T. Skauli, P. S. Kuo, K. L. Vodopyanov, T. J. Pinguet, O. Levi, L. A. Eyres, J. S. Harris, M. M. Fejer, B. Gerard, L. Becouarn, and E. Lallier, "Improved dispersion relations for GaAs and applications to nonlinear optics," *Journal of Applied Physics*, vol. 94, p. 6447, Oct. 2003.

[2] Y. C. Xin, Y. Li, V. Kovanis, A. L. Gray, L. Zhang, and L. F. Lester, "Reconfigurable quantum dot monolithic multisectionpassive mode-locked lasers," *Opt. Express*, vol. 15, pp. 7623–7633, June 2007.

[3] M. Kobrinsky and B. Block, "On-Chip Optical Interconnects," *Intel Technology Journal*, vol. 08, no. 02, pp. 129–142, 2004.

[4] C. Y. Lin, Y. C. Xin, Y. Li, F. L. Chiragh, and L. F. Lester, "Cavity design and characteristics of monolithic long-wavelength InAs/InP quantum dash passively mode-locked lasers," *Optics express*, vol. 17, pp. 19739–19748, Oct. 2009.

[5] K. Lau and J. Paslaski, "Condition for short pulse generation in ultrahigh frequency mode-locking of semiconductor lasers," *Photonics Technology Letters, IEEE*, vol. 3, pp. 974–976, Aug. 1991.

[6] N. N. Ledentsov, M. Grundmann, F. Heinrichsdorff, D. Bimberg, V. M. Ustinov, a. E. Zhukov, M. V. Maximov, Z. Alferov, and J. A. Lott, "Quantum-dot heterostructure lasers," *IEEE Journal of Selected Topics in Quantum Electronics*, vol. 6, pp. 439–451, May 2000.

[7] Y. C. Xin, Y. Li, A. Martinez, T. J. Rotter, H. Su, L. Zhang, A. L. Gray, S. Luong, K. Sun, Z. Zou, J. Zilko, P. M. Varangis, L. F. Lester, and S. Member, "Optical gain and absorption of quantum dots measured using an alternative segmented contact method," *Quantum Electronics, IEEE Journal of*, vol. 42, pp. 725–732, July 2006.

[8] L. Lester, N. Naderi, and F. Grillot, "Strong optical injection and the differential gain in a quantum dash laser," *Optics express*, vol. 22, no. 6, pp. 1308–1314, 2014.

[9] M. T. Crowley, D. Murrell, N. Patel, M. Breivik, C.-Y. Lin, Y. Li, B.-O. Fimland, and L. F. Lester, "Analytical Modeling of the Temperature Performance of Monolithic Passively {Mode-Locked} Quantum Dot Lasers," *IEEE Journal of Quantum Electronics*, vol. 47, p. 1059, Feb. 2011.

[10] J. K. Mee, M. T. Crowley, N. Patel, D. Murrell, R. Raghunathan, A. Aboketaf, A. Elshaari, S. F. Preble, P. Ampadu, and L. F. Lester, "A passively mode-locked quantum-dot laser operating over a broad temperature range," *Applied Physics Letters*, vol. 101, pp. 71112–71114, Aug. 2012.

[11] J. K. Mee, M. T. Crowley, D. Murrell, R. Raghunathan, L. F. Lester, and S. Member, "Temperature Performance of Monolithic Passively Mode-Locked Quantum Dot Lasers: Experiments and Analytical Modeling," *Selected Topics in Quantum Electronics, IEEE Journal of*, vol. 19, p. 1101110, July 2013.

[12] B. Kochman, A. Stiff-Roberts, S. Chakrabarti, J. Phillips, S. Krishna, J. Singh, and P. Bhattacharya, "Absorption, carrier lifetime, and gain in inas∼gaas quantum-dot infrared photodetectors," *IEEE Journal of Quantum Electronics*, vol. 39, pp. 459–467, Mar. 2003.

[13] M. G. Thompson, A. R. Rae, M. Xia, R. V. Penty, and I. H. White, "InGaAs Quantum-Dot Mode-Locked Laser Diodes," *Selected Topics in Quantum Electronics, IEEE Journal of*, vol. 15, pp. 661–672, May 2009.

[14] H. Simos, M. Rossetti, C. Simos, C. Mesaritakis, T. Xu, P. Bardella, I. Montrosset, and D. Syvridis, "Numerical Analysis of Passively Mode-Locked Quantum-Dot Lasers With Absorber Section at the Low-Reflectivity Output Facet," *IEEE Journal of Quantum Electronics*, vol. 49, pp. 3–10, Jan. 2013.

[15] G. T. Liu, K. J. Malloy, A. Stintz, H. Li, and L. F. Lester, "Extremely low room-temperature threshold current density diode lasers using {InAs} dots in {$In_{0.15}Ga_{0.85}As$} quantum well," *Electronics Letters*, vol. 35, pp. 1163–1165, July 1999.

[16] R. Rosales, K. Merghem, C. Calo, G. Bouwmans, I. Krestnikov, A. Martinez, and A. Ramdane, "Optical pulse generation in single section InAs/GaAs quantum dot edge emitting lasers under continuous wave operation," *Applied Physics Letters*, vol. 101, no. 22, pp. 221113+, 2012.

[17] K. J. Vahala, M. A. Newkirk, and T. R. Chen, "The optical gain lever: A novel gain mechanism in the direct modulation of quantum well semiconductor lasers," *Applied Physics Letters*, vol. 54, no. 25, p. 2506, 1989.

[18] C. Y. Lin, Y. C. Xin, J. H. Kim, C. G. Christodoulou, and L. F. Lester, "Compact Optical Generation of Microwave Signals Using a Monolithic Quantum Dot Passively {Mode-Locked} Laser," *IEEE Photonics Journal*, vol. 1, pp. 236–244, Oct. 2009.

[19] G. Atmazakis, D. Murrell, C. G. Christodoulou, and L. F. Lester, "Injection Locking Properties of a Photonic Microwave Oscillator Based on a Quantum Dot Mode Locked Laser," in *URSI National Radio Science Meeting*, (Boulder, CO), Jan. 2013.

[20] G. Atmatzakis, D. Murrell, C. G. Christodoulou, and L. F. Lester, "A microwave antenna array with injection locked quantum dot laser sources," in *2013 IEEE Antennas and Propagation Society International Symposium (APSURSI)*, pp. 1810–1811, IEEE, July 2013.

[21] K. Brown, B. Wysocki, M. Fanto, J. Malowicki, V. Kovanis, and L. Lester, "Control over spectral content via differential pumping of a monolithic passively mode-locked quantum dot laser," *Proceedings of SPIE*, vol. 6572, pp. 65720A+, May 2007.

Chapter 6

Conclusions

6.1 Concluding Remarks

The power of predictive modeling in the design of experimental systems provides insight and allows for efficient application of experimental resources. Leveraging fundamental device parameters of the Quantum Dot Mode Locked Laser (QDMLL) by way of their gain and loss values [1] allows for the forecasting of mode locking operation under extreme conditions; these forecasts allow for the analytical evaluation of new cavity geometries before any photolithography masks are patterned. Expansion from gain modulation phasor approaches [2], into ratioed cavity models [3], and next to extreme thermal forecasting [4] all provide bountiful experimental branches to explore.

This research examined three cases of the application of gain and loss analysis as a predictive model and demonstrated fitness in each case. Research into next generation communication systems [5] like the QDMLL [6] is vital for managing the forecasted demand on worldwide communications systems [7]. My research into analytical modeling of QDMLLs and the demonstration of the resilience of these devices experimentally verifies their fitness for applications where module mass, power consumption, radiation hardness, and thermal flexibility are vital.

6.2 The Quantum Dot Mode Locked Laser

The QDMLL is a layered semiconductor structure [8] that has a gain material that devises its unique properties from the quantum confinement [9] of fine structures [6]. Effects of the QDMLL [10] that allow for low threshold current density [8], low spontaneous emission noise in the output pulses [11], broad gain bandwidth from an inhomogeneously broadened system [12], abrupt gain saturation with carrier density [13], and others derive from the reduced density of states in the Quantum Dot system. Growth of the devices used in this study was performed using Molecular Beam Epitaxy (MBE) [14] which allows for fine control of the laser's structure. The behavior of these dots in the bandgap structure [15] depends on the arrangement of the dot relative to the parent semiconductor. This engineering can lead to hole trapping, electron trapping, or both depending on the intended design.

The theory used to conduct the baseline analysis of the QDMLLs is based on a gain modulation phasor approach [2] that allows for the projection of mode locking operation for differing cavity geometries [16] and differing environmental conditions [1]. The fitness of this model evolved [3] before this work and has provided excellent framework for recent experiments [17]. Thus, it provided a great foundation on which to build.

6.3 Predictive Analytic Modeling of the Quantum Dot Mode Locked Laser Over Temperature

The first section of work in this dissertation was to expand the gain modulation phasor model of QDMLL mode locking [2] after it had been further reworked into a ratioed expression [3]. Incorporating a lasing threshold parameter to provide the lower bound to mode locking projections to the ratioed expressions of mode locking prediction allows for the prediction of ideal length ratios in two section devices to achieve mode locking across a broad range of temperatures [1]. It was found that the ideal absorber to gain section length ratio for the 8 layered QDMLL under examination was 0.08 based on the measured device parameters. A two section test device that had an absorber to gain length ratio of 0.15 was used to show remarkable agreement with threshold mode locking in line with the predictive model. This test device's absorber to gain length ratio was arrived upon using a previous empirical method where many different ratios were exhaustively tested. This explains the fitness of that device but the lower resolution of the empirical study did not allow for that study to arrive at the ideal ratio of 0.08 found in the theoretical investigation.

The power of this technique is that the gain and loss data necessary for the input to the model can be gathered from the processed device material using the segmented contact method [16]. Any degradation to the gain curves caused either by thermal effects or others can be incorporated into mode locking prediction. The next extension of this theory follows using these predictive models towards other types of damage to the gain material.

6.4 Radiation Hardness in Quantum Dot Media

The hardiness of Quantum Dot media to high energy gamma radiation has been studied before in consideration of the lasing threshold condition. It was found that Quantum Dot Lasers required extraordinary doses (>100 MRad) [18] of high energy photons before they became inoperative. These doses far exceed [19] the expected values from spaceflight missions in Earth orbit. Examination of QDMLLs and the effect of irradiation on their mode locking had not yet been studied and was an interesting extension of previous work. Unprocessed materials with three different epitaxial structures were examined using Photoluminescence (PL) after 3 irradiation sessions with a variety of sources and intensity. The PL studies showed that all of the gain materials tested exhibited remarkable resilience to radiation damage with little variance in the observed spectra. From these results, examinations with fully processed devices continued.

The final examination in the radiation hardness study utilized two processed QDMLLs that had been characterized for both gain and loss as well as the mode locking threshold conditions. These devices were irradiated with a high energy ^{60}Co source and evaluated afterwards for mode locking fitness. They were found to continue to function. This demonstrates their fitness for flight applications in orbit as the radiation doses given also exceed the expected dose over a mission lifetime. However, survivability is only one of the traits that would be required for a space mission. Ever higher communications bandwidth will also be demanded to get the most out of the hardware. To this end, examination into increased repetition rates for these QDMLLs was the next logical step.

6.5 Expansion of Repetition Rates in QDMLLs

The fundamental repetition rate of the QDMLL is determined by the length of the cavity and the material that the cavity is made from. This provides the minimum rate at which the mode locked pulses can be generated but it is far from the maximum. Repetition rates of QDMLLs can be increased by creating cavity geometries that excite higher order harmonics of the fundamental rate [20]. This is commonly done by strategically positioning the absorber sections in the cavity so that higher order repetition rates are observed. Until now, a study on the fundamental limit of how fast these techniques can push the repetition rate had not been conducted on the QDMLLs. The gain and loss data for the 6 layered 789 QDMLL used previously [20] to explore higher repetition rates was then analyzed under each of the reported conditions to determine material limitations on repetition rates using extensions of the gain modulation phasor model [2, 3]. It was found that the highest repetition rate predicted under the most favorable device configuration was 187.81 GHz which shows that there is some additional improvement that can be made in achieving higher harmonic mode locking from previously reported results. Additionally, the expressions were recast again to express the maximum repetition rate as a function of the contrast of the absorption to the internal loss. This provides a design guideline as both parameters can be engineered for higher potential repetition rates.

The limitation in previous studies with multisection devices [20] was that the finite size of the segments of the laser limited the minimum length of the absorber in the cavity. This means that much higher harmonics are hard to isolate because the minimum absorber section is too long. Simulations of mode locking effects on absorber position in the cavity [21] and an observation that a single section device could mode lock [22] provided the motivation to apply theoretical rigor to a new type of cavity design. The Quantum Dot Gain Lever is a proposed device that operates with two sections in forward bias and leverages the gain contrast between the two

sections to achieve mode locking using an extension of the gain modulation phasor model [2, 3]. This approach provides regions of predicted mode locking for both the ground and excited state of the Quantum Dots while both sections are producing gain. Unfortunately, materials to test this model as projected experimentally were unavailable but would provide fertile content for additional study.

However, existing two section devices that had a large length disparity between both sections were available to examine in forward bias. These devices were originally engineered to have a long section to provide device gain and a short section to act as a saturable absorber [23]. In this experiment the absorber section becomes the "control" section of our Quantum Dot Gain Lever. These devices did not have a long enough control section to match the predictive model for the Quantum Dot Gain Lever but characterizing them under differential bias was informative. It was found that mode locking persisted in these devices as both sections were operated in forward bias so long as the shorter control section was biased below some fraction of the open circuit voltage of the diode. The two packaged devices used in this study both exhibited a cutoff point at a nearly constant fraction of the open circuit voltage that was unique for each device. This information and the pulse characterization from the forward bias conditions is informative even though mode locking operation could not be observed with both sections forward biased sufficiently to produce gain. Two section devices engineered with larger control section relative to the gain section are predicted to have better performance.

6.6 Recommendations for Future Work

There are two natural extensions to the work in this dissertation that are most worthy of detailed study. First is the short duration of the radiation study on the QDMLL. This work could not be conducted with a large enough radiation dose to totally

eliminate the mode locking behavior of the devices under test. It would be useful to conduct a long term test that has a cumulative dose of radiation >100 Mrad where gain and loss profile data is taken at several intermediate points. Additionally, the mode locking map of the device and pulse quality measured at each radiation interval would be of great interest. Such a test would require a large amount of irradiation time or a radiation source that is far more active that was available for this study.

The second investigation would be an extension of the Quantum Dot Gain Lever using a new cavity design that exploits multiple bias points to achieve the necessary cavity geometry as suggested in figure 6.1.

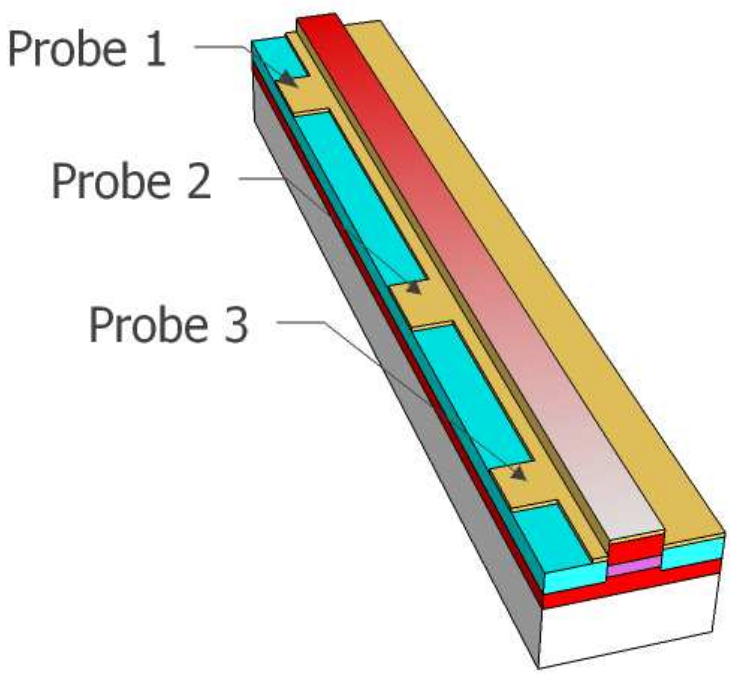

Figure 6.1: A proposed biasing scheme to examine new cavity geometries in a Quantum Dot Gain Levered laser showing differential biasing using separate electrical probes

Such a configuration could be used to examine differential biasing effects that could be introduced deliberately through nonuniform metalization on cavity design. Such a device could be used to explore higher order mode locking harmonics previously unreachable in multisection studies [20]. Any scholars who wish to proceed along these paths have my profound well wishes and I hope that this dissertation provides an excellent foundation for such ventures.

References for Chapter 6

[1] M. T. Crowley, D. Murrell, N. Patel, M. Breivik, C.-Y. Lin, Y. Li, B.-O. Fimland, and L. F. Lester, "Analytical Modeling of the Temperature Performance of Monolithic Passively {Mode-Locked} Quantum Dot Lasers," *IEEE Journal of Quantum Electronics*, vol. 47, p. 1059, Feb. 2011.

[2] K. Lau and J. Paslaski, "Condition for short pulse generation in ultrahigh frequency mode-locking of semiconductor lasers," *Photonics Technology Letters, IEEE*, vol. 3, pp. 974–976, Aug. 1991.

[3] C. Y. Lin, Y. C. Xin, J. H. Kim, C. G. Christodoulou, and L. F. Lester, "Compact Optical Generation of Microwave Signals Using a Monolithic Quantum Dot Passively {Mode-Locked} Laser," *IEEE Photonics Journal*, vol. 1, pp. 236–244, Oct. 2009.

[4] J. K. Mee, M. T. Crowley, D. Murrell, R. Raghunathan, L. F. Lester, and S. Member, "Temperature Performance of Monolithic Passively Mode-Locked Quantum Dot Lasers: Experiments and Analytical Modeling," *Selected Topics in Quantum Electronics, IEEE Journal of*, vol. 19, p. 1101110, July 2013.

[5] A. Shacham, K. Bergman, and L. P. Carloni, "Photonic Networks-on-Chip for Future Generations of Chip Multiprocessors," *IEEE Transactions on Computers*, vol. 57, pp. 1246–1260, Sept. 2008.

[6] N. N. Ledentsov, M. Grundmann, F. Heinrichsdorff, D. Bimberg, V. M. Ustinov, a. E. Zhukov, M. V. Maximov, Z. Alferov, and J. A. Lott, "Quantum-dot heterostructure lasers," *IEEE Journal of Selected Topics in Quantum Electronics*, vol. 6, pp. 439–451, May 2000.

[7] Sandvine, "Sandvine Global Internet Phenomena Report 1H-2013," tech. rep., Sandvine Corporation, Waterloo, ON, Canada, 2013.

[8] G. T. Liu, K. J. Malloy, A. Stintz, H. Li, and L. F. Lester, "Extremely low room-temperature threshold current density diode lasers using {InAs} dots in {$In_{0.15}Ga_{0.85}As$} quantum well," *Electronics Letters*, vol. 35, pp. 1163–1165, July 1999.

[9] P. Holmström, L. Thylén, and A. Bratkovsky, "Dielectric function of quantum dots in the strong confinement regime," *Journal of Applied Physics*, vol. 107, no. 6, pp. 064307+, 2010.

[10] M. G. Thompson, A. R. Rae, M. Xia, R. V. Penty, and I. H. White, "InGaAs Quantum-Dot Mode-Locked Laser Diodes," *Selected Topics in Quantum Electronics, IEEE Journal of*, vol. 15, pp. 661–672, May 2009.

[11] C.-Y. Y. Lin, F. Grillot, N. a. Naderi, Y. Li, and L. F. Lester, "Rf Linewidth Reduction in a Quantum Dot Passively Mode-Locked Laser Subject To External Optical Feedback," *Applied Physics Letters*, vol. 96, no. 5, pp. 051118+, 2010.

[12] H. Su and L. F. Lester, "Dynamic properties of quantum dot distributed feedback lasers: high speed, linewidth and chirp," *Journal of Physics D: Applied Physics*, vol. 38, pp. 2112+, July 2005.

[13] S. W. Osborne, P. Blood, P. M. Smowton, J. Lutti, Y. C. Xin, A. Stintz, D. L. Huffaker, and L. F. Lester, "Energy distributions of carriers in quantum dot laser structures," in *Proc. SPIE 5349, Physics and Simulation of Optoelectronic Devices XII* (M. Osinski, H. Amano, and F. Henneberger, eds.), vol. 5349, pp. 63–68, June 2004.

[14] L. Li, G. Patriarche, N. Chauvin, P. Ridha, M. Rossetti, J. Andrzejewski, G. Sek, J. Misiewicz, and A. Fiore, "Controlling the Aspect Ratio of Quantum Dots: From Columnar Dots to Quantum Rods," *IEEE Journal of Selected Topics in Quantum Electronics*, vol. 14, no. 4, pp. 1204–1213, 2008.

[15] X. M. Wen, L. V. Dao, P. Hannaford, S. Mokkapati, H. H. Tan, and C. Jagadish, "The state filling effect in p-doped InGaAs/GaAs quantum dots," *Journal of Physics: Condensed Matter*, vol. 19, p. 386213, Sept. 2007.

[16] Y. C. Xin, Y. Li, A. Martinez, T. J. Rotter, H. Su, L. Zhang, A. L. Gray, S. Luong, K. Sun, Z. Zou, J. Zilko, P. M. Varangis, L. F. Lester, and S. Member, "Optical gain and absorption of quantum dots measured using an alternative segmented contact method," *Quantum Electronics, IEEE Journal of*, vol. 42, pp. 725–732, July 2006.

[17] J. K. Mee, M. T. Crowley, R. Raghunathan, D. Murrell, and L. F. Lester, "Characteristics of passively mode-locked quantum dot lasers from 20 to 120C,"

in *SPIE OPTO* (B. Witzigmann, M. Osinski, F. Henneberger, and Y. Arakawa, eds.), p. 86190B, International Society for Optics and Photonics, Mar. 2013.

[18] J. W. Mares, J. Harben, A. V. Thompson, D. W. Schoenfeld, and W. V. Schoenfeld, "Gamma Radiation Induced Degradation of Operating Quantum Dot Lasers," *IEEE Transactions on Nuclear Science*, vol. 55, pp. 763–768, Apr. 2008.

[19] B. R. Bhat, N. Upadhyaya, and R. Kulkarni, "Total radiation dose at geostationary orbit," *IEEE Transactions on Nuclear Science*, vol. 52, pp. 530–534, Apr. 2005.

[20] Y. C. Xin, Y. Li, V. Kovanis, A. L. Gray, L. Zhang, and L. F. Lester, "Reconfigurable quantum dot monolithic multisectionpassive mode-locked lasers," *Opt. Express*, vol. 15, pp. 7623–7633, June 2007.

[21] H. Simos, M. Rossetti, C. Simos, C. Mesaritakis, T. Xu, P. Bardella, I. Montrosset, and D. Syvridis, "Numerical Analysis of Passively Mode-Locked Quantum-Dot Lasers With Absorber Section at the Low-Reflectivity Output Facet," *IEEE Journal of Quantum Electronics*, vol. 49, pp. 3–10, Jan. 2013.

[22] R. Rosales, K. Merghem, C. Calo, G. Bouwmans, I. Krestnikov, A. Martinez, and A. Ramdane, "Optical pulse generation in single section InAs/GaAs quantum dot edge emitting lasers under continuous wave operation," *Applied Physics Letters*, vol. 101, no. 22, pp. 221113+, 2012.

[23] T. G. T. Dziura, "Beyond mean field and plane wave theories of bistable semiconductor lasers," *IEEE Journal of Quantum Electronics*, vol. 22, pp. 651–654, May 1986.